NAVAL POSTGRADUATE SCHOOL

MONTEREY, CALIFORNIA

THESIS

BI-SPECTRAL METHOD FOR RADAR TARGET RECOGNITION

by

Jiunn Wah Yeo

December 2006

Thesis Advisor:	Brett Borden
Co-Advisor:	Donald L. Walters

Approved for public release; distribution is unlimited

THIS PAGE INTENTIONALLY LEFT BLANK

REPORT DOCUMENTATION PAGE			Form Approved OMB No. 0704-0188
Public reporting burden for this collection of information is estimated to average 1 hour per response, including the time for reviewing instruction, searching existing data sources, gathering and maintaining the data needed, and completing and reviewing the collection of information. Send comments regarding this burden estimate or any other aspect of this collection of information, including suggestions for reducing this burden, to Washington headquarters Services, Directorate for Information Operations and Reports, 1215 Jefferson Davis Highway, Suite 1204, Arlington, VA 22202-4302, and to the Office of Management and Budget, Paperwork Reduction Project (0704-0188) Washington DC 20503.			
1. AGENCY USE ONLY ***(Leave blank)***	**2. REPORT DATE** December 2006	**3. REPORT TYPE AND DATES COVERED** Master's Thesis	
4. TITLE AND SUBTITLE: Bi-Spectral Method for Radar Target Recognition			**5. FUNDING NUMBERS**
6. AUTHOR(S) Jiunn Wah Yeo			
7. PERFORMING ORGANIZATION NAME(S) AND ADDRESS(ES) Naval Postgraduate School Monterey, CA 93943-5000			**8. PERFORMING ORGANIZATION REPORT NUMBER**
9. SPONSORING /MONITORING AGENCY NAME(S) AND ADDRESS(ES) N/A			**10. SPONSORING/MONITORING AGENCY REPORT NUMBER**
11. SUPPLEMENTARY NOTES The views expressed in this thesis are those of the author and do not reflect the official policy or position of the Department of Defense or the U.S. Government.			
12a. DISTRIBUTION / AVAILABILITY STATEMENT Approved for public release; distribution is unlimited.			**12b. DISTRIBUTION CODE** A

13. ABSTRACT (maximum 200 words)

Target recognition and identification in battlefields has been a crucial determinant to the ultimate success or failure of modern military campaigns. Since World War II, the Identification of Friend or Foe (IFF) systems installed in radar systems have served as the primary cooperative target identification techniques based on the "question and answer" interrogation loop of unidentified aircraft. However, the IFF system has a number of limitations that pose significant challenges in the positive identification of hostile and neutral aircrafts, which can lead to catastrophic outcome of fratricide and possible elimination of a friendly or commercial aircraft.

To reduce the probability of fratricide and enhance the effectiveness and robustness of target identification, this research will examine the radar Non-Cooperative Target Recognition (NCTR) technique of using the bi-spectral signatures of backscattered radar signals. The basic idea is that the geometry of the target scatterers and their mutual interactions impose features in the reflected radar signal that are typical and unique to the target of interests. The bi-spectrum can be used to detect these multiple interactions features which may then be used to match against a reference database that contains signatures of different target types for recognition and identification.

14. SUBJECT TERMS Bi-spectrum, Non-Cooperative Target Recognition (NCTR) Techniques, High Order Spectra Analysis, Backhoe Data Dome.			**15. NUMBER OF PAGES** 89
			16. PRICE CODE
17. SECURITY CLASSIFICATION OF REPORT Unclassified	**18. SECURITY CLASSIFICATION OF THIS PAGE** Unclassified	**19. SECURITY CLASSIFICATION OF ABSTRACT** Unclassified	**20. LIMITATION OF ABSTRACT** UL

NSN 7540-01-280-5500 Standard Form 298 (Rev. 2-89)
Prescribed by ANSI Std. 239-18

THIS PAGE INTENTIONALLY LEFT BLANK

Approved for public release; distribution is unlimited

BI-SPECTRAL METHOD FOR RADAR TARGET RECOGNITION

Jiunn Wah Yeo
Civilian, Republic of Singapore
B.Eng., Nanyang Technology University, Singapore, 1997

Submitted in partial fulfillment of the
requirements for the degree of

MASTER OF SCIENCE IN COMBAT SYSTEMS SCIENCES AND TECHNOLOGY

from the

NAVAL POSTGRADUATE SCHOOL
December 2006

Author: Jiunn Wah Yeo

Approved by: Brett Borden
Thesis Advisor

Donald L. Walters
Co-Advisor

James Luscombe
Chairman, Department of Physics

THIS PAGE INTENTIONALLY LEFT BLANK

ABSTRACT

Target recognition and identification in battlefields has been a crucial determinant to the ultimate success or failure of modern military campaigns. Since World War II, the Identification of Friend or Foe (IFF) systems installed in radar systems have served as the primary cooperative target identification techniques based on the "question and answer" interrogation loop of unidentified aircraft. However, the IFF system has a number of limitations that pose significant challenges in the positive identification of hostile and neutral aircrafts, which can lead to a catastrophic outcome of fratricide and the possible elimination of a friendly or commercial aircraft.

To reduce the probability of fratricide and enhance the effectiveness and robustness of target identification, this research will examine the radar Non-Cooperative Target Recognition (NCTR) technique of using the bi-spectral signatures of backscattered radar signals. The basic idea is that the geometry of the target scatterers and their mutual interactions impose features in the reflected radar signal that are typical and unique to the target of interests. The bi-spectrum can be used to detect these multiple interactions features which may then be used to match against a reference database that contains signatures of different target types for recognition and identification.

THIS PAGE INTENTIONALLY LEFT BLANK

TABLE OF CONTENTS

LIST OF FIGURES

LIST OF TABLES

THIS PAGE INTENTIONALLY LEFT BLANK

ACKNOWLEDGMENTS

I wish to thank my wife, Charlene, for her love and encouragement throughout the course of my research and study at the NPS.

I would like to thank my thesis advisor, Professor Brett Borden, for his excellent guidance and knowledge-sharing during my entire thesis research and learning process. I also wish to thank my thesis co-advisor, Professor Donald L. Walters, for his invaluable advice and discussions.

I am thankful to my fellow coursemates, Major Charles Chua, Major Anthony Lee, Captain James Neo and Mr. Yeo Eng Choon, for their friendship, encouragement and support.

THIS PAGE INTENTIONALLY LEFT BLANK

I. INTRODUCTION

> Know the enemy and know yourself; in a hundred battles you will never be in peril. Know yourself but not the enemy; for every victory gained you will also suffer a defeat. Know neither the enemy nor yourself; you will succumb in every battle.
>
> — Sun Tzu, Chinese General and Military Strategist (1971)

A. MOTIVATION

Situation awareness has always been the key determinant for the ultimate victory or defeat of all warfare and military campaigns. Through situation awareness, one must be able to ascertain the four "Ws" of one's own forces as well as one's enemies, which are:

1. Where are they: azimuth, elevation, range, etc?
2. When will they arrive: heading, velocity, time of flight, etc?
3. Who are they: friendly, hostile or neutral? and
4. What are they: fighter jet, commercial aircraft, tank, school bus, etc?

While "Where" and "When" are adequately addressed by the early RAdio Detection And Ranging (Radar) systems used primarily as sensors to detect and track targets since World War II, "Who" and "What" or more specifically, target recognition and identification, can pose significant challenges, as only limited information pertaining to the characteristics of the target being detected has been available from the radar backscattered signal.

As such, early radar systems were merely "blob" detectors, as detections of target presences from the reflected radar signal were usually displayed as phosphor "blips" on the radar system's Plan Position Indicator (PPI) (Skolnik, 2001). Information on the target's location in range, azimuth and elevation and velocity could then be extracted from the PPI, but could not provide further detail on the target's type and identity.

This limitation of the early radar systems, together with the vital need for situation awareness as a force multiplier to enhance combat effectiveness, provided the impetus for the development of the IFF system and various other radar target recognition techniques.

1. IFF System and Cooperative Target Recognition

The IFF system is a two-channel interrogator / transponder system, with one frequency used for the interrogating signals and another for the response, that uses pulse-coded radio frequency transmissions to positively identify friendly aircraft, ships, and army units from those of the enemy forces. It serves as a cooperative technique for target recognition, based on the "Question" interrogation and "Answer" response loop of unidentified targets of interests, as depicted in Figure 1.

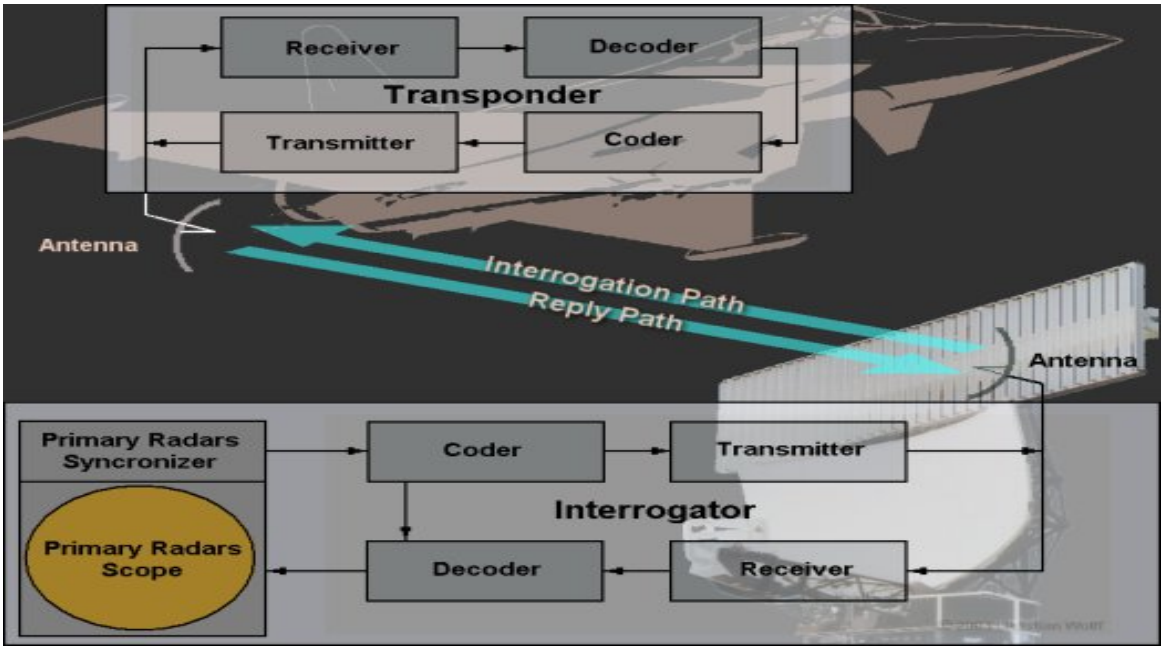

Figure 1 IFF "Question and Answer" Loop (Wolff, 1997)

The IFF interrogator system initiates the "Question and Answer" loop by transmitting a pulse-coded radio frequency signal, also referred to as the "challenge" that asks a series of questions, one of which is "Who are you?" to the unidentified target of interest. The interrogation code or challenge is then received by an electronic system known as a transponder that is installed onboard the target. If the target is friendly and equipped with a compatible transponder, it automatically interprets the challenge and

responds by transmitting the requested identification code back to the interrogator system. After successfully receiving and decoding the acknowledgement, the target is tagged as a friendly target by the interrogating radar system.

Conversely, if the target is neutral or hostile, it is assumed that the challenge cannot be decoded and interpreted by the onboard transponder. Henceforth, the transponder is unable to respond with a correct answer and will be tagged as an unknown or foe target by the interrogating radar system.

Although the IFF system plays a significant role in contributing toward target recognition, it can only perform positive recognition of friendly targets, and it requires the active and cooperative participation of the targets which are under interrogation.

Moreover, IFF systems have a number of limitations, and cooperative systems have historically been plagued with the following fundamental issues:

a. If the IFF system is inoperative, due to a malfunction, or an operator intentionally turns it off, there is no inherent method for a weapon system to distinguish the resulting lack of response from that of an enemy target.

b. Hostile targets may intercept / listen to and re-transmit an acknowledgement from a “friendly” target, in which case the hostile target will be tagged as “friendly.”

c. Commercial airliners are fitted with transponders that conform to open international civil aviation standards, which enable terrorists or enemy forces the opportunity to be equipped with such transponders on their aircrafts. Consequently, they can masquerade as passenger airliners for the purpose of infiltrating the air defence system.

Hence, it is obvious that the IFF system is not infallible and any interruption in the IFF “Question and Answer” loop, resulting in the absence of a response or correct acknowledgement, can potentially draw the inference that the unidentified target is hostile. This seriously reduces the utility of neutral or allied forces and can potentially lead to catastrophic outcomes of fratricide and the erroneous elimination of a friendly or commercial aircraft.

2. Tragic Incidents of Fratricide

To illustrate the devastating consequences of erroneous target recognition and identification, a few examples of wrongful engagements of neutral civilian and friendly targets from recent history are referenced from V.G Nebabin's *Methods and Techniques of Radar Recognition* (1995) and P. Tait's *Introduction to Radar Target Recognition* (2005).

a. In 1980, a DC-9 Italian passenger plane was shot down by mistake with a missile (supposedly American or French made) near the Island of Sicily. It is believed that the missile was re-aimed by mistake because of incorrect IFF and discrimination of the type of plane. Eighty-one passengers died.

b. In 1983, a Boeing 747 passenger plane, South Korean Airlines Flight 007, flying from New York and Anchorage to Korea, was shot down by the USSR Air Defense SU-15 fighter as a result of incorrect recognition. The Boeing 747 was recognized as an RC-135 reconnaissance aircraft. Two-hundred and sixty-nine passengers from Korea, Japan, the U.S. and other countries died.

c. In 1988, an Iranian A-300B Airbus passenger plane, Flight 655, flying from Bender-Abba, Iran, to Dubai, United Arab Emirates was shot down by an SM-2 Standard Missile under control of the Aegis system of the cruiser USS Vincennes in the Persian Gulf. The A-300B was recognized erroneously as an F-14 fighter. Two-hundred and ninety-eight people died.

d. In 1994, two U.S. Blackhawk military helicopters were shot down in the north of Iraq by two U.S. F-15 fighters. The passengers and crews of the helicopters had been performing a humanitarian mission. They had been recognized erroneously as Iraqi helicopters flying in the no-fly zone. Fourteen men died.

e. During the 2003 Iraq war, there were several incidents of ground troops being killed by friendly fire from the air. A UK Tornado aircraft was shot down by a Patriot missile, apparently being mistaken for a Scud ballistic missile, and two British soldiers were killed apparently in an exchange of fire between two British Challenger tanks.

3. Non-Cooperative Target Recognition (NCTR)

To prevent the catastrophic outcome of fratricide and enhance the robustness of the air defense system, NCTR, which encompasses the techniques and technologies to extract and examine the characteristics of target signatures in order to provide further insight on the target's type and identity without its active cooperative participation, has been developed and adopted over the years (Tait, 2005).

A variety of active and passive sensor systems can be utilized to perform NCTR and establish a target's type and identity. A discussion of the various sensor systems and their strengths and limitations in target recognition performance is presented in the following sections.

a. Electro-Optical (EO) and Infrared (IR) Systems

An EO system uses optics for the surveillance, tracking and recognition of a target and depends on external illumination for the conversion of photons into amplifier electrical signals for imaging. An IR system detects the heat emission of the target and can operate in total darkness without external illumination of the target as it is dependent on the temperature differences between the target and its background, for imaging. Both EO and IR systems are passive sensor systems that are ideal for covert operations and have strength in providing high-resolution images for target recognition. However, their performances are adversely affected by weather effects, such as rain, fog and haze, and by atmospheric attenuation due to scattering and absorption.

b. Electronic Warfare (EW) and Electronic Support Measure (ESM) Systems

EW and ESM systems use passive receivers for the detection and analysis of signal in the electromagnetic spectrum. The characteristics of the intercept signal are measured and used to isolate, identify and locate the emitter. Identification of the emitter through the use of finger-printing techniques of its measured signal, along with a library of reference signals can then be used to recognize the associate platform. Although EW and ESM systems have good range performance, due to the one-way propagation of the emitter signal, their effectiveness is completely reliant on the target's electromagnetic

emission for locating and possibly identifying it. Hence an Emission Control (EMCON) imposed by an incoming target will easily overcome the EW and ESM systems' NCTR capability.

c. Acoustics System

The acoustics system uses an array of microphones to discern sound waves from the noisy environment for the detection, localization and possible recognition of sound generating targets, such as human speech, the engine of a moving vehicle and the chopping blades of a hovering helicopter, etc. While the acoustics signal from these targets may be discriminating and recognisable, the acoustics sensor is generally limited in performance due to the slow speed of sound, which is about 330 m/s in air, and limited sensitivity to background noise. The acoustics system is also affected by atmospheric propagation attenuation and is only considered for very short-range applications.

d. Radar System

By far, a radar system is considered the sensor of choice for NCTR, as it offers the most potential. It is able to perform round-the-clock 24/7 surveillance, can perform detection and tracking of targets at ranges much further than EO and IR systems, and is not affected by adverse weather conditions. Furthermore, unlike EW and ESW systems, radar systems are not dependent on the target emissions. Technological advancements have created a system that formerly could only detect and track targets to one that is capable of high resolution imaging and target recognition.

According to Van Der Heigen's "Aircraft Recognition with Radar Range Profiles (1998)," Radar NCTR techniques are rooted on the basic concept that the geometry of the target or the moving parts on the target impose characteristic features in the reflected radar signal that are typical and are unique to the targets of interest. These features may then be used to match against a reference database that contains signatures of different target types for target recognition and identification.

B. SCOPE AND ORGANIZATION

1. Thesis Scope

This thesis first discusses the two fundamental methods of High Range Resolution (HRR) imaging and Signal Modulation analysis, developed to perform target recognition and identification using a radar system. Several conventional NCTR techniques based on these two fundamental methods are then reviewed and evaluated based on their relative merits and limitations.

Next, the thesis focuses on developing a complementary radar NCTR technique of using the bi-spectral signatures of backscattered radar signals to augment the knowledge that conventional NCTR techniques already offer. Derivation and theoretical calculations of the bi-spectrum of radar target signature were performed to extract the multiple scattering interaction features which may then be used to match against a reference database that contains signatures of different target types for target recognition and identification.

2. Research Objectives

The objectives of this thesis are two-fold:

a. To study and mathematically model the direct and indirect multiple interactions scattering mechanisms of radar backscattered signal.

b. To develop the radar NCTR technique of using the bi-spectral signatures of backscattered radar signals for characterization of a target's multiple interactions features.

3. Outline and Organization

Chapter II provides a review of the current conventional NCTR techniques based on the two fundamental classes of HRR imaging and Signal Modulation analysis, developed to perform target recognition and identification using radar systems. A comparison of the NCTR techniques and their relative advantages and disadvantages in target recognition performance is presented.

Chapter III examines the radar principles and scattering mechanisms of electromagnetic waves when a radar signal intersects any target in its propagation path. A mathematical model to represent direct specular and indirect multiple scattering interactions of the backscattered radar signal is presented.

Chapter IV introduces the definitions and mathematical derivations of the bi-spectrum, bi-time and bi-range of the radar backscattered signal. The concept of using the bi-spectral signatures, also known as the characteristic bi-range profiles of backscattered radar signal for target recognition and identification, is presented and studied through an example of a simple 3-points scatterer target.

Chapter V further investigates the potential of using bi-spectra technique for radar target recognition by conducting experimentation based on the Air Force Research Laboratory, “Backhoe Data Dome.” The results and findings for three different test cases are presented and analyzed.

Chapter VI discusses the conclusions made in this thesis and recommends objectives for follow-on research work.

II. NCTR CLASSES AND TECHNIQUES

A. FUNDAMENTAL RADAR TARGET RECOGNITION CLASSES

NCTR is generally categorized into two fundamental classes: High Range Resolution (HRR) imaging and Signal Modulation analysis to perform radar target recognition and identification (Tait, 2005; Van Der Heigen, 1998). The HRR imaging class of NCTR exploits the radar signatures of a target's physical shape, while the Signal Modulation analysis class of NCTR exploits the radar signatures of the target or the dynamics of its moving-parts. A discussion of the concepts, relative merits and limitations of the current conventional NCTR techniques based on these two fundamental classes is presented in the following sections.

B. HRR IMAGING

The basis of the HRR imaging class of NCTR is established on the ability for high radial and cross range resolutions radar to resolve the individual scattering centers of a target and perform radar imaging for target recognition. NCTR techniques from this family include one-dimensional HRR profile or, simply, radial range profile and two-dimensional Inverse Synthetic Aperture Radar (2D-ISAR) imaging (Skolnik, 2001; Tait, 2005; Van Der Heigen, 1998).

1. Radial Range Profile

The radial range profiles of a target of interest essentially represent the one-dimensional images of the target as viewed from different aspect angles. The dominant individual scatterering centers or subcomponents, i.e. the parts on the target that present large Radar Cross-Sections (RCS) and subsequently return a strong radar reflection, are projected onto the line-of-sight between the radar system and the target.

An example of a one-dimensional image that can be can be created by the HRR radar system is illustrated in Figure 2. Figure 2 shows the radial range profile of a target generated by the computer prediction code using the Computer Aided Design (CAD) model of an aircraft viewed from the left hand side. Impulse responses, created using the

Fourier transform of the backscattered radar signal from the aircraft dominant scatterers (dots), are then projected onto the line-of-sight in order to generate a radial range profile.

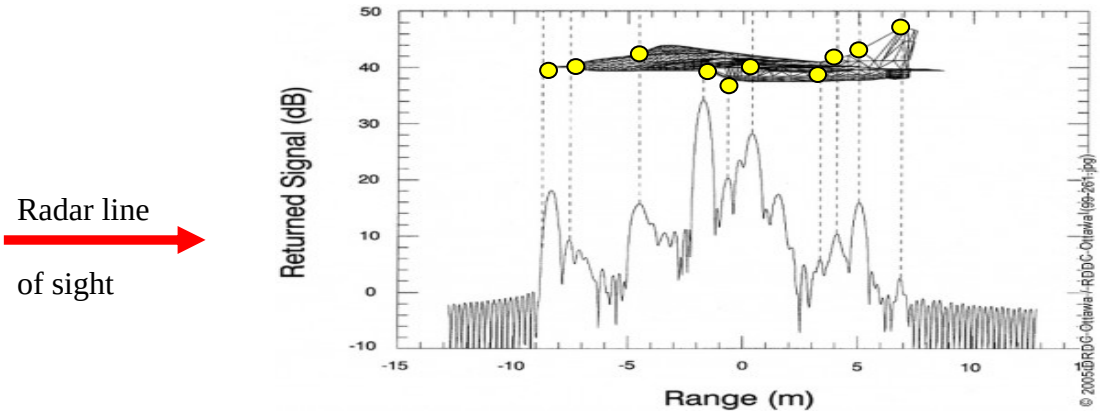

Figure 2 Radial Range Profile of a CAD modeled aircraft (Defence Research and Development Canada).

The radial range profile contains information on the geometry and heuristic features of the target and can be used to infer the type characteristic of the target. This information, together with collected reference databases of measured and / or stimulated (i.e. generated using RCS prediction tools and CAD models) target signatures of different target types (e.g. aircraft, ship and vehicle) and orientations, can then be processed by target recognition and identification algorithms to classify the unknown target into broader categories, such as small jet, large jumbo jet, missile and tank, etc. down to the specific platform type, such as F-16 fighter jet, Boeing-747 passenger plane, Kh-31 Anti-Radiation Missile and M-1 Main Battle Tank, etc.

The merits and limitations of the radial range profile NCTR technique according to Van der Heigen (1998)are summarized in Table 1:

Advantages	Disadvantages
a. Applicable to all target aspect angles.	a. Radial range profile is highly dependent on the target aspect angle. Hence large data sets of target signatures covering all expected target types and orientations are required.
b. Requires relatively short time on target.	

Table 1 Summary of Radial Range Profile's Advantages and Disadvantages

2. 2D-ISAR Imaging

Unlike the radial range profile which only uses the line-of-sight or down range information of the backscattered radar signal for HRR imaging, 2D-ISAR imaging uses information in both the down range and cross-range directions to form two-dimensional images of the target of interests. The cross-range resolution in 2D-ISAR can be thought of in terms of the high resolution in the Doppler-frequency domain. Since each of the major individual scatterer of a moving target can have a different relative velocity with respect to the radar system, resolution in Doppler-frequency, especially for the rotation components of the target's motion, will make it possible to separate these scatterers in the cross-range direction. Figure 3 shows an example of an ISAR image. The target is a B727 jetliner with orientation as in inset (Borden, 1998).

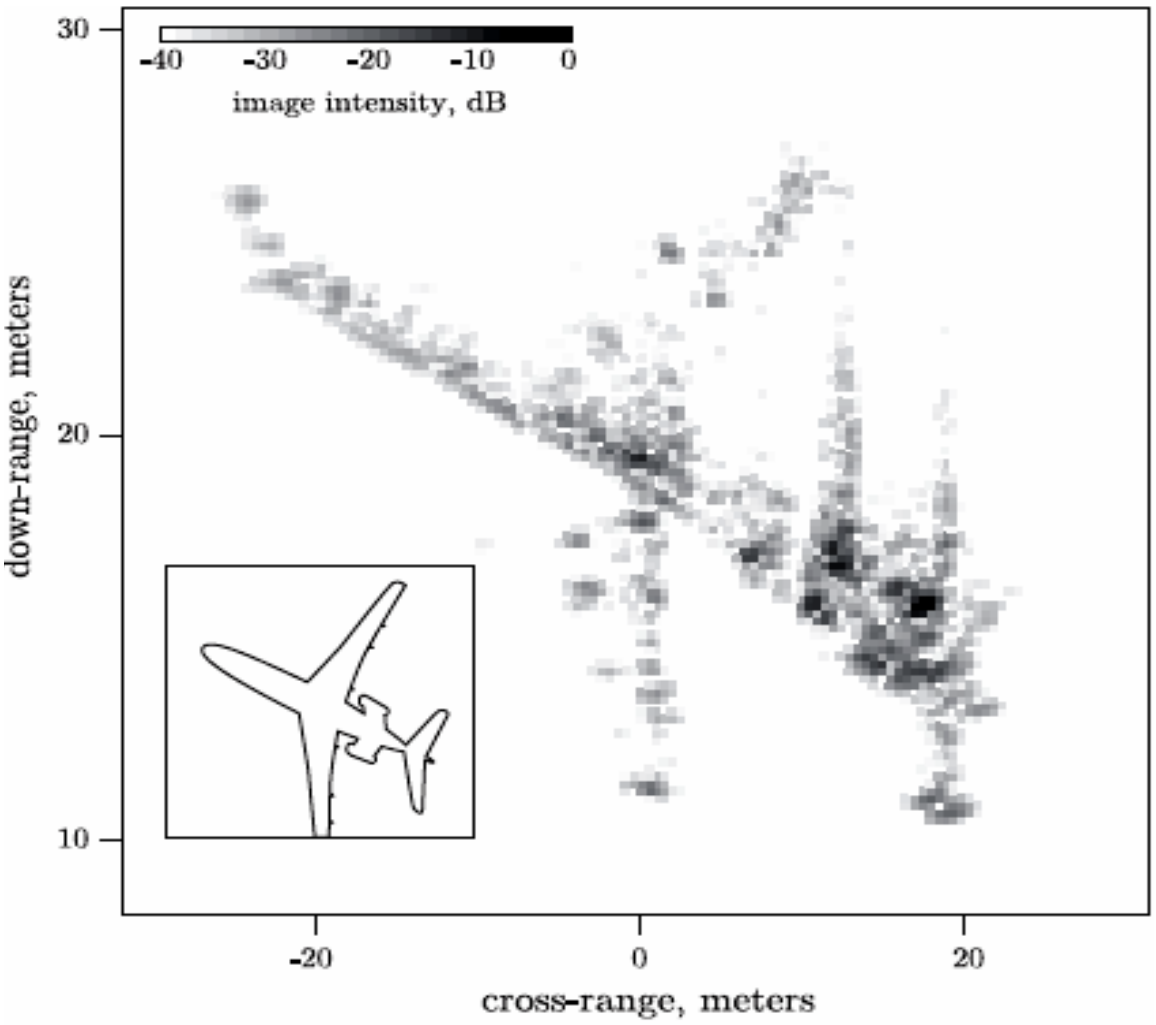

Figure 3 ISAR Image of a B727 Jetliner (Borden, 1998).

The merits and limitations of the 2D-ISAR imaging NCTR technique according to Van Der Heigen (1998) are summarized in Table 2:

<table>
<tr><th>Advantages</th><th>Disadvantages</th></tr>
<tr><td>a. Better fidelity in mapping the geometry of the target due to the additional resolution in the cross-range dimension.</td><td>a. Requires rotational components of target's motion perpendicular to the line-of-sight. Hence target with weak angular rotation (i.e. pitch, roll and yaw motions) will have poor cross-range resolution.</td></tr>
<tr><td rowspan="2">b. More photographic-like 2D image which is better suited for human interpretation.</td><td>b. Requires complex motion compensation and auto-focusing algorithm of 2D-ISAR images which is computationally heavy.</td></tr>
<tr><td>c. Limited knowledge on the precise project plane for the rotation vectors, making recognition complicated.</td></tr>
</table>

Table 2 Summary of 2D-ISAR Imaging's Advantages and Disadvantages

C. SIGNAL MODULATION ANALYSIS

The Signal Modulation analysis class of NCTR is based on the characterizations of the reflected radar modulation signals from the rotating parts of the engine, such as the compressor blades in a jet engine, propellers on a propeller-aircraft and rotors on a helicopter, in the Doppler domain. The NCTR techniques from this family are prominently used to perform target recognition and the identification of aircrafts and include the following: Jet Engine Modulation (JEM), Propeller ROtor Modulation (PROM) and HElicopter Rotor Modulation (HERM) (Skolnik, 2001; Tait, 2005; Van Der Heigen, 1998).

1. JEM, PROM and HERM

The compressor blades in a jet engine, aircraft propellers and rotating blades and hub of a helicopter, each produces a unique and distinctive modulation of the radar target signatures. These modulations in the characteristic spectrums of JEM, PROM and

HERM can be analysed, and attributes pertaining to the information on engines / propellers / rotors types, quantities, number of blades, ranges of rotation frequencies, etc, can be extracted. Examples of the JEM spectrum of a twin-engine aircraft, PROM spectrum of a DC-7 four-engine aircraft and HERM spectrum of a hovering helicopter are shown in Figures 4, 5 and 6 respectively.

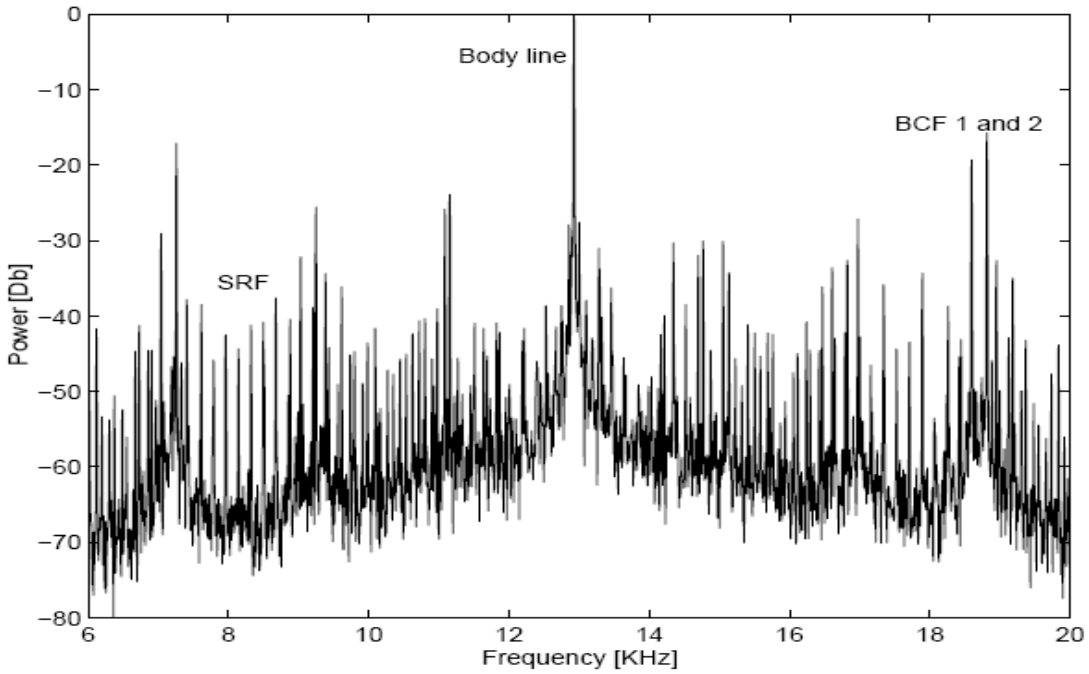

Figure 4 JEM Spectrum of a Twin-Engine Aircraft (Van Der Heigen, 1998)

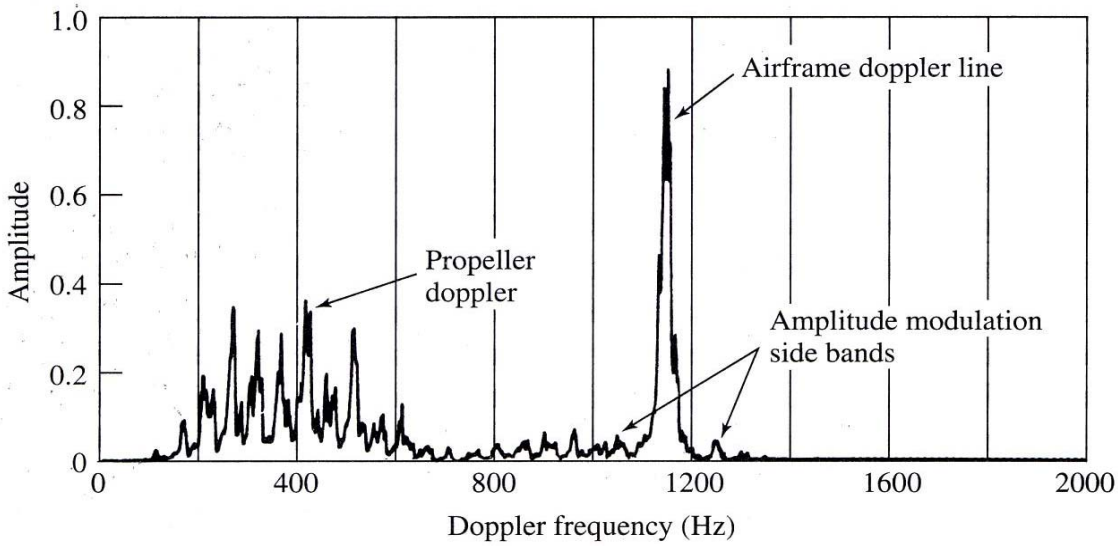

Figure 5 PROM Spectrum of a DC-7 four-engine aircraft (Skolnik, 2001)

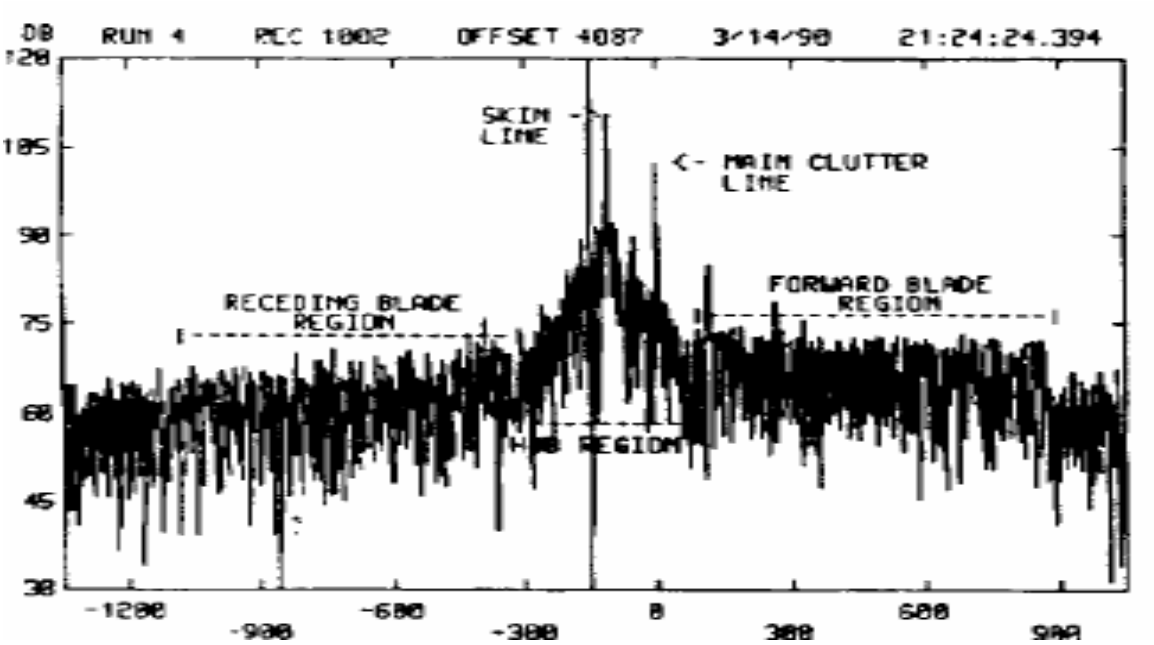

Figure 6 HERM of a Hovering Helicopter (Bullard & Dowdy, 1991)

Since each aircraft has a unique engine, propeller or rotor, these characteristic parameters can be matched against a reference database or table that contains specifications for a variety of target engines / propellers / rotor types for engines associated target recognition and identification.

The merits and limitations of JEM, PROM and HERM analysis NCTR techniques according to Van Der Heigen (1998) are summarized in Table 3:

Advantages	Disadvantages
a. Small and simple target database since it is comprised of engine specification rather than radar target signature or image.	a. Dependent on the target aspect angle. Useful spectrums mostly in the head-on or tail-on orientation.
b. Requires relatively short time on target.	b. Requires strong signal-to-noise ratio for effective classification. Hence techniques limited to relatively short ranges
c. Fast classification since almost all aircrafts have a unique engine type.	

Table 3 Summary of JEM, PROM and HERM Analysis's Advantages and Disadvantages

III. RADAR PRINCIPLES AND TARGET SCATTERING

A. OVERVIEW OF RADAR CONCEPT

RAdio Detection And Ranging (RADAR) is a method of using electromagnetic waves to remotely sense the presence and extract information pertaining to the position, velocity and identifying characteristics of targets of interest. An overview of the basic radar operating principle and electromagnetic wave propagation theory is presented in the following sections.

1. Principle of Radar Operation

The basic radar block diagram and principle of radar operation is illustrated in Figure 7.

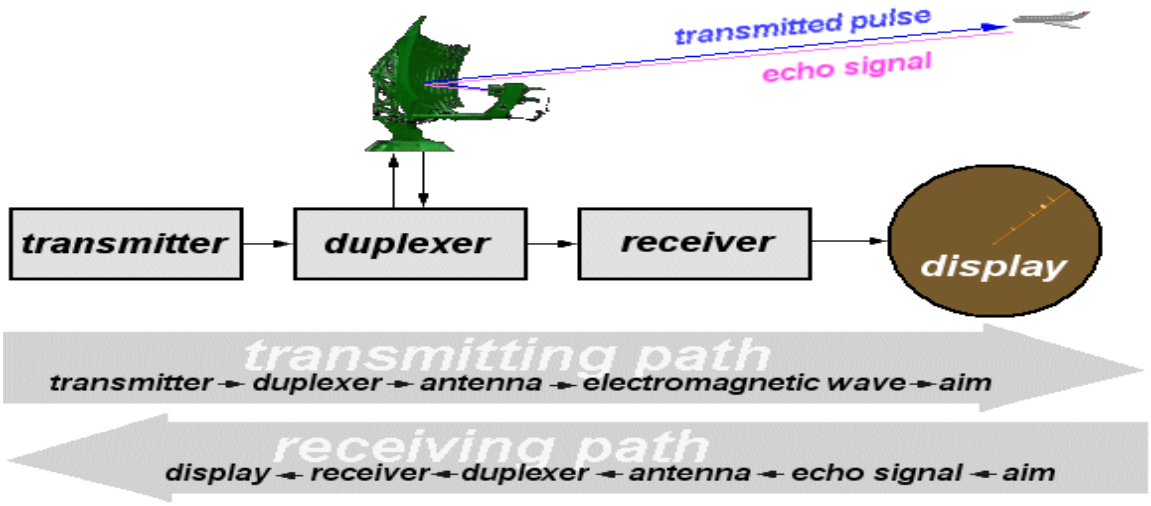

Figure 7 Basic Radar Block Diagram and Operating Principle (Wolff, 1997)

Using a transmitter, the radar system first generates an electromagnetic signal (such as a short sinusoidal pulse) that is radiated into free space through a duplexer and an antenna. The duplexer switches the antenna of monostatic single-antenna systems between the transmitter and receiver, allowing the antenna to be shared for both transmitting and receiving functions, while the antenna is used to concentrate and direct the electromagnetic energy towards the target.

As the electromagnetic wave propagates in free space, a fraction of the transmitted electromagnetic energy is intercepted by the target and scattered in all directions. The reflected energy of the echo signal directed back towards the radar system**,** which is also known as the radar backscattered signal, is then collected by the same antenna and redirected to the receiver through the duplexer. Thereafter, the receiver performs the signal processing of the received echo signal in order to detect the presence of the target and extract information pertaining to its position, velocity and identifying characteristics. The process is completed with the presentation of this information on an operator display.

2. Theory of Electromagnetic Wave Propagation

The fundamental laws of electricity and magnetism, also known as Maxwell's equations, predicted the phenomenon of electromagnetic waves in the form of sinusoidal electric E-field and magnetic H-field, which are oscillating at the wave's frequency and mutually orthogonal to the direction of propagation, as depicted in Figure 8.

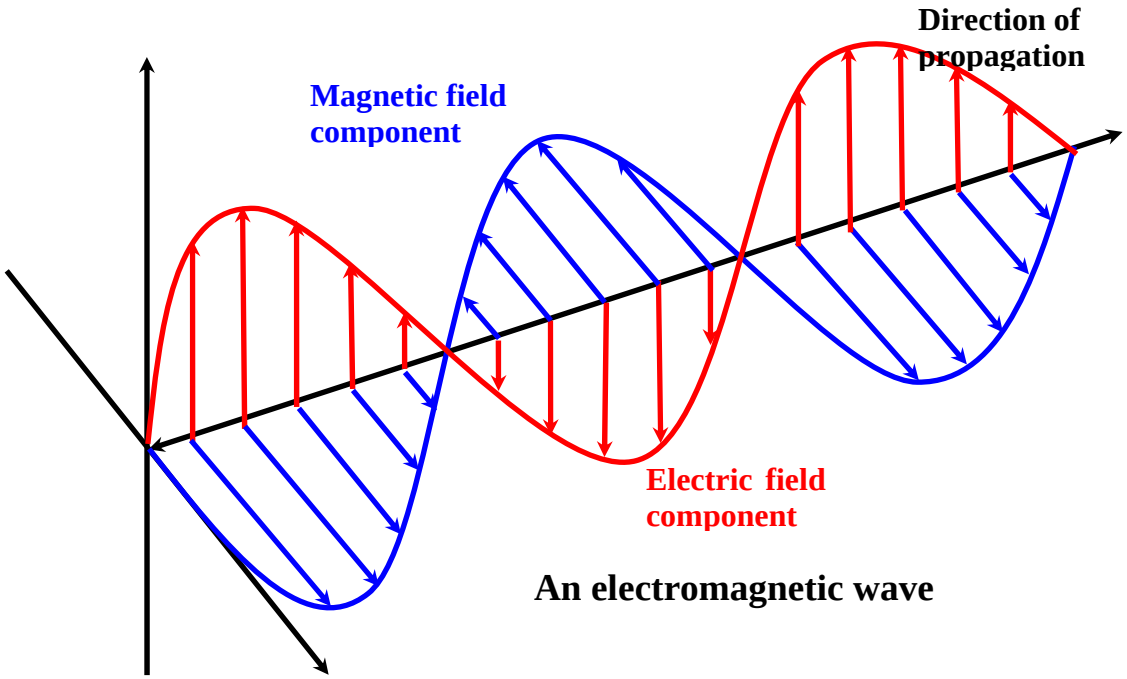

Figure 8 Electromagnetic Wave With Mutually Orthogonal E-Field, H-Field and Direction of Propagation Components

By convention, the electric E-field is usually adopted in the representation of the electromagnetic wave. A derivation of the electric E-field wave equation from Maxwell's equations is presented according to Sadiku's *Elements of Electromagnetics* (2001). Beginning from Maxwell's equations for a vacuum:

$$\nabla \cdot \boldsymbol{E} = 0 \tag{3.1}$$

$$\nabla \times \boldsymbol{E} = -\mu_0 \frac{\partial}{\partial \mathrm{t}} \boldsymbol{H} \tag{3.2}$$

$$\nabla \cdot \boldsymbol{H} = 0 \tag{3.3}$$

$$\nabla \times \boldsymbol{H} = \varepsilon_0 \frac{\partial}{\partial \mathrm{t}} \boldsymbol{E} \tag{3.4}$$

where

∇ is the vector differential operator,

μ_0 = $4\pi \times 10^{-7}$ H/m is the permeability of the vacuum and

ε_0 = 8.854×10^{-12} F/m is the permittivity of the vacuum.

Taking the curl of equation (3.2):

$$\nabla \times \left(\nabla \times \boldsymbol{E} \right) = \nabla \times \left(-\mu_0 \frac{\partial}{\partial \mathrm{t}} \boldsymbol{H} \right) \tag{3.5}$$

Evaluating the left hand side of equation (3.5) with the vector identity of $\nabla \times \left(\nabla \times \boldsymbol{A} \right) = \nabla \left(\nabla \cdot \boldsymbol{A} \right) - \nabla^2 \boldsymbol{A}$ and simplifying the expression using equation (3.1),

$$\nabla \times \left(\nabla \times \boldsymbol{E} \right) = \nabla \left(\nabla \cdot \boldsymbol{E} \right) - \nabla^2 \boldsymbol{E} = -\nabla^2 \boldsymbol{E} \tag{3.6}$$

Evaluating the right hand side of equation (3.5) and simplifying the expression using equation (3.4),

$$\nabla \times \left(-\mu_0 \frac{\partial}{\partial \mathrm{t}} \boldsymbol{H} \right) = -\mu_0 \frac{\partial}{\partial \mathrm{t}} \left(\nabla \times \boldsymbol{H} \right) = -\mu_0 \varepsilon_0 \frac{\partial^2}{\partial \mathrm{t}^2} \boldsymbol{E} \tag{3.7}$$

Equating equations (3.6) and (3.7), results in a differential equation for the electric E-field wave equation,

$$\nabla^2 \boldsymbol{E} - \mu_0 \varepsilon_0 \frac{\partial^2}{\partial t^2} \boldsymbol{E} = 0 \tag{3.8}$$

where

$\mu_0 \varepsilon_0$ $= 1/c^2$ and

c $= 2.998 \times 10^8$ m/sec is the speed of light.

3. Radar Signal

By solving the electric E-field wave equation in equation (3.8), the radar signal for an electromagnetic wave propagating from a radar system can be represented as a general form of a complex sinusoid electric E-field varying in both time and space and expressed as

$$E(r,t) = A(\omega)\left[cos(\omega t - k \cdot r) - i\, sin(\omega t - k \cdot r)\right] \tag{3.9}$$

where

A is the amplitude of the E-field signal,

ω $= 2\pi f$ is the radial frequency,

k $= \dfrac{2\pi}{\lambda}$ is the wave number,

λ is the wavelength,

r is the range from the radar system and

t is the time duration elapsed.

Using Euler's formula, $e^{-ix} = cosx - i\, sinx$, the radar signal at a given position and time, $E(r, t)$ can be rewritten in the exponential form as

$$E(r,t) = A(\omega) e^{-i(\omega t - k \cdot r)} \tag{3.10}$$

To compute the echo signal collected at the radar receiver, the range from the radar system is set to zero, $r = 0$, hence the received radar signal in the time domain is

$$E(t) = A(\omega)e^{-i(\omega t)} \tag{3.11}$$

While the corresponding received radar signal in the frequency domain is

$$H(\omega) = A(\omega)e^{-i(\omega t)} \tag{3.12}$$

B. TARGET SCATTERING MECHANISMS

The mechanisms by which target scattering occurs, are important considerations for determining the physical size, shape, orientation and material composition of the target, which then account for the portion of electromagnetic energy that is reflected back in the direction of the radar system and consequently the probability of target detection, recognition and identification.

As discussed in Tait (2005), the main interactions of the electromagnetic wave with the target are: reflection; absorption; refraction; diffraction and creeping surface waves. Figure 9 illustrates the interaction effects of reflection, absorption and refraction.

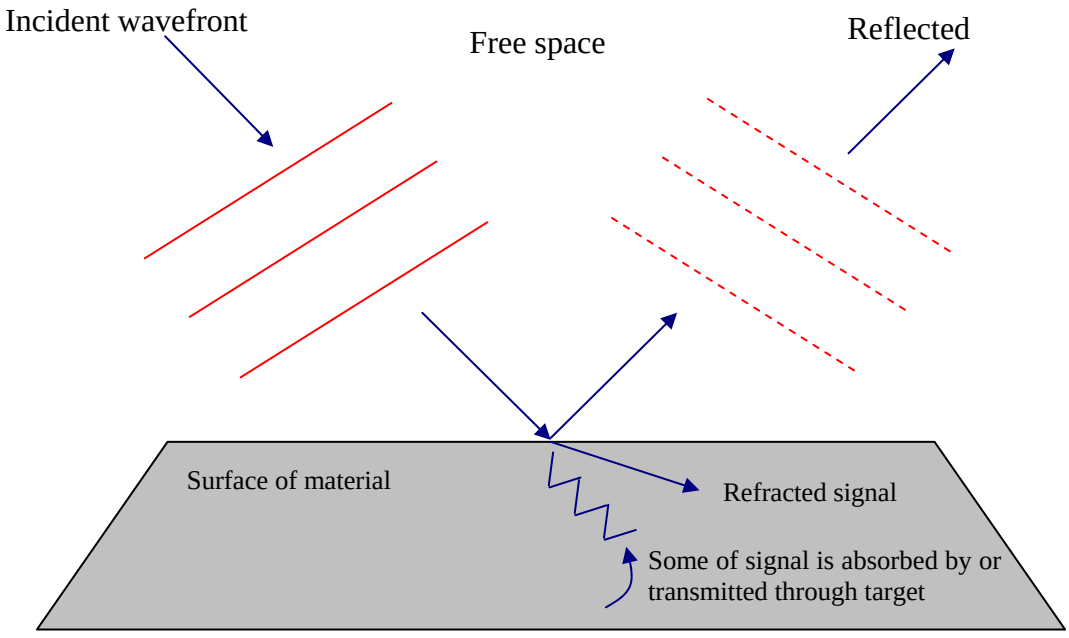

Figure 9 Target Scattering Mechanisms of Radar Wave (Tait, 2005)

At the surface boundary of the target, the incident electromagnetic energy is reflected, refracted and absorbed by the interactions of the radar wave with the target. It can be observed that the fraction of incident electromagnetic energy reflected back towards the radar system is dependent on the portion of energy that is absorbed and refracted into the material, as well as the angle of incidence to the material surface.

Another form of scattering mechanism, through the interaction of the radar wave with the target, is diffraction. This knife-edge effect is explained by Huygens' Principle, which states that a well-defined obstruction to an electromagnetic wave acts as a secondary source and creates a new wavefront. This new wavefront then propagates into the geometric optics shadow area of the obstacle, enabling the radar wave to bend around the edges of the target, propagate into the target's structure through openings and detect the interior parts of the target that would be considered as non line-of-sight as shown in Figure 10.

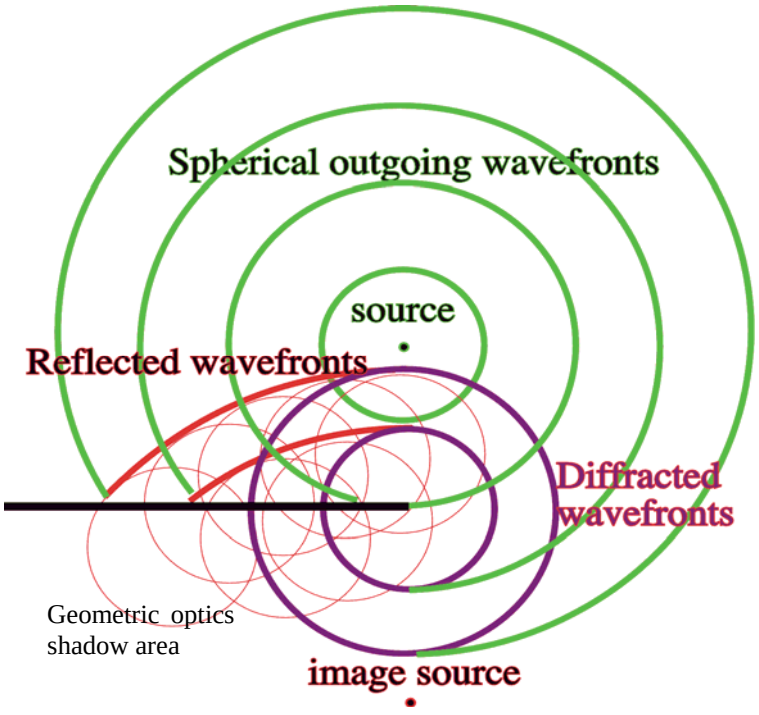

Figure 10 Huygens' Principle of Diffraction (Potter)

Finally the creeping surface wave interaction effect allows for the propagation of radar electromagnetic wave along the surface of a target using surface wave to access the geometric optics' blind region.

C. REPRESENTATION OF RADAR BACKSCATTERED SIGNAL

Targets are generally composed of many individual discrete specular scatterers, each with different scattering properties which correspond to a physical feature of the target, for example the nose, engines, main and tail wings of an aircraft.

Each scatterer, when intercepted by a radar electromagnetic wave, will reflect an echo signal characterized by an amplitude and a phase back towards the direction of the radar system, which will then sum up to a resultant radar backscattered signal at the radar receiver. In addition, there will be contributions from the interactions between the multiple individual scatterers that will further complicate the target characteristics.

A simple mathematical model for the direct specular and indirect multiple scattering interactions of the backscattered radar signal is discussed and presented in the following sections as referenced from Borden (1998) and Jouny (1994).

1. Mathematical Model for Direct Specular Scattering

The radar backscattered signal is assumed to be composed of two major components. The first component represents the specular direct scattering response from the individual scatterers, distributed over the target. The propagation path of the signal can be represented in Figure 11 as:

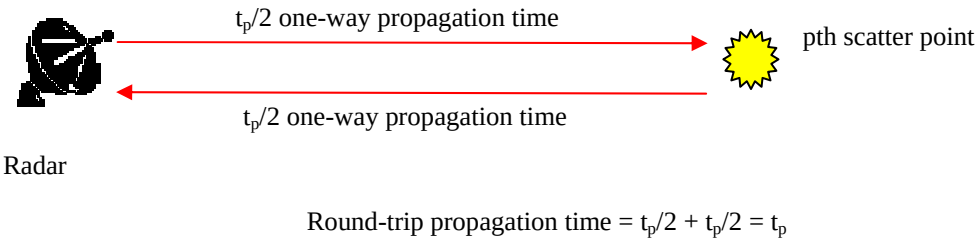

Figure 11 Propagation Path of Direct Specular Scattering Response from Individual Scatterers

Using equation 3.12, this component of the backscatter signal can be expressed mathematically as a summation of the reflected echo signals from all of the individual discrete specular scatterers:

$$H_1(\omega) = \sum_{p=1}^{m} A_p(\omega) e^{-i(\psi_p + \omega t_p)} \tag{3.13}$$

where

m is the number of scattering centers,

A_p is the amplitude of the scattered signal from the pth scattering centre,

ψ_p is the phase shift due to pth scatterer and statistically characterized by the uniform probability density distribution over the interval $(0, 2\pi)$,

ω is the radial frequency ($=2\pi f$) and

t_p is the round-trip propagation time between the radar and the pth scattering centre.

2. Mathematical Model for Indirect Multiple Scatter Interactions

The second major component of the radar backscattered signal represents the effect of interaction between multiple scattering points. The 1st order interaction between any two scattering points is represented in Figure 12 as:

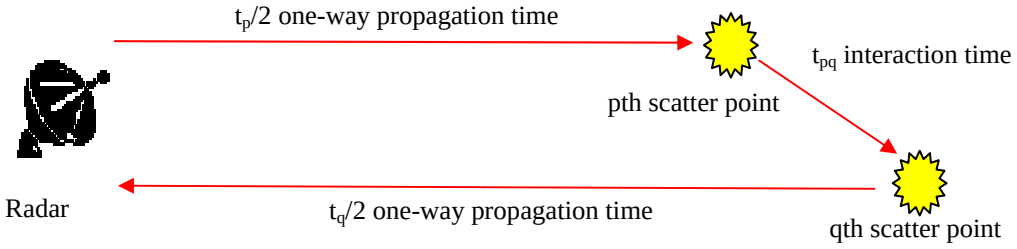

Round-trip propagation time = $t_p/2+(t_{pq})+t_q/2= (t_p+t_q)/2 + t_{pq}$

Figure 12 Propagation Path of Indirect Scattering Response from Multiple Scatterers' Interactions

Using equation 3.12, this second component can also possibly be modeled mathematically as a summation of the reflected echo signals from all of the multiple scatterers' interactions:

$$H_2(\omega) = \sum_{p=1}^{m} \sum_{q=1, q\neq p}^{m} A_{pq}(\omega) e^{-i\left[\psi_p + \psi_q + \omega\left(\frac{t_p + t_q}{2} + t_{pq}\right)\right]} + \ldots higher\text{-}order\ interaction \tag{3.14}$$

where

A_{pq} is the amount of coupling between the pth and qth scattering points,

ψ_q is the phase (uniformly distributed over 2π) of the of qth scatter,

t_q is the round-trip propagation time between the radar and the qth scattering centers and

t_{pq} is the interaction time between the pth and qth scattering centers.

Since the interaction time, t_{pq} between the pth and qth scattering centers is generally unknown for complex targets, it is assumed to be equivalent to $(t_p+t_q)/2$ for the present (although this can be easily generalized). The radar backscattered signal due to multiple interactions is then scattered at a round-trip propagation time of $(t_p+t_q)/2+(t_p+t_q)/2 = t_p+t_q$ and the second major component of this signal can be rewritten as:

$$H_2(\omega) = \sum_{p=1}^{m} \sum_{q=1, q\neq p}^{m} A_{pq}(\omega) e^{-i\left[\psi_p + \psi_q + \omega\left(t_p + t_q\right)\right]} + \ldots. higher\text{-}order\ interaction \tag{3.15}$$

3. Mathematical Model for Combined Direct Specular and Indirect Multiple Scattering Interactions

Collectively, the coherent radar backscattered signal of the target, $H(\omega)$ at radial frequency, $\omega=2\pi f$, is a combination of both the direct specular and multiple scatter interaction terms of $H_1(\omega)$ and $H_2(\omega)$.

Ignoring the effect of higher-order interactions and assuming that the signal amplitudes are frequency-independent, the radar backscattered signal, $H(\omega)$ is given as:

$$H(\omega) = H_1(\omega) + H_2(\omega)$$
$$= \sum_{p=1}^{m} A_p e^{-i(\psi_p + \omega t_p)} + \sum_{p=1}^{m} \sum_{q=1, q\neq p}^{m} A_{pq} e^{-i[\psi_p + \psi_q + \omega(t_p + t_q)]} \quad (3.16)$$

However in target range profiling, the point scatterer data are often observed in terms of relative range instead of the round-trip propagation times. As such, the radar backscattered signal can be rewritten using the radar range relationship of $t=2r/c$ as:

$$H(f) = \sum_{p=1}^{m} A_p e^{-i\left(4\pi R_p \frac{f}{c} + \psi_p\right)} + \sum_{p=1}^{m} \sum_{q=1, q\neq p}^{m} A_{pq} e^{-i\left[4\pi(R_p + R_q)\frac{f}{c} + \psi_p + \psi_q\right]} \quad (3.17)$$

where

R_p is the range between the radar and the pth scatter point,

R_q is the range between the radar and the qth scatter point,

f is the frequency and

c is the speed of light.

D. EXAMPLE: RADAR BACKSCATTERED SIGNAL FROM A SIMPLE 3-POINT SCATTERERS TARGET

To illustrate mathematical modeling of the backscattered radar signal, consider a 3-point scatterers hypothetical target with scatter points at ranges of R_1, R_2 and R_3 from the radar as shown in Figure 13.

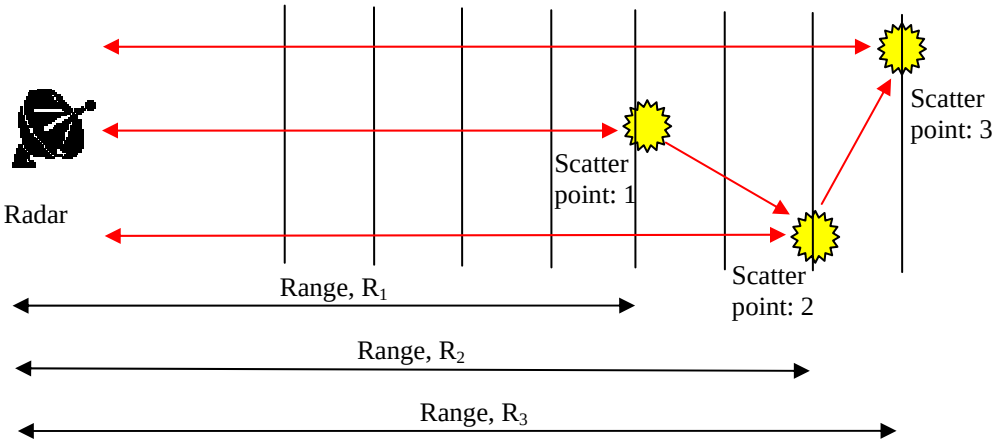

Figure 13 Direct and Indirect Propagation Path of a 3-Point Scatterers Target

Using equation 3.17, the radar backscatter signal for a given frequency, f is given as:

$$
\begin{aligned}
H(f) = & \sum_{p=1}^{3} A_p e^{-i\left(4\pi R_p \frac{f}{c}+\psi_p\right)} + \sum_{p=1}^{3}\sum_{q=1,q\neq p}^{3} A_{pq} e^{-i\left[4\pi\left(R_p+R_q\right)\frac{f}{c}+\psi_p+\psi_q\right]} \\
= & A_1 e^{-i\left(4\pi R_1 \frac{f}{c}+\psi_1\right)} + A_2 e^{-i\left(4\pi R_2 \frac{f}{c}+\psi_2\right)} + A_3 e^{-i\left(4\pi R_3 \frac{f}{c}+\psi_3\right)} \\
& + A_{12} e^{-i\left[4\pi\left(R_1+R_2\right)\frac{f}{c}+\psi_1+\psi_2\right]} + A_{13} e^{-i\left[4\pi\left(R_1+R_3\right)\frac{f}{c}+\psi_1+\psi_3\right]} \\
& + A_{21} e^{-i\left[4\pi\left(R_1+R_2\right)\frac{f}{c}+\psi_1+\psi_2\right]} + A_{23} e^{-i\left[4\pi\left(R_2+R_3\right)\frac{f}{c}+\psi_2+\psi_3\right]} \\
& + A_{31} e^{-i\left[4\pi\left(R_1+R_3\right)\frac{f}{c}+\psi_1+\psi_3\right]} + A_{32} e^{-i\left[4\pi\left(R_2+R_3\right)\frac{f}{c}+\psi_2+\psi_3\right]}
\end{aligned}
$$

When R_1 = 0 m, R_2 = 1.5 m and R_3 = 3.6 m, the corresponding radar backscatter signal can be rewritten as:

$$
H(f) = C_1 + C_2 e^{-i\left[4\pi(1.5)\frac{f}{c}\right]} + C_3 e^{-i\left[4\pi(3.6)\frac{f}{c}\right]} + C_4 e^{-i\left[4\pi(5.1)\frac{f}{c}\right]}
$$

where

C_1, C_2, C_3 and C_4 are constants.

E. EXAMPLE: RADIAL RANGE PROFILE OF A SIMPLE 3-POINT SCATTERERS TARGET

To better understand and visualize the contributions of individual scatterers and their multiple interactions in the radar backscattered signal, the radial range profile of the target is examined. The radial range profile of any target can be generated by evaluating the amplitudes and phases of the radar backscattered signals over a frequency band of evenly spaced frequency intervals and performing Fourier Transform to convert the signals into the time domain (Jouny, 1994). The radial range profile is a plot of the magnitude of the impulse response versus the projected down range along the line-of-sight between the radar system and the target, where scatterings from the individual specular scatterers and their multiple interactions will appear as peak responses.

The radial range profile of the simple 3-point scatterers target, computed using MATLAB's Fast Fourier Transform of the associated radar backscattered signals over a frequency band from 5.0 GHz to 6.0 GHz, is illustrated in Figure 14. The related MATLAB program, "backscatter_signal.m" and source code used to generate this plot can be found in Appendix A.

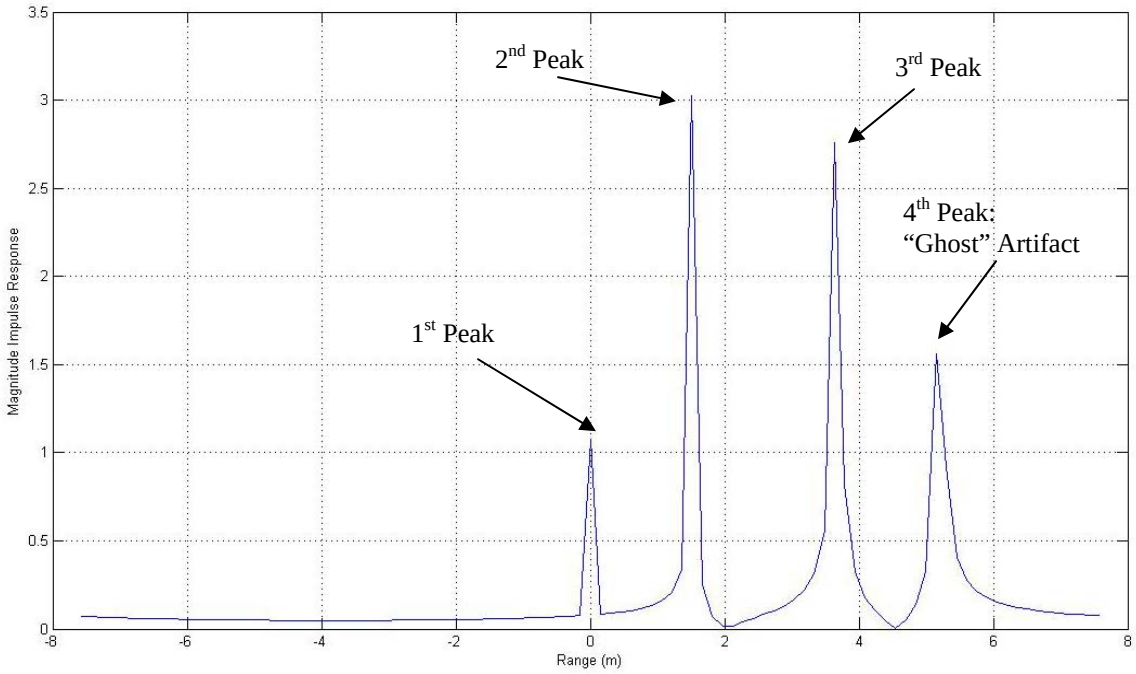

Figure 14 Radial Range Profile of 3-Point Scatterers Target

From Figure 14, it can be observed that the first three peak impulse responses are consistent with the relative positions and geometry of the 3-points scatterers at ranges R_1 = 0 m, R_2 = 1.5 m and R_3 = 3.6 m, while the fourth peak impulse response is a "ghost" artifact that does not map to any scatterers and represents the collective summation of the multiple scatters interaction terms between the 2nd and 3rd scattering points at a range equivalent to $R_2 + R_3$ = 1.5 m + 3.6 m = 5.1 m. (Borden, 1998; Jouny, 1994).

IV. BI-SPECTRAL NCTR TECHNIQUE

A. OVERVIEW OF BI-SPECTAL METHOD

While the radial range profile NCTR technique proves to be a viable means of performing target recognition, its application is predominantly based on the correct mapping and correlation of the peak impulse responses from the direct specular scatterers to the actual physical layout of the target structure and its characteristic features.

However, as discussed and observed in the last section of Chapter III, some of these peak impulse responses in the radial range profile do not correspond to any target structures and represent the multiple interactions between major individual scatterers instead. Thus, a bi-spectral method, to differentiate the direct specular scattering responses from the multiple scatterers interaction responses, is proposed in Jouny (1994), Botha & Spoelstra (1992), Garber, Jouny & Moses (1995) and Jounty & Walton (1990) as another HRR imaging class of NCTR technique to augment the radial range profile in performing radar target recognition and identification.

1. Definition of Bi-Spectrum

In Higher-Orders Statistic (HOS) signal processing, the bi-spectrum of a continuous-time signal, *h*(t) is defined as the Fourier Transform of the third-order cumulant-generating function and is given in Jouny (1994), Botha & Spoelstra (1992), Garber, Jouny & Moses (1995) and Jounty & Walton (1990):

$$B(\omega_1, \omega_2) = \int_{-\infty}^{\infty} \int_{-\infty}^{\infty} C_3(t_1, t_2) e^{-i(\omega_1 t_1 + \omega_2 t_2)} dt_1 dt_2 \tag{4.1}$$

where

C_3 represents the triple correlation of the signal and is expressed as:

$$C_3(t_1, t_2) = \int_{-\infty}^{\infty} h^*(t) h(t + t_1) h(t + t_2) dt = E\{h^*(t) h(t + t_1) h(t + t_2)\} \tag{4.2}$$

$E\{\ \}$ denoted the expectation and

* superscript asterisk denoted a complex conjugate.

2. Definition of Bi-Time

However, in radar signal processing, the radar backscattered signals are often processed and analyzed as discrete signals in the frequency-domain (i.e. expressed as a function of frequency). The third-order cumulant or triple correlation of the frequency-domain signal, $H(\omega)$ is then defined by Jouny (1994), Botha & Spoelstra (1992), Garber, Jouny & Moses (1995) and Jounty & Walton (1990) as:

$$\begin{aligned} C_3(\omega_1,\omega_2) &= \int_{-\infty}^{\infty} H^*(\omega)H(\omega+\omega_1)H(\omega+\omega_2)d\omega \\ &= E\left\{H^*(\omega)H(\omega+\omega_1)H(\omega+\omega_2)\right\} \end{aligned} \tag{4.3}$$

The equivalent bi-spectrum, expressed as a function of time after applying the Fourier Transform, is known as the bi-time. The bi-time of a discrete time-domain bi-spectral signature is then expressed as:

$$B(t_1,t_2) = \sum_{\omega_1=-\infty}^{\infty}\sum_{\omega_2=-\infty}^{\infty} C_3(\omega_1,\omega_2)e^{-i(\omega_1 t_1+\omega_2 t_2)} \tag{4.4}$$

and can be represented in terms of impulse response as:

$$B(t_1,t_2) = E\left\{h(t_1)h(t_2)h^*(t_1+t_2)\right\} \tag{4.5}$$

where

h(t) is the impulse response as a function of time

3. Definition of Bi-Range

The bi-time can be further expressed as a function of range using the radar range and round-trip propagation time relation of:

$$r = \frac{ct}{2} \Rightarrow t = \frac{2r}{c} \tag{4.6}$$

where

r is the range from the radar to the target,

t is the round-trip propagation time needed for the radar signal to propagate to the target and back, and

c is the speed of light.

Substituting $t=2r/c$ and $f=\omega/2\pi$ into the expression for bi-time, derives the corresponding bi-range as (Jouny (1994), Botha & Spoelstra (1992), Garber, Jouny & Moses (1995) and Jounty & Walton (1990):

$$\begin{aligned} B(r_1, r_2) &= \sum_{f_1=-\infty}^{\infty} \sum_{f_2=-\infty}^{\infty} C_3(f_1, f_2) e^{-i\left[2\pi f_1\left(\frac{2r_1}{c}\right)+2\pi f_2\left(\frac{2r_2}{c}\right)\right]} \\ &= \sum_{f_1=-\infty}^{\infty} \sum_{f_2=-\infty}^{\infty} C_3(f_1, f_2) e^{\left[-i\frac{4\pi}{c}(f_1 r_1 + f_2 r_2)\right]} \end{aligned} \tag{4.7}$$

and bi-range can then be represented in terms of impulse response as:

$$B(r_1, r_2) = E\left\{h(r_1)h(r_2)h^*(r_1 + r_2)\right\} \tag{4.8}$$

where

$h(\mathrm{r})$ is the impulse response as a function of range.

From equation 4.7, it can be deduced that if the range profile for a given radar target contains three responses, $h(r_1)$, $h(r_2)$ and $h(r_3)$, two of which, $h(r_1)$ and $h(r_2)$ are due to direct specular scattering, and one is due to an interaction between the direct scatterers, $h(r_3)$, the bi-range will only detect this term if the interaction term appears at a distance from the radar equal to the sum of the distances of the direct terms, i.e. at $r_3 = r_1 + r_2$ according to Jouny (1994).

B. EXAMPLE: BI-RANGE OF A SIMPLE 3-POINT SCATTERERS TARGET

Using the same simple 3-point scatterers target example as described in Chapter III, the bi-range of the target can be computed mathematically using equation 4.7 as:

$$\begin{aligned} B(r_1, r_2) &= E\left\{h(r_1)h(r_2)h^*(r_1 + r_2)\right\} \\ &= \sum_{p=1}^{4} \sum_{q=1}^{4} A_p A_q A_{pq} \left[\delta(r_1 - R_p, r_2 - R_q) + \delta(r_1 - R_q, r_2 - R_p)\right] \end{aligned} \tag{4.9}$$

Expanding the terms for the above expression:

$$
\begin{aligned}
B(r_1, r_2) = {} & A_1 A_1 A_{11}\left[\delta(r_1 - R_1, r_2 - R_1) + \delta(r_1 - R_1, r_2 - R_1)\right] \\
& + A_1 A_2 A_{12}\left[\delta(r_1 - R_1, r_2 - R_2) + \delta(r_1 - R_2, r_2 - R_1)\right] \\
& + A_1 A_3 A_{13}\left[\delta(r_1 - R_1, r_2 - R_3) + \delta(r_1 - R_3, r_2 - R_1)\right] \\
& + A_1 A_4 A_{14}\left[\delta(r_1 - R_1, r_2 - R_4) + \delta(r_1 - R_4, r_2 - R_1)\right] \\
& + A_2 A_1 A_{21}\left[\delta(r_1 - R_2, r_2 - R_1) + \delta(r_1 - R_1, r_2 - R_2)\right] \\
& + A_2 A_2 A_{22}\left[\delta(r_1 - R_2, r_2 - R_2) + \delta(r_1 - R_2, r_2 - R_2)\right] \\
& + A_2 A_3 A_{23}\left[\delta(r_1 - R_2, r_2 - R_3) + \delta(r_1 - R_3, r_2 - R_2)\right] \\
& + A_2 A_4 A_{24}\left[\delta(r_1 - R_2, r_2 - R_4) + \delta(r_1 - R_4, r_2 - R_2)\right] \\
& + A_3 A_1 A_{31}\left[\delta(r_1 - R_3, r_2 - R_1) + \delta(r_1 - R_1, r_2 - R_3)\right] \\
& + A_3 A_2 A_{32}\left[\delta(r_1 - R_3, r_2 - R_2) + \delta(r_1 - R_2, r_2 - R_3)\right] \\
& + A_3 A_3 A_{33}\left[\delta(r_1 - R_3, r_2 - R_3) + \delta(r_1 - R_3, r_2 - R_3)\right] \\
& + A_3 A_4 A_{34}\left[\delta(r_1 - R_3, r_2 - R_4) + \delta(r_1 - R_4, r_2 - R_3)\right] \\
& + A_4 A_1 A_{41}\left[\delta(r_1 - R_4, r_2 - R_1) + \delta(r_1 - R_1, r_2 - R_4)\right] \\
& + A_4 A_2 A_{42}\left[\delta(r_1 - R_4, r_2 - R_2) + \delta(r_1 - R_2, r_2 - R_4)\right] \\
& + A_4 A_3 A_{43}\left[\delta(r_1 - R_4, r_2 - R_3) + \delta(r_1 - R_3, r_2 - R_4)\right] \\
& + A_4 A_4 A_{44}\left[\delta(r_1 - R_4, r_2 - R_4) + \delta(r_1 - R_4, r_2 - R_4)\right]
\end{aligned}
$$

Substituting R_1 = 0 m, R_2 = 1.5 m, R_3 = 3.6 m and R_4 = 5.1 m, the bi-range can be rewritten as:

$$
\begin{aligned}
B(r_1, r_2) = {} & C_1'\left[\delta(r_1, r_2)\right] + C_2'\left[\delta(r_1 - 1.5, r_2 - 1.5)\right] \\
& + C_3'\left[\delta(r_1 - 3.6, r_2 - 3.6)\right] + C_4'\left[\delta(r_1 - 5.1, r_2 - 5.1)\right] \\
& + C_5'\left[\delta(r_1, r_2 - 1.5) + \delta(r_1 - 1.5, r_2)\right] \\
& + C_6'\left[\delta(r_1, r_2 - 3.6) + \delta(r_1 - 3.6, r_2)\right] \\
& + C_7'\left[\delta(r_1, r_2 - 5.1) + \delta(r_1 - 5.1, r_2)\right] \\
& + C_8'\left[\delta(r_1 - 1.5, r_2 - 3.6) + \delta(r_1 - 3.6, r_2 - 1.5)\right] \\
& + C_9'\left[\delta(r_1 - 1.5, r_2 - 5.1) + \delta(r_1 - 5.1, r_2 - 1.5)\right] \\
& + C_{10}'\left[\delta(r_1 - 3.6, r_2 - 5.1) + \delta(r_1 - 5.1, r_2 - 3.6)\right]
\end{aligned}
$$

where C_1', C_2', C_3', C_4', C_5', C_6', C_7', C_8', C_9' and C_{10}' are constants.

Graphically, the bi-range of the 3-point scatterers target can be computed using MATLAB's two-dimensional (2-D) discrete Fourier Transform of the third-order cumulant function of the radar backscatter signal. The results are then plotted as the three-dimensional (3-D) and 2-D (contour plot) bi-range profiles of the 3-point scatterers

target in Figure 15 and 16 respectively. The related MATLAB programs, “bispectral.m” and source code used to generate these plots can be found in Appendix B.

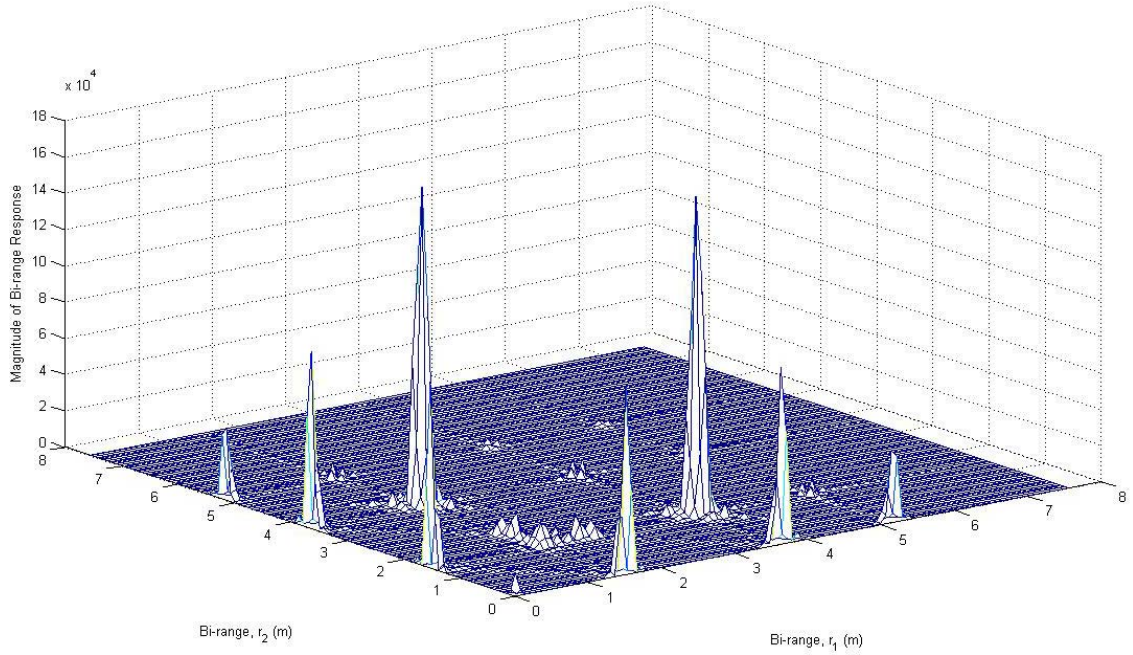

Figure 15 3-D Bi-Range Profile of 3-Point Scatterers Target

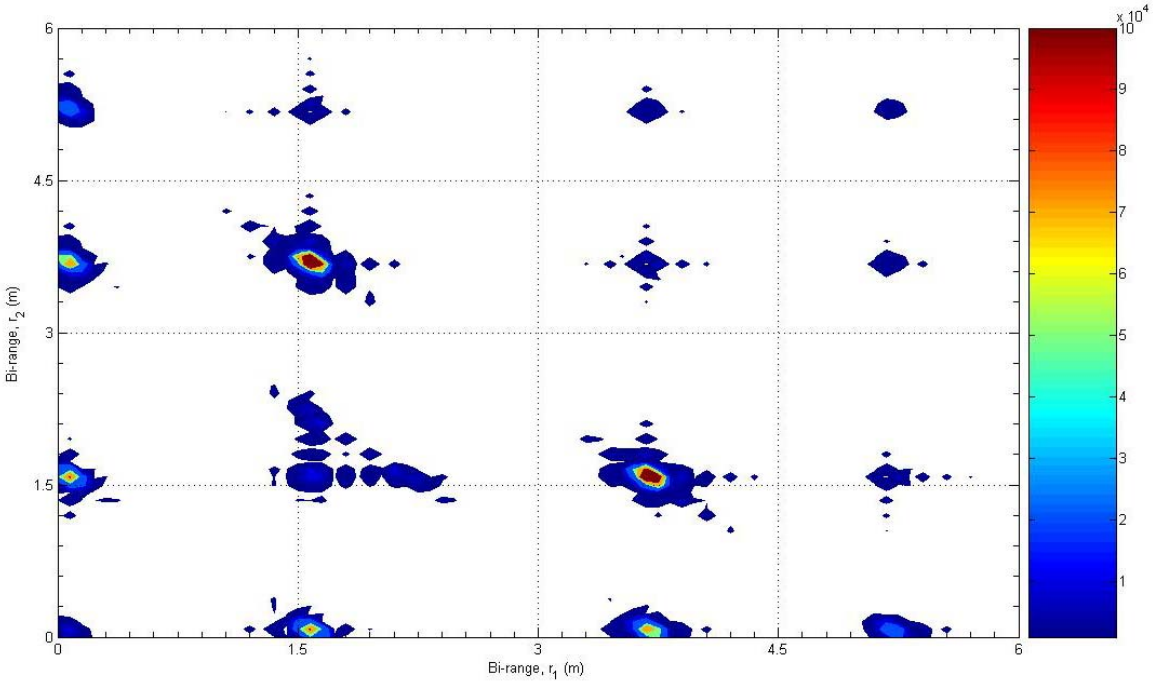

Figure 16 2-D Bi-Range Profile of 3-Point Scatterers Target

From Figures 15 and 16, it can be observed that the bi-range profiles are generated by responses at the range pairs (R_p and R_q) for p and q = 1,…. 4 with amplitude of $A_pA_qA_{pq}$. The locations of the responses are also noted to be consistent with the theoretically computed positions.

C. CHARACTERISTIC BI-RANGE PROFILE

Since a non-zero bi-range response is an outcome arising from the correlated interaction between the responses at range r_1 and r_2, it is clear that the peak responses in the bi-range profile of the radar backscattered signals represent strong additive multiple interactions between the scatterers or subcomponents of the target.

Therefore, the characteristic bi-range profile of a target, which highlights the defining peak responses (within an order of magnitude) at coordinates (r_1, r_2) can potentially be employed to characterize the unique composition and layout of the target for recognition and identification. The characteristic bi-range profile, showcasing the peak responses of the 3-points-scatterer target example is illustrated in Figure 17.

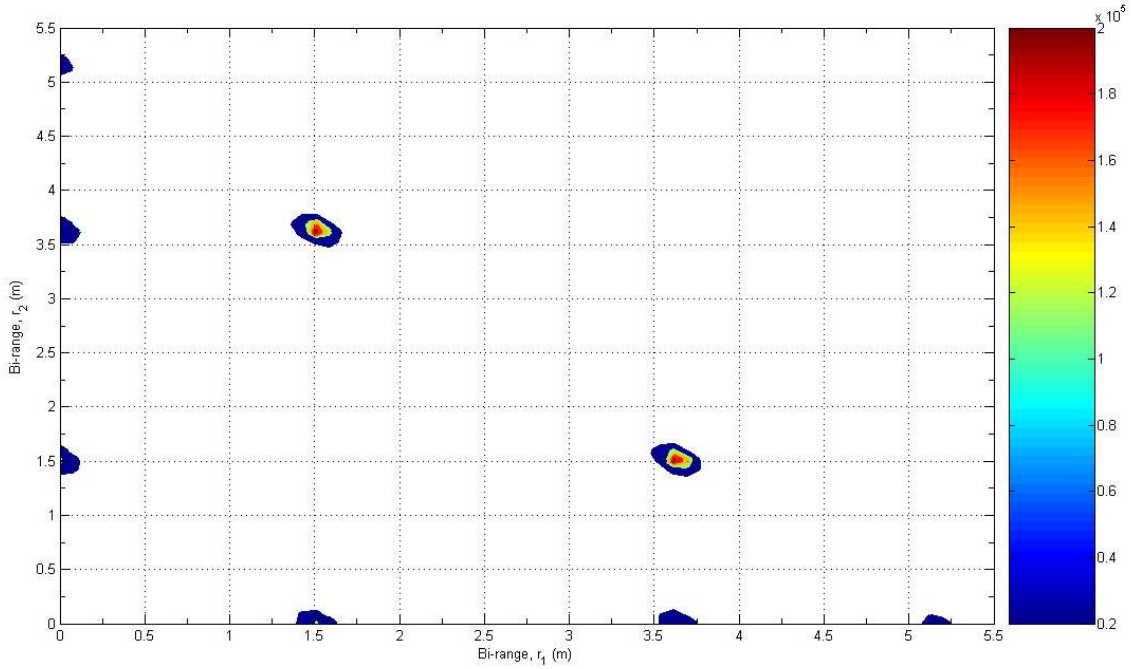

Figure 17 2-D Characteristic Bi-Range Profile of 3-Point Scatterers Target

It can be observed from Figure 17 that the peak responses in the bi-range profile of the 3-points scatterer target at (r_1, r_2) = (1.5m, 3.6m) corresponded to the resulting multiple interactions between the 2nd scattering point at 1.5m and 3rd scattering point at 3.6m, as expected.

The merits and limitations of bi-range profile NCTR technique according to Bao, Shi & Zhang (2001) and Bao, Pei & Xing (2001) are summarized in Table 4:

Advantages	**Disadvantages**
a. Retains both the amplitude and phase information of a signal. Hence bi-spectral signatures are translation (or shift) invariant and robust to aspect dependence.	a. Requires intensive computation of two-dimensional high range resolution data. The number of bi-spectral data is the square of the HRR profile.
b. Good clutter and noise rejection performance due to ability to statistically suppress the clutter or noise characterized by zero-mean Gaussian probability density distribution.	

Table 4 Summary of Bi-range Profile's Advantages and Disadvantages

THIS PAGE INTENTIONALLY LEFT BLANK

V. BI-SPECTRAL NCTR EXPERIMENTATION

A. "BACKHOE DATA DOME" EXPERIMENTATION

To further examine the potential of using the characteristic bi-range profile of a complex target for NCTR and identification, experimentation based on the Air Force Research Laboratory (AFRL), "Backhoe Data Dome, Version 1.0" by Lin & Naidu (2004) are performed and presented in the following sections.

1. AFRL "Backhoe Data Dome Version 1.0"

The "Backhoe Data Dome, Version 1.0" consists of simulated wideband (7-13 GHz), full polarization, complex backscatter data from a backhoe loader generated using a Computer-Aided-Design (CAD) model in free space as shown in Figure 18. The MATLAB program "plotfacet.m" available from the Air Force Research Laboratory Sensor Data Management System was used to plot all 3-D graphics of the backhoe loader.

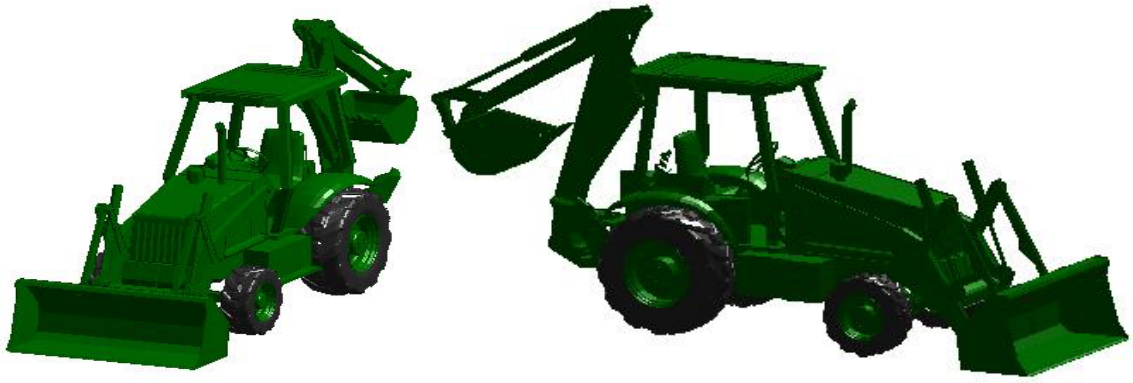

Figure 18 CAD Model of Backhoe Loader

The backscatter data are then synthetically generated over a full 2π steradian viewing hemisphere with 14 samples per degree in both azimuth and elevation. There is one sample every 11.75 MHz over the 6 GHz bandwidth and full polarizations; i.e. horizontal linear polarization on transmit and receive (HH), vertical linear polarization on transmit and receive (VV) and horizontal linear polarization on transmit and vertical linear polarization on receive (HV).

A representation of the k-space data dome is as shown in Figure 19.

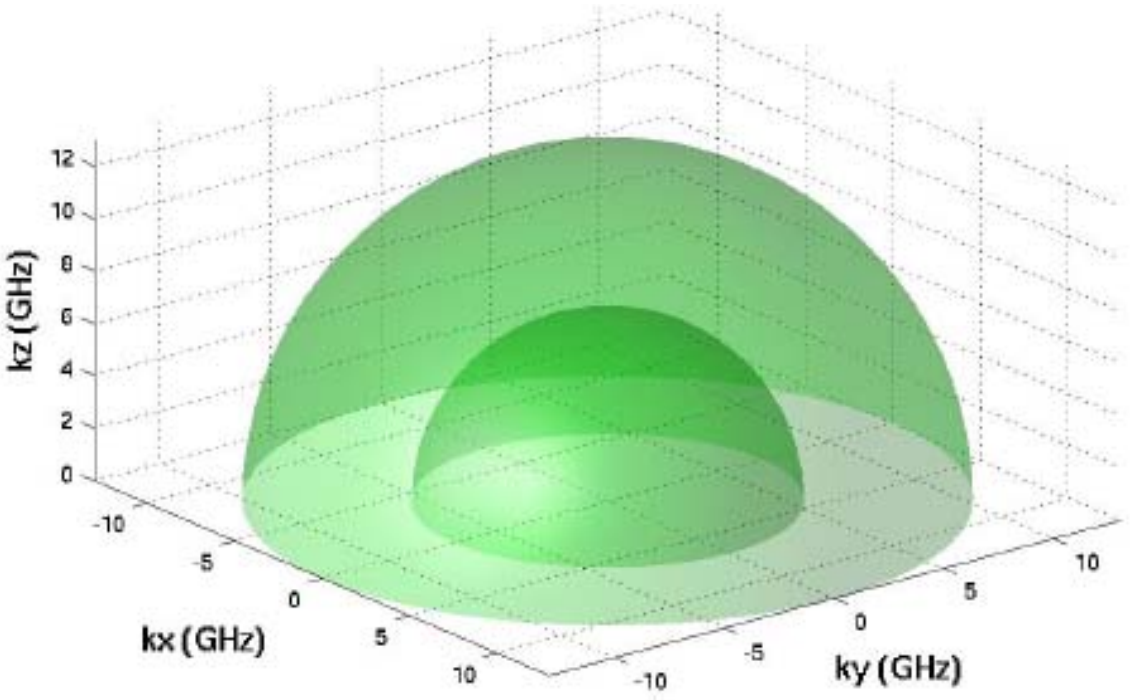

Figure 19 Backhoe Data Dome Representation in k-Space (Lin & Naidu, 2004)

In this experiment, two sets of 2-D backhoe backscattered data which contained VV, HH and HV polarized k-space data from a 110 degree azimuth cut (from 350 degrees to 100 degrees in azimuth) available through Lin & Naidu (2004) are used, one at 0 degree elevation and the other at 30 degree elevation.

With the method described in the preceding Chapters, characteristic bi-range profiles analysis on the 2-D k-space data is performed for three different test cases, with the backhoe loader setup in the following orientation and using the specified polarization:

a. Test Case 1: Orientation of backhoe loader at 0 degree azimuth and 0 degree elevation with VV, HH and HV polarizations.

b. Test Case 2: Orientation of backhoe loader at 90 degree azimuth and 0 degree elevation with VV, HH and HV polarizations.

c. Test Case 3: Orientation of backhoe loader at 60 degree azimuth and 30 degree elevation with VV, HH and HV polarizations.

2. Test Case 1: Setup and Results ($\theta_{azimuth}$=0°, $\varphi_{elevation}$=0°)

In Test case 1, the backhoe loader is orientated at 0 degree azimuth and 0 degree elevation with reference to the radar direction as depicted in Figure 20:

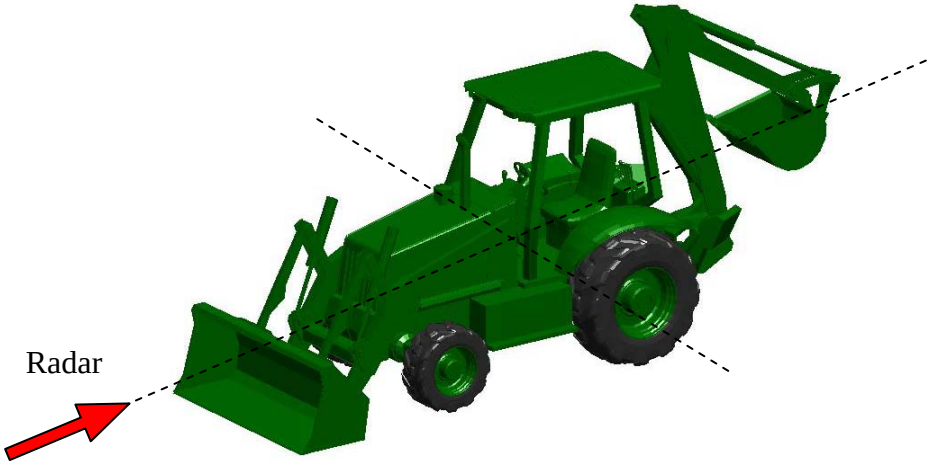

Figure 20 Orientation of CAD-Modeled Backhoe Loader at Aspect Viewing Angles of Azimuth, ($\theta_{azimuth}$)=0° and Elevation, ($\varphi_{elevation}$)=0°

The radial range profiles of the backhoe loader are computed using MATLAB's Fast Fourier Transform of the associated radar backscattered signals, while the 3-D and 2 -D bi-range profiles are computed using MATLAB's two-dimensional (2-D) discrete Fourier Transform of the third-order cumulant function of the radar backscatter signals.

Both radial range and bi-range profiles are processed over a frequency bandwidth of 5.9058 GHz (from 7.0472 to 12.953 GHz) with VV, HH and HV polarizations for the target's aspect viewing angle of azimuth, ($\theta_{azimuth}$) = 0° and elevation, ($\varphi_{elevation}$) = 0°. The related MATLAB program, "test_case1.m" and source code used to generate this plot can be found in Appendix C.

a. Radial Range Profile ($\theta_{azimuth}$=0°, $\varphi_{elevation}$=0°)

The radial range profiles of the backhoe loader with VV, HH and HV polarizations are illustrated in Figure 21, 22 and 23 respectively.

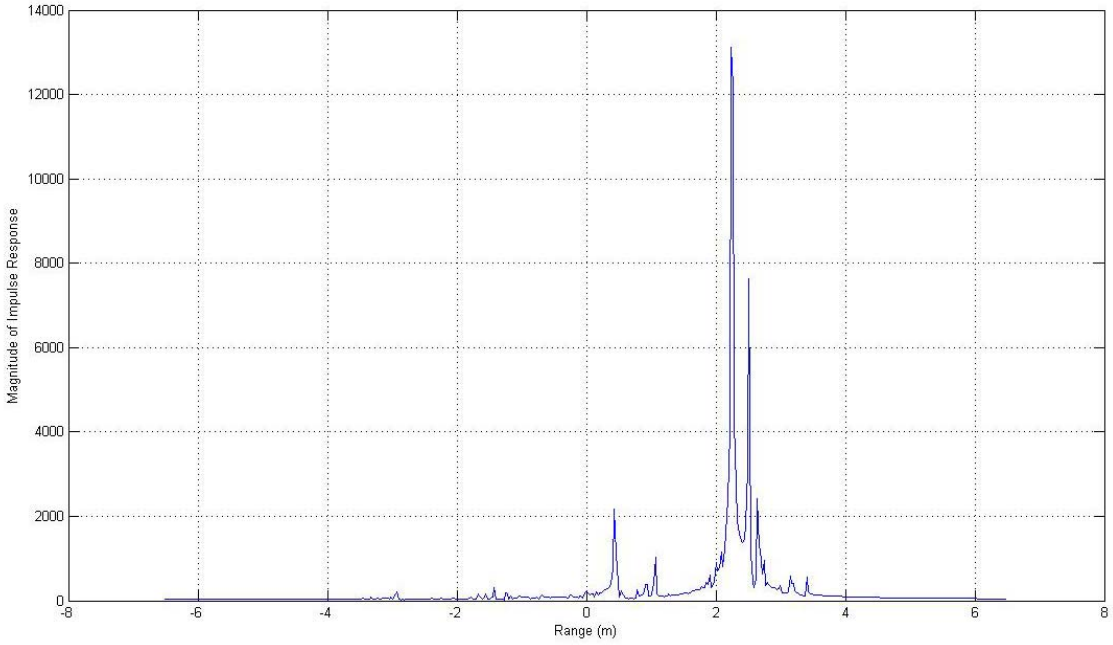

Figure 21 Radial Range Profile of Backhoe Loader at Aspect Angles of $\theta_{azimuth}$=0° and $\varphi_{elevation}$=0° with VV Polarization

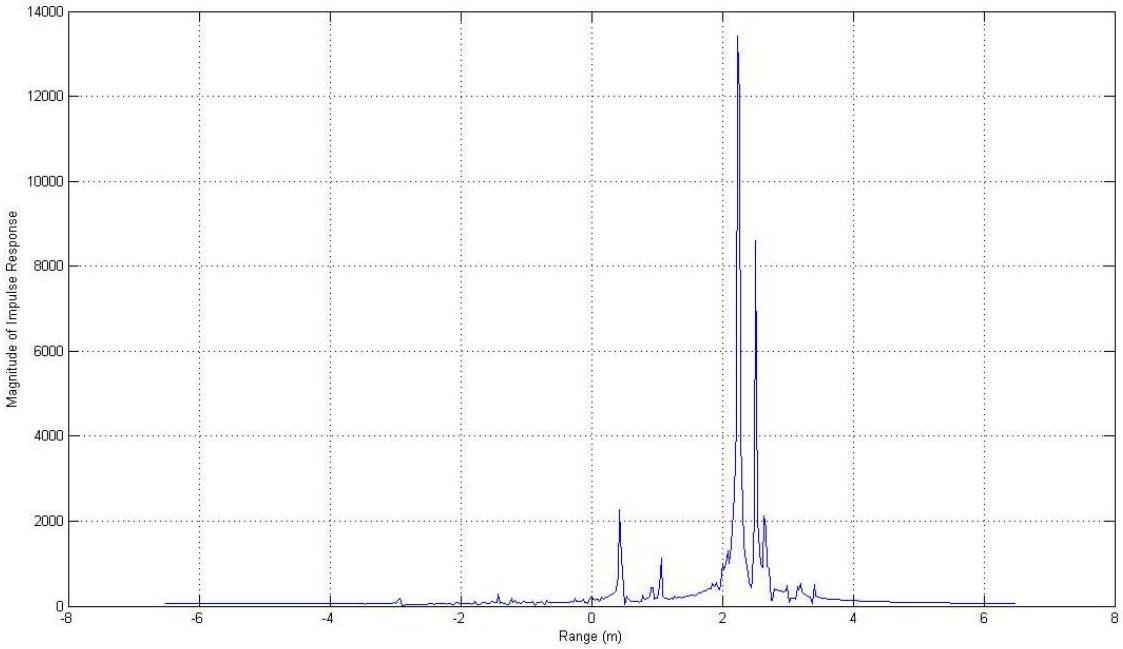

Figure 22 Radial Range Profile of Backhoe Loader at Aspect Angles of $\theta_{azimuth}$=0° and $\varphi_{elevation}$=0° with HH Polarization

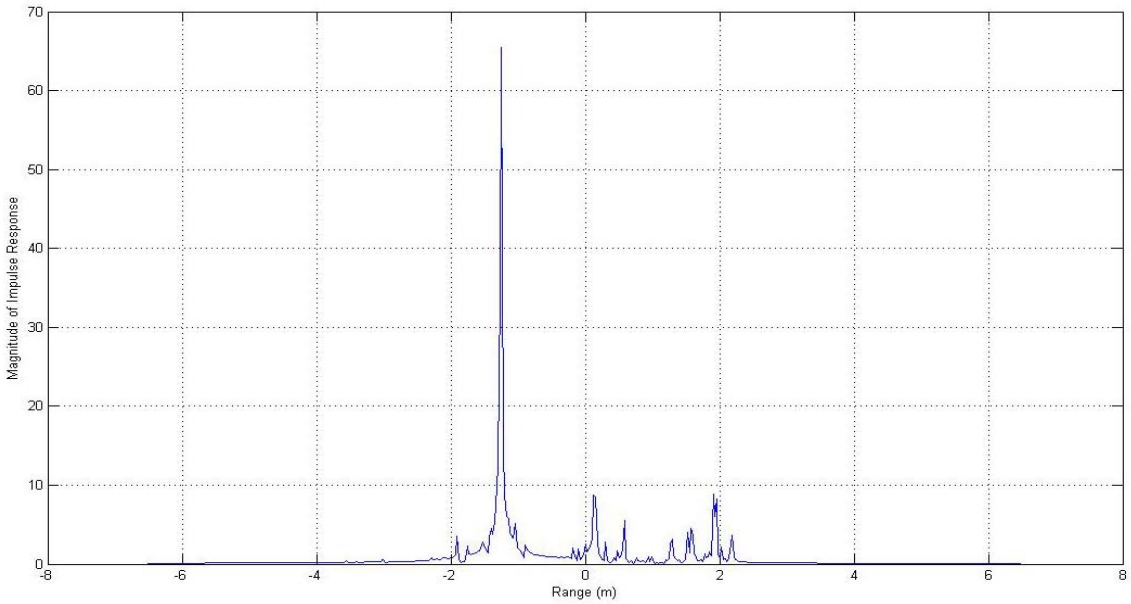

Figure 23 Radial Range Profile of Backhoe Loader at Aspect Angles of $\theta_{azimuth}$=0° and $\varphi_{elevation}$=0° with HV Polarization

b. 3-D Bi-Range Profile ($\theta_{azimuth}$=0°, $\varphi_{elevation}$=0°)

The corresponding 3-D bi-range profiles of the backhoe loader with VV, HH and HV polarizations are shown in Figure 23, 24 and 25 respectively.

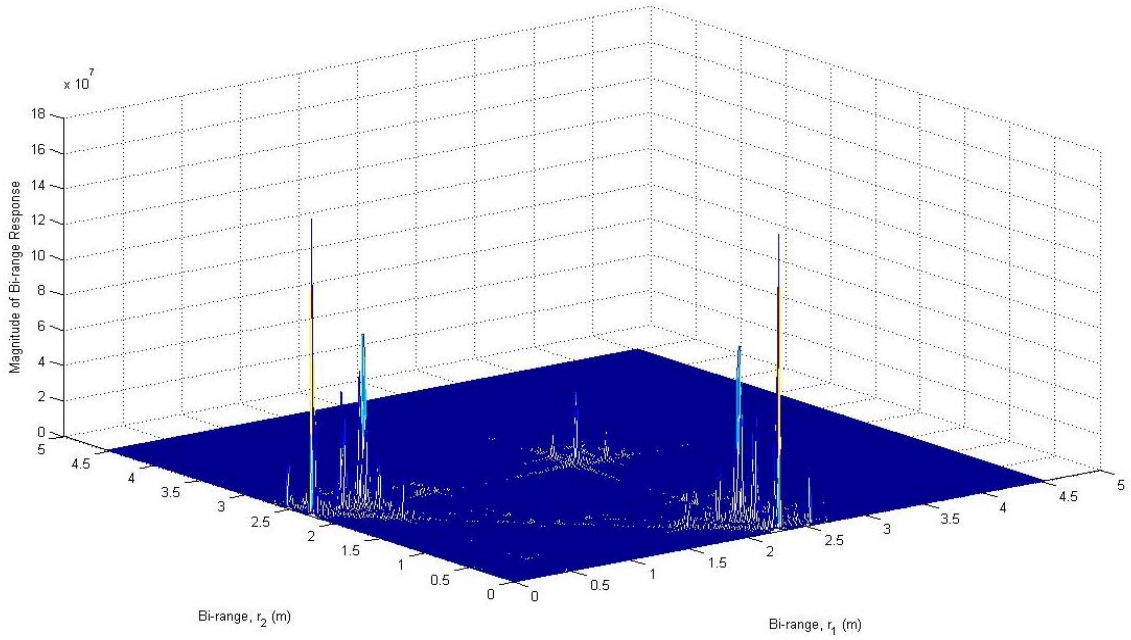

Figure 24 3-D Bi-Range Profile of Backhoe Loader at Aspect Angles of $\theta_{azimuth}$=0° and $\varphi_{elevation}$=0° with VV Polarization

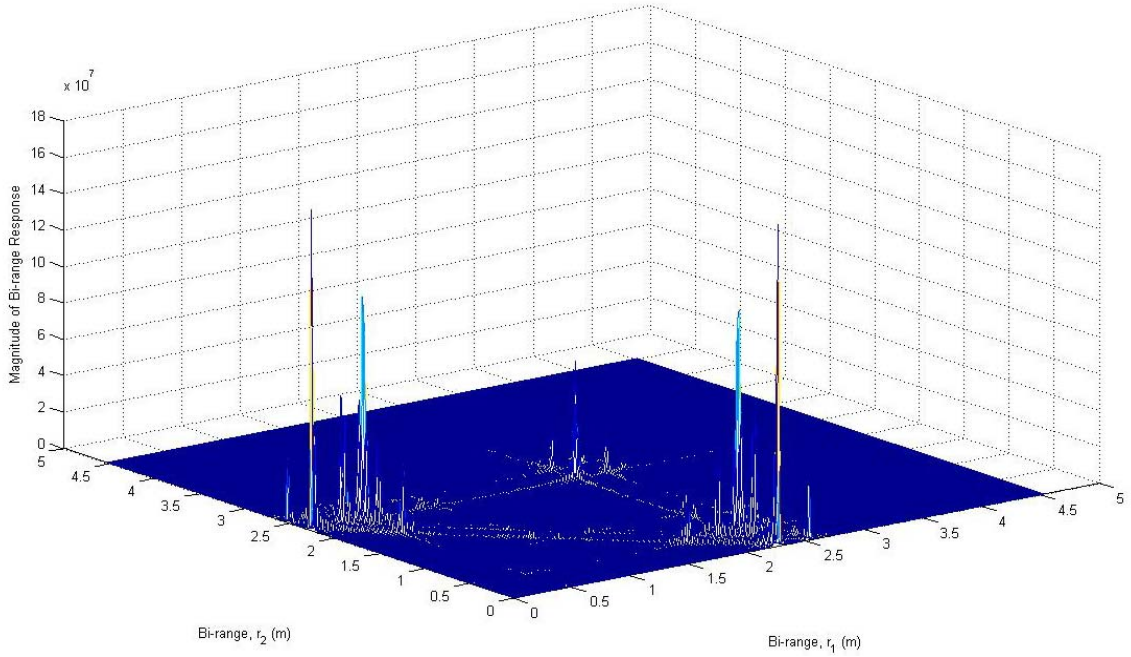

Figure 25 3-D Bi-Range Profile of Backhoe Loader at Aspect Angles of $\theta_{azimuth}$=0° and $\varphi_{elevation}$=0° with HH Polarization

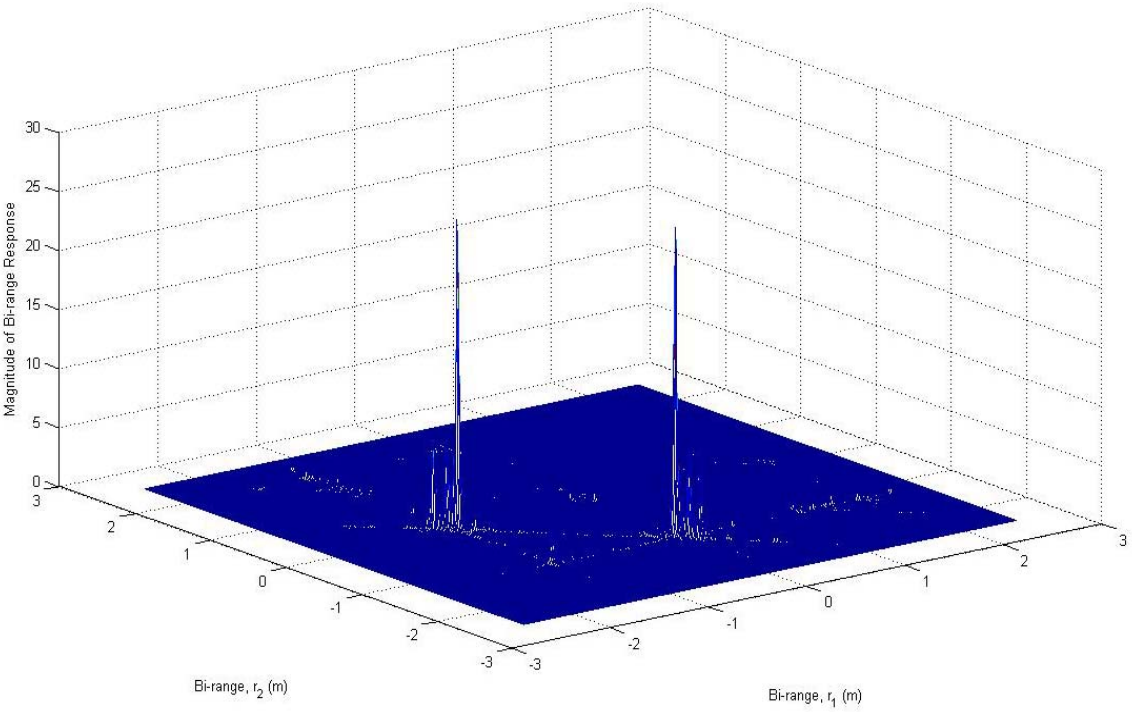

Figure 26 3-D Bi-Range Profile of Backhoe Loader at Aspect Angles of $\theta_{azimuth}$=0° and $\varphi_{elevation}$=0° with HV Polarization

c. 2-D Characteristic Bi-Range Profile ($\theta_{azimuth}$=0°, $\varphi_{elevation}$=0°)

The resulting 2-D characteristic bi-range profiles of the backhoe loader with VV, HH and HV polarizations are shown in Figure 25, 26 and 27 respectively.

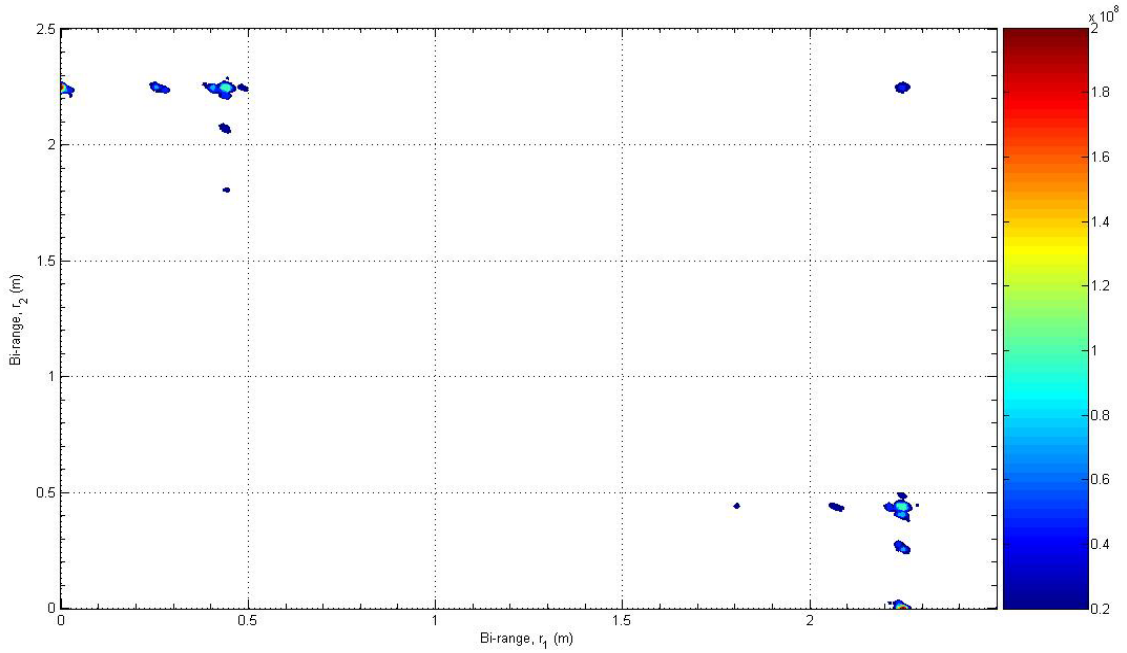

Figure 27 2-D Characteristic Bi-Range Profile of Backhoe Loader at Aspect Angles of $\theta_{azimuth}$=0° and $\varphi_{elevation}$=0° with VV Polarization

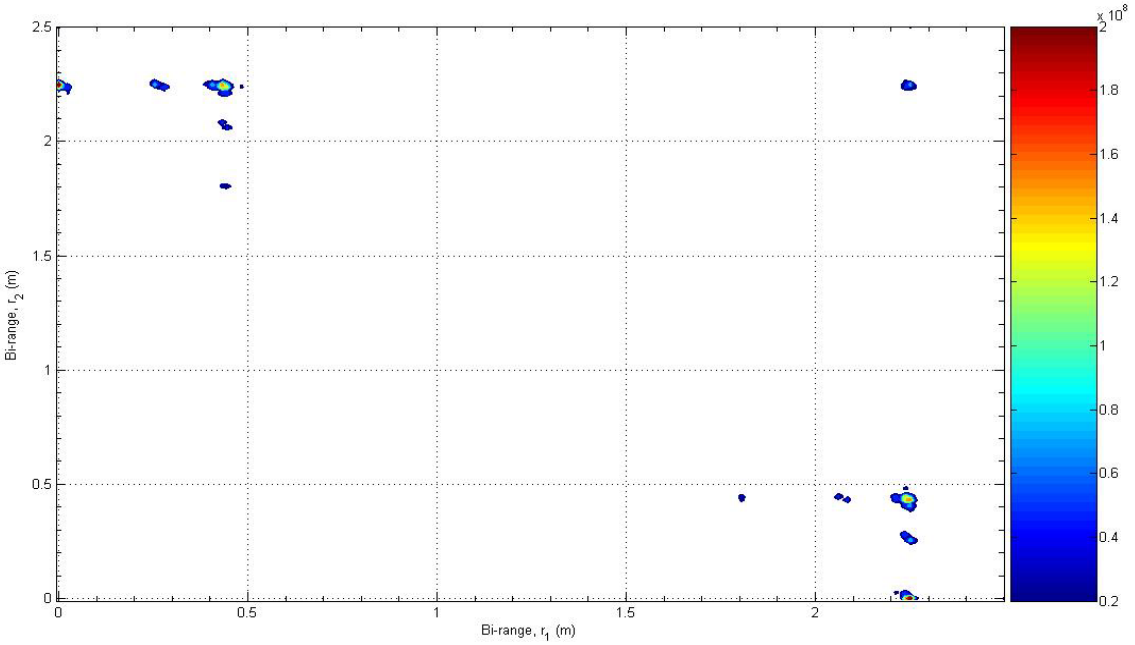

Figure 28 2-D Characteristic Bi-Range Profile of Backhoe Loader at Aspect Angles of $\theta_{azimuth}$=0° and $\varphi_{elevation}$=0° with HH Polarization

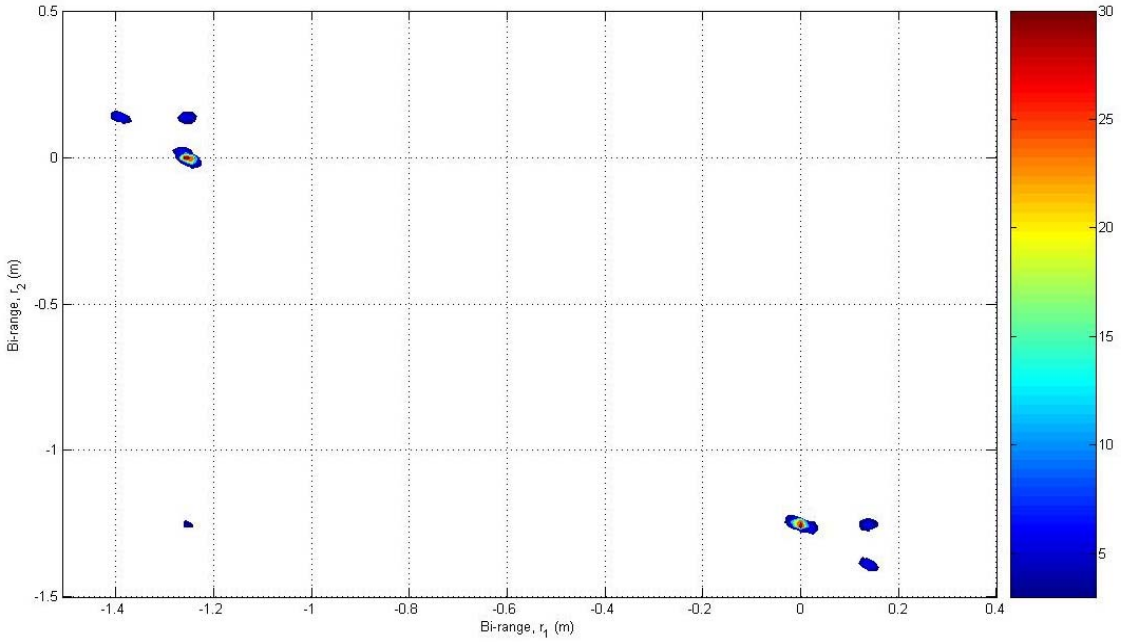

Figure 29 2-D Characteristic Bi-Range Profile of Backhoe Loader at Aspect Angles of $\theta_{azimuth}$=0° and $\varphi_{elevation}$=0° with HV Polarization

3. Test Case 2: Setup and Results ($\theta_{azimuth}$=90°, $\varphi_{elevation}$=0°)

In Test Case 2, the backhoe loader is orientated at 90 degree azimuth and 0 degree elevation with reference to the radar direction as depicted in Figure 30:

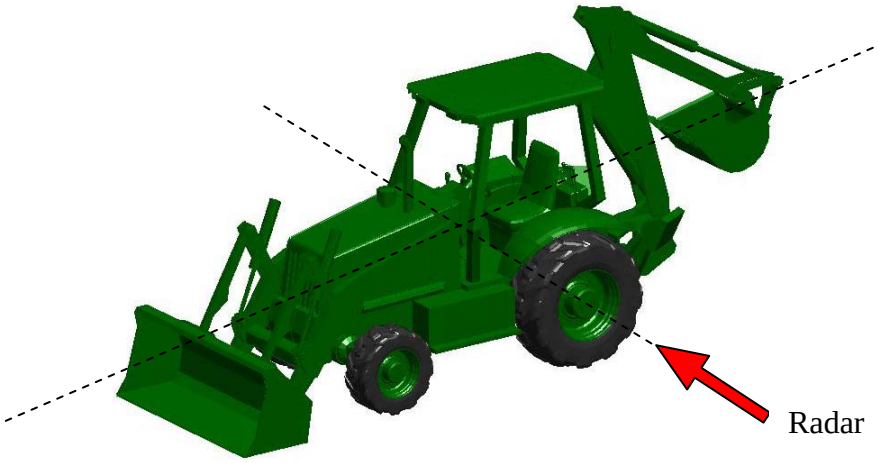

Figure 30 Orientation of CAD-Modeled Backhoe Loader at Aspect Viewing Angles of Azimuth, ($\theta_{azimuth}$)=90° and Elevation, ($\varphi_{elevation}$)=0°

The radial range profiles of the backhoe loader are computed using MATLAB's Fast Fourier Transform of the associated radar backscattered signals, while the 3-D and 2 -D bi-range profiles are computed using MATLAB's two-dimensional (2-D) discrete Fourier Transform of the third-order cumulant function of the radar backscatter signals.

Both radial range and bi-range profiles are processed over a frequency bandwidth of 5.9058 GHz (from 7.0472 to 12.953 GHz) with VV, HH and HV polarizations for the target's aspect viewing angle of azimuth, ($\theta_{azimuth}$) = 90° and elevation, ($\varphi_{elevation}$) = 0°. The related MATLAB program, "test_case2.m" and source code used to generate this plot can be found in Appendix D.

a. Radial Range Profile ($\theta_{azimuth}$=90°, $\varphi_{elevation}$=0°)

The radial range profiles of the backhoe loader with VV, HH and HV polarizations are illustrated in Figure 31, 32 and 33 respectively.

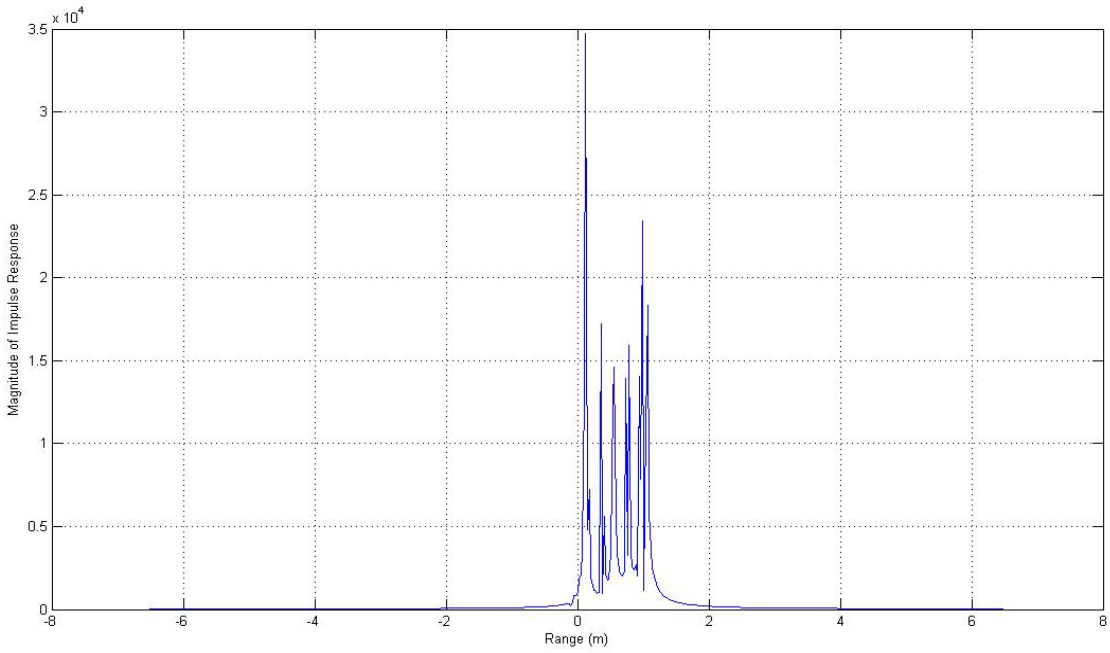

Figure 31 Radial Range Profile of Backhoe Loader at Aspect Angles of $\theta_{azimuth}$=90° and $\varphi_{elevation}$=0° with VV Polarization

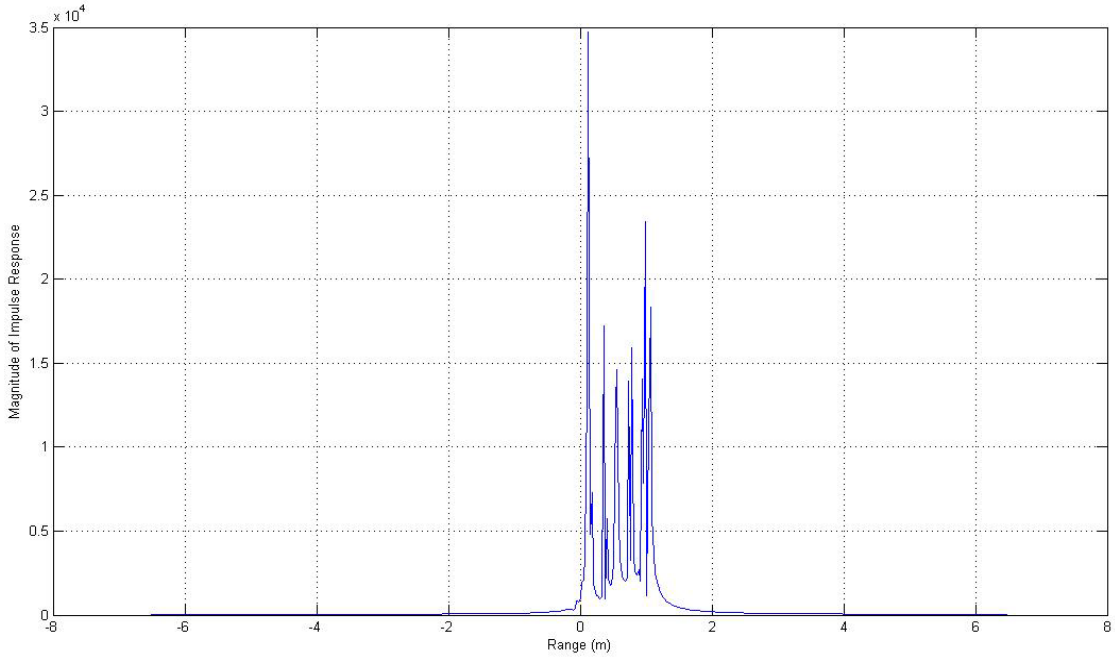

Figure 32 Radial Range Profile of Backhoe Loader at Aspect Angles of $\theta_{azimuth}$=90° and $\varphi_{elevation}$=0° with HH Polarization

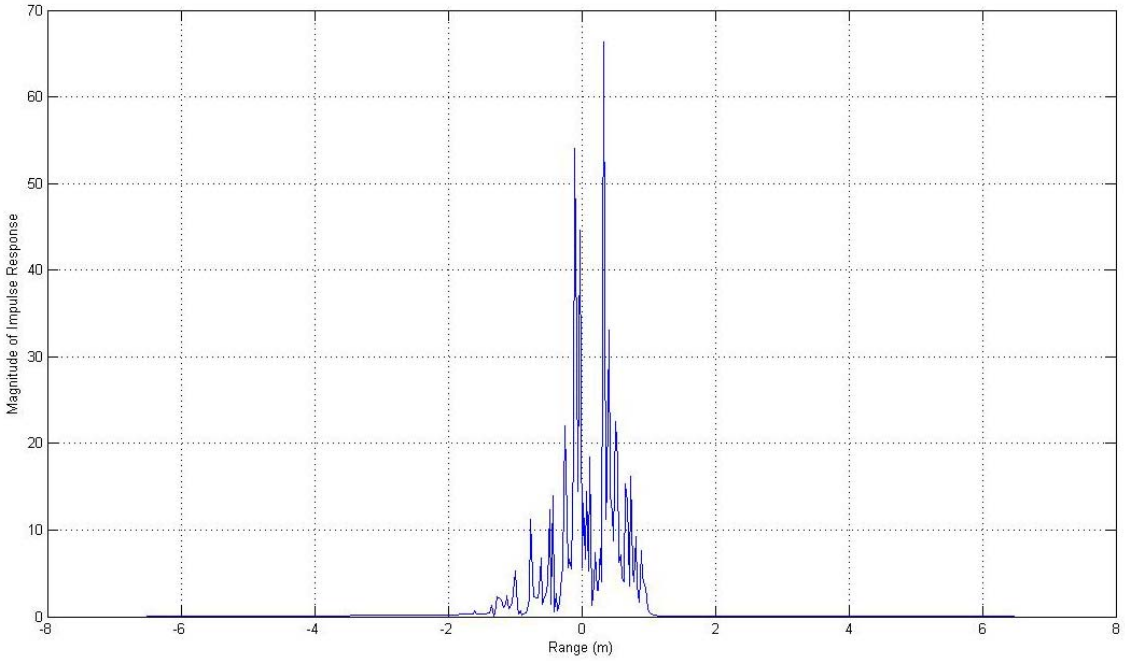

Figure 33 Radial Range Profile of Backhoe Loader at Aspect Angles of $\theta_{azimuth}$=90° and $\varphi_{elevation}$=0° with HV Polarization

b. 3-D Bi-Range Profile ($\theta_{azimuth}$=90°, $\varphi_{elevation}$=0°)

The corresponding 3-D bi-range profiles of the backhoe loader with VV, HH and HV polarizations are shown in Figure 34, 35 and 36 respectively.

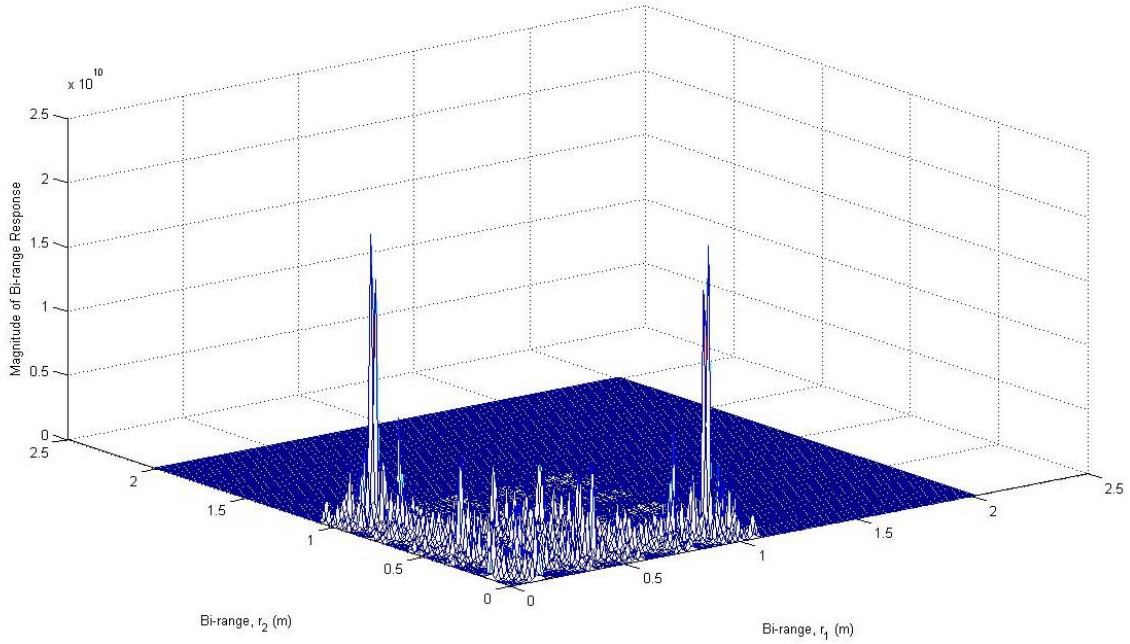

Figure 34 3-D Bi-Range Profile of Backhoe Loader at Aspect Angles of $\theta_{azimuth}$=90° and $\varphi_{elevation}$=0° with VV Polarization

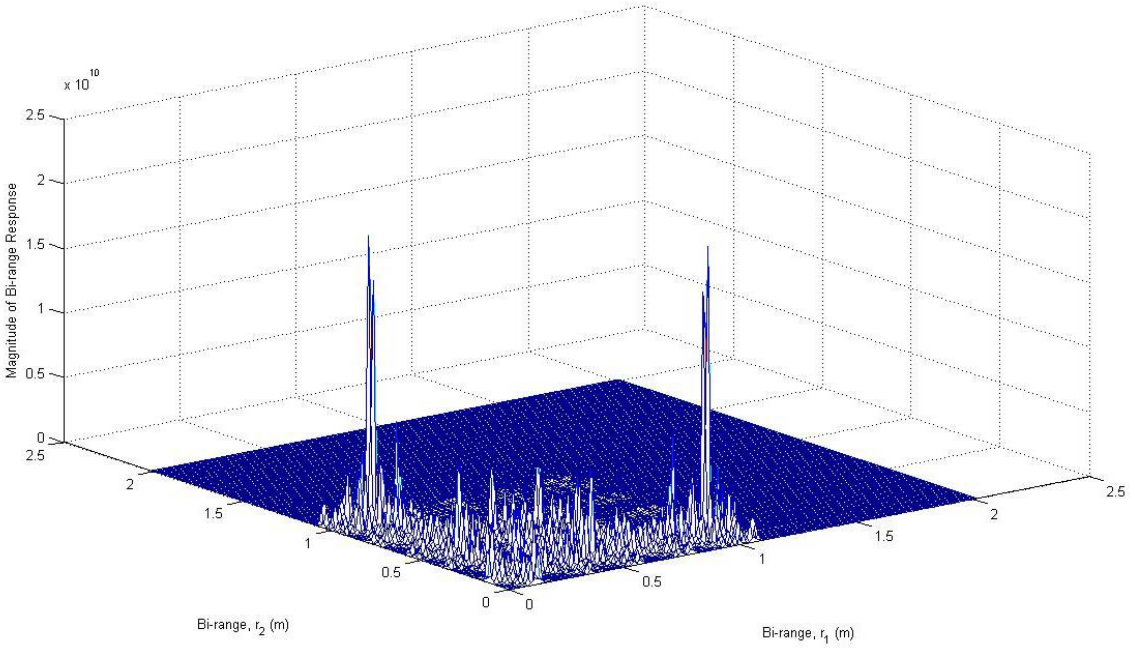

Figure 35 3-D Bi-Range Profile of Backhoe Loader at Aspect Angles of $\theta_{azimuth}$=90° and $\varphi_{elevation}$=0° with HH Polarization

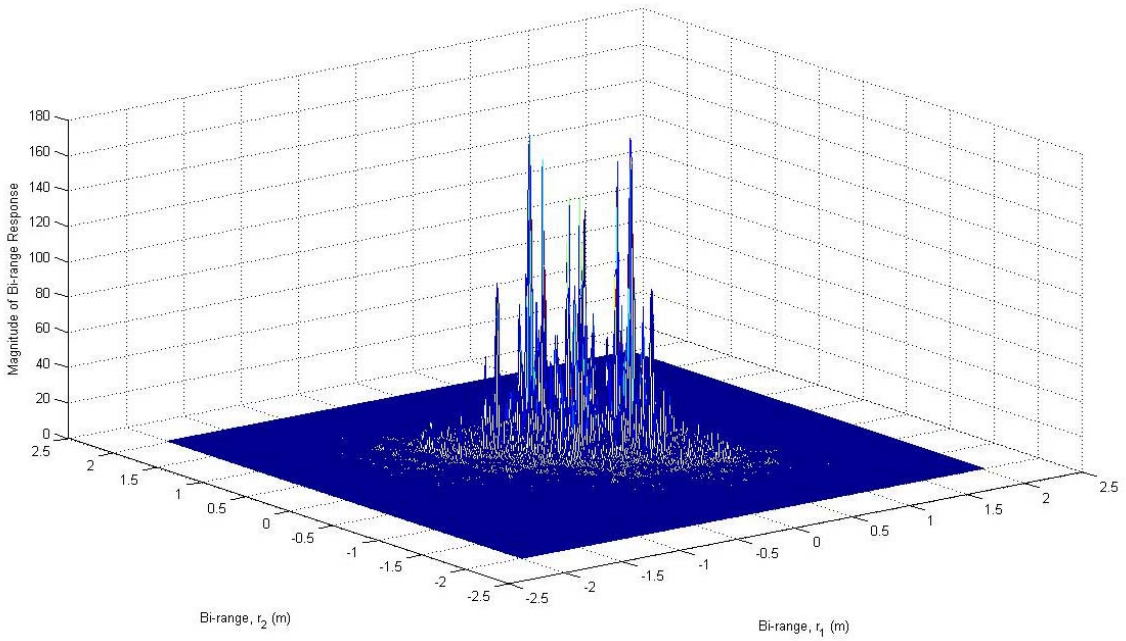

Figure 36 3-D Bi-Range Profile of Backhoe Loader at Aspect Angles of $\theta_{azimuth}$=90° and $\varphi_{elevation}$=0° with HV Polarization

c. 2-D Characteristic Bi-Range Profile ($\theta_{azimuth}$=90°, $\varphi_{elevation}$=0°)

The resulting 2-D characteristic bi-range profiles of the backhoe loader with VV, HH and HV polarizations are shown in Figure 37, 38 and 39 respectively.

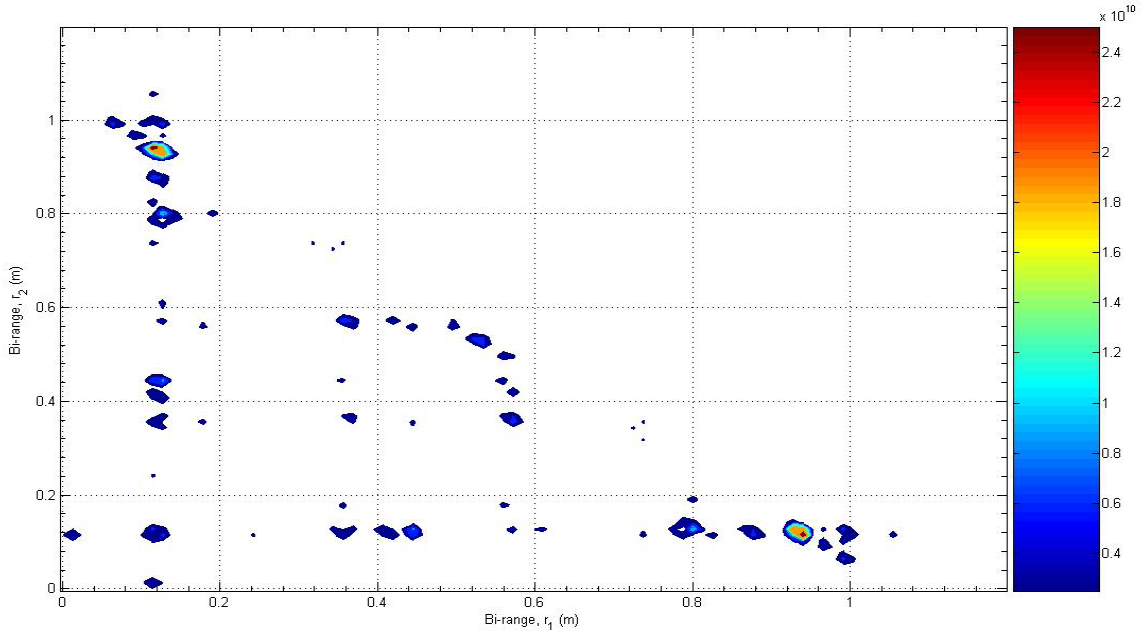

Figure 37 2-D Characteristic Bi-Range Profile of Backhoe Loader at Aspect Angles of $\theta_{azimuth}$=90° and $\varphi_{elevation}$=0° with VV Polarization

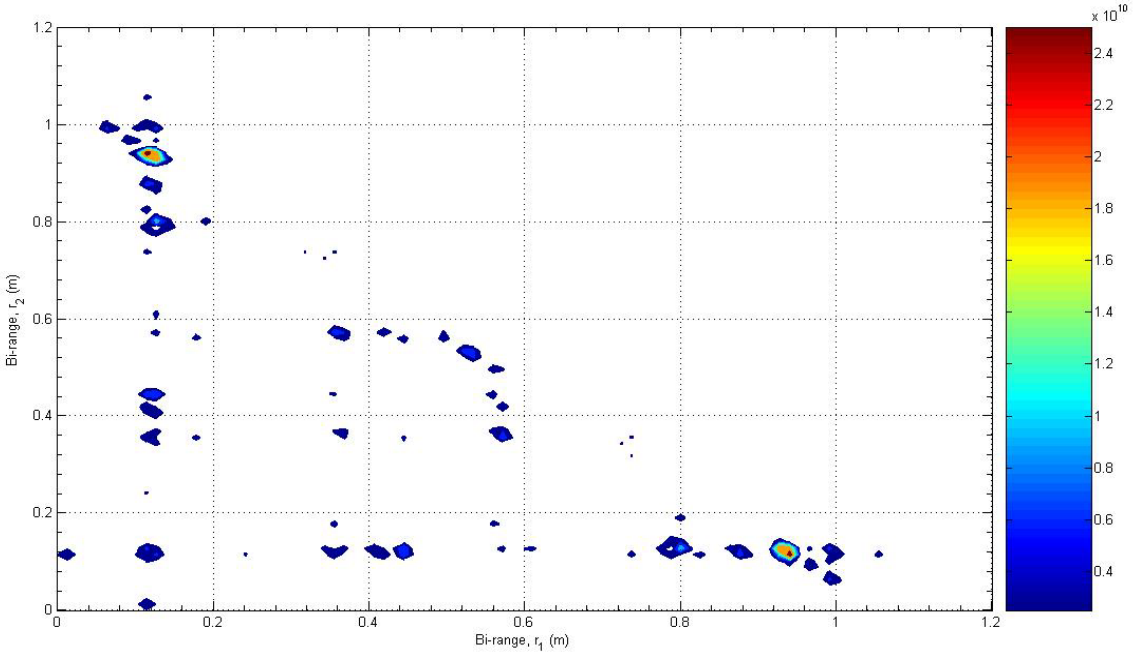

Figure 38 2-D Characteristic Bi-Range Profile of Backhoe Loader at Aspect Angles of $\theta_{azimuth}$=90° and $\varphi_{elevation}$=0° with HH Polarization

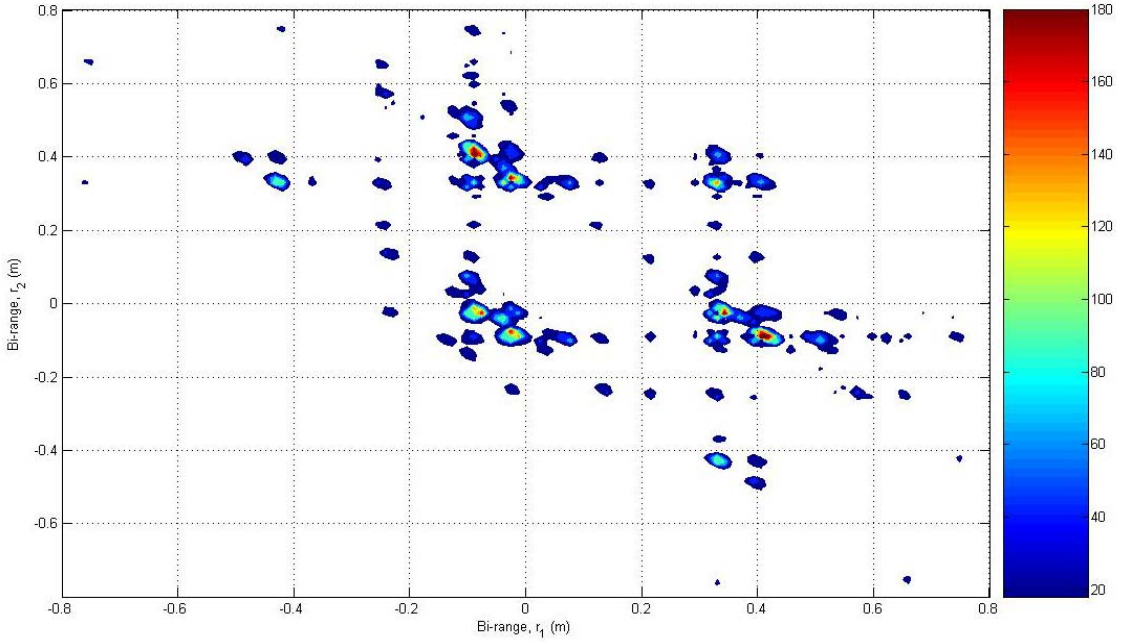

Figure 39 2-D Characteristic Bi-Range Profile of Backhoe Loader at Aspect Angles of $\theta_{azimuth}$=90° and $\varphi_{elevation}$=0° with HV Polarization

4. Test Case 3: Setup and Results ($\theta_{azimuth}$=60°, $\varphi_{elevation}$=30°)

In Test Case 3, the backhoe loader is orientated at 60 degree azimuth and 30 degree elevation with reference to the radar direction as depicted in Figure 40:

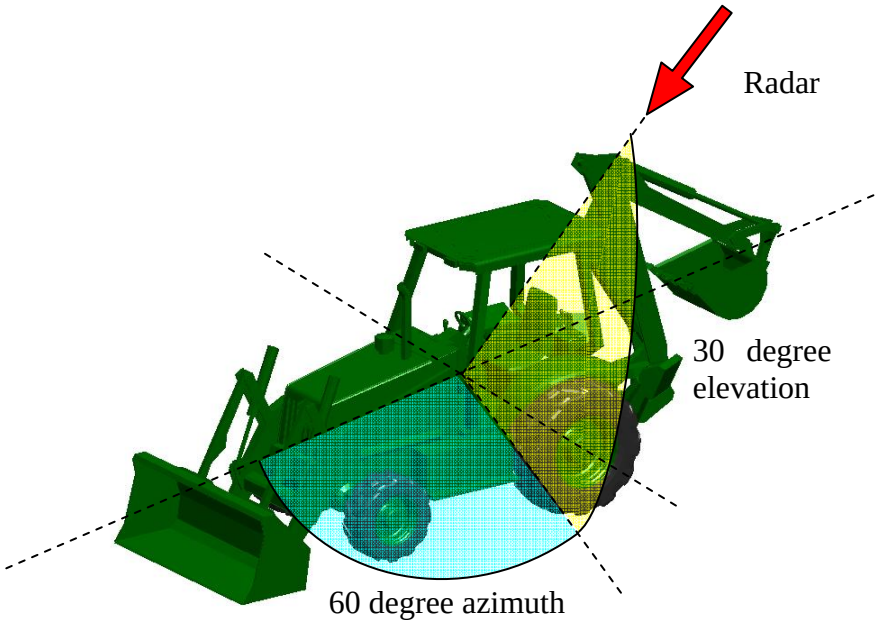

Figure 40 Orientation of CAD-Modeled Backhoe Loader at Aspect Viewing Angles of Azimuth, ($\theta_{azimuth}$)=60° and Elevation, ($\varphi_{elevation}$)=30°

The radial range profiles of the backhoe loader are computed using MATLAB's Fast Fourier Transform of the associated radar backscattered signals, while the 3-D and 2 -D bi-range profiles are computed using MATLAB's two-dimensional (2-D) discrete Fourier Transform of the third-order cumulant function of the radar backscatter signals.

Both radial range and bi-range profiles are processed over a frequency bandwidth of 5.9058 GHz (from 7.0472 to 12.953 GHz) with VV, HH and HV polarizations for the target's aspect viewing angle of azimuth, ($\theta_{azimuth}$) = 60° and elevation, ($\varphi_{elevation}$) = 30°. The related MATLAB program, "test_case3.m" and source code used to generate this plot can be found in Appendix E.

a. Radial Range Profile ($\theta_{azimuth}$=60°, $\varphi_{elevation}$=30°)

The radial range profiles of the backhoe loader with VV, HH and HV polarizations are illustrated in Figure 41, 42 and 43 respectively.

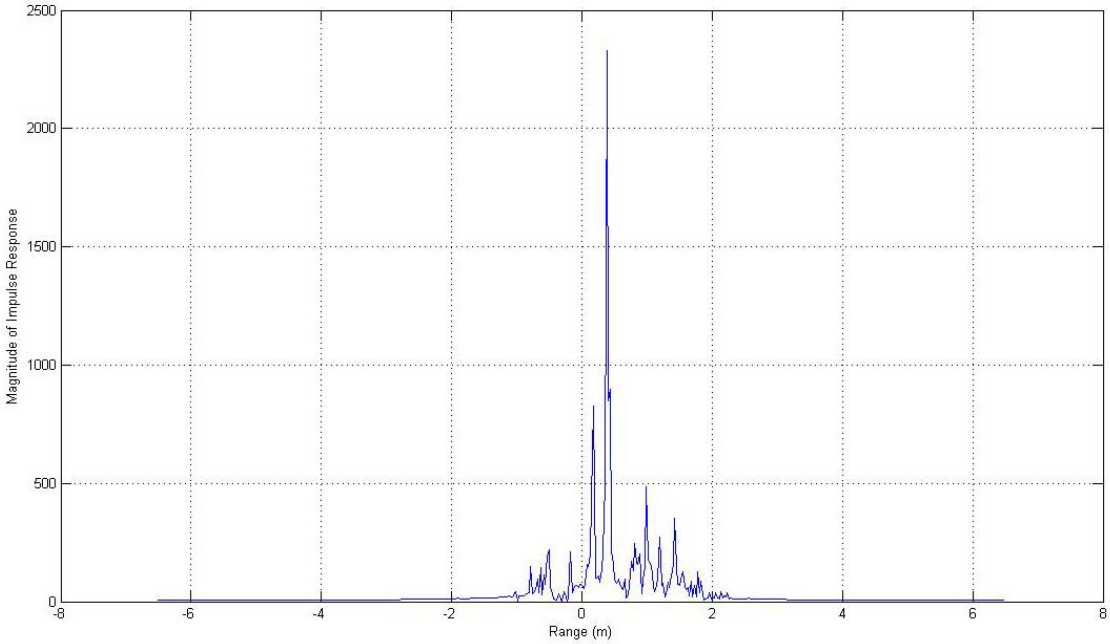

Figure 41 Radial Range Profile of Backhoe Loader at Aspect Angles of $\theta_{azimuth}$=60° and $\varphi_{elevation}$=30° with VV Polarization

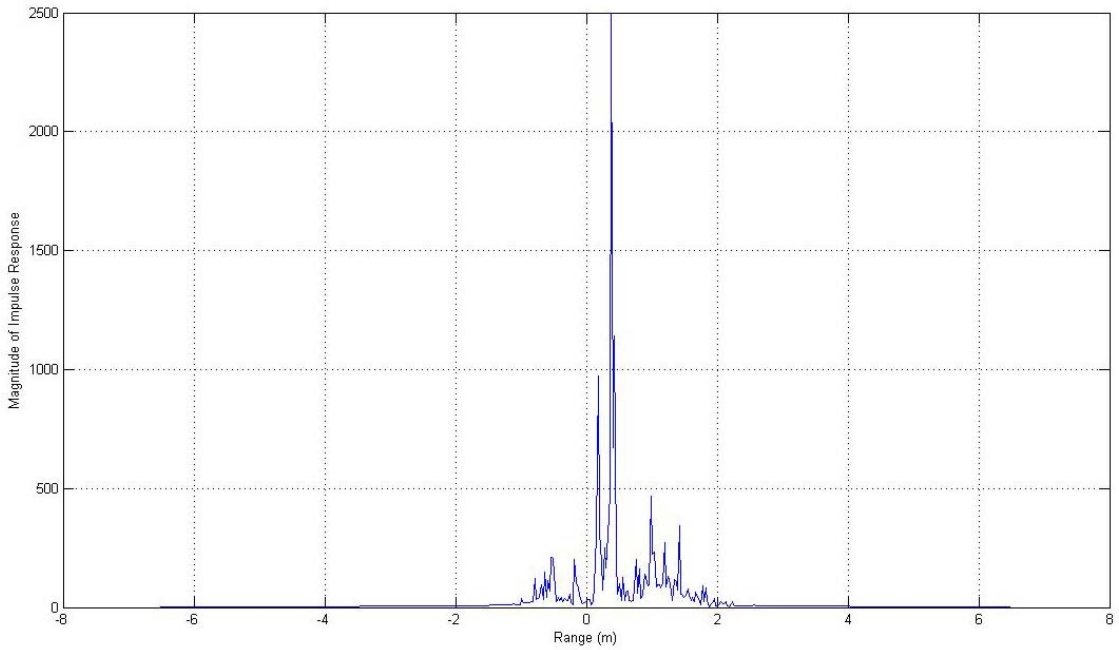

Figure 42 Radial Range Profile of Backhoe Loader at Aspect Angles of $\theta_{azimuth}$=60° and $\varphi_{elevation}$=30° with HH Polarization

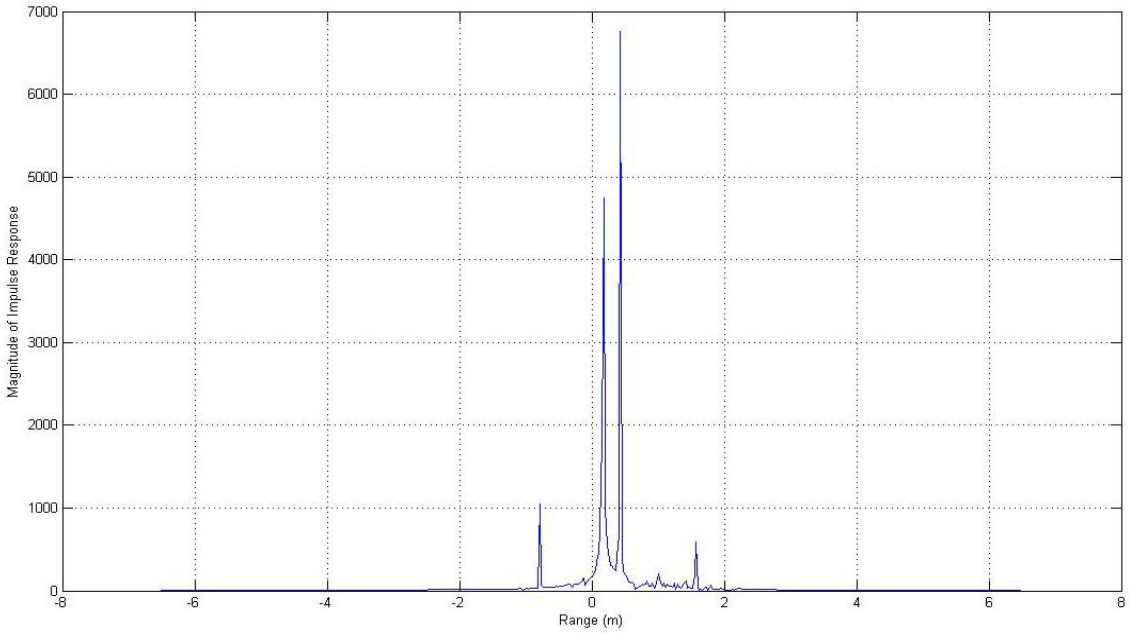

Figure 43 Radial Range Profile of Backhoe Loader at Aspect Angles of $\theta_{azimuth}$=60° and $\varphi_{elevation}$=30° with HV Polarization

b. 3-D Bi-Range Profile ($\theta_{azimuth}$=60°, $\varphi_{elevation}$=30°)

The corresponding 3-D bi-range profiles of the backhoe loader with VV, HH and HV polarizations are shown in Figure 44, 45 and 46 respectively.

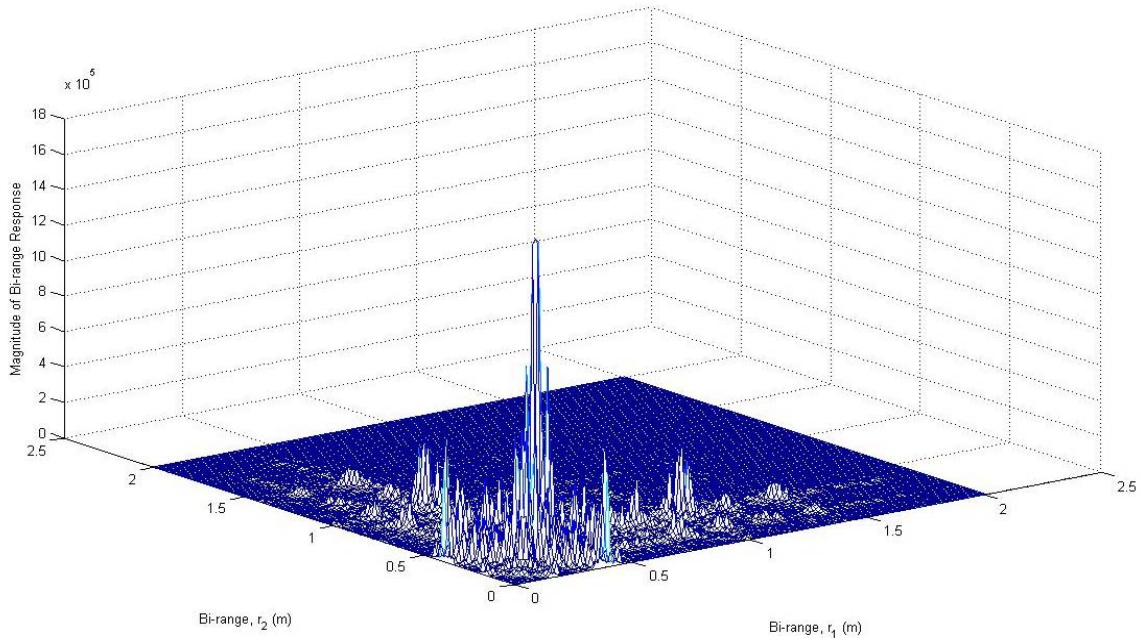

Figure 44 3-D Bi-Range Profile of Backhoe Loader at Aspect Angles of $\theta_{azimuth}$=60° and $\varphi_{elevation}$=30° with VV Polarization

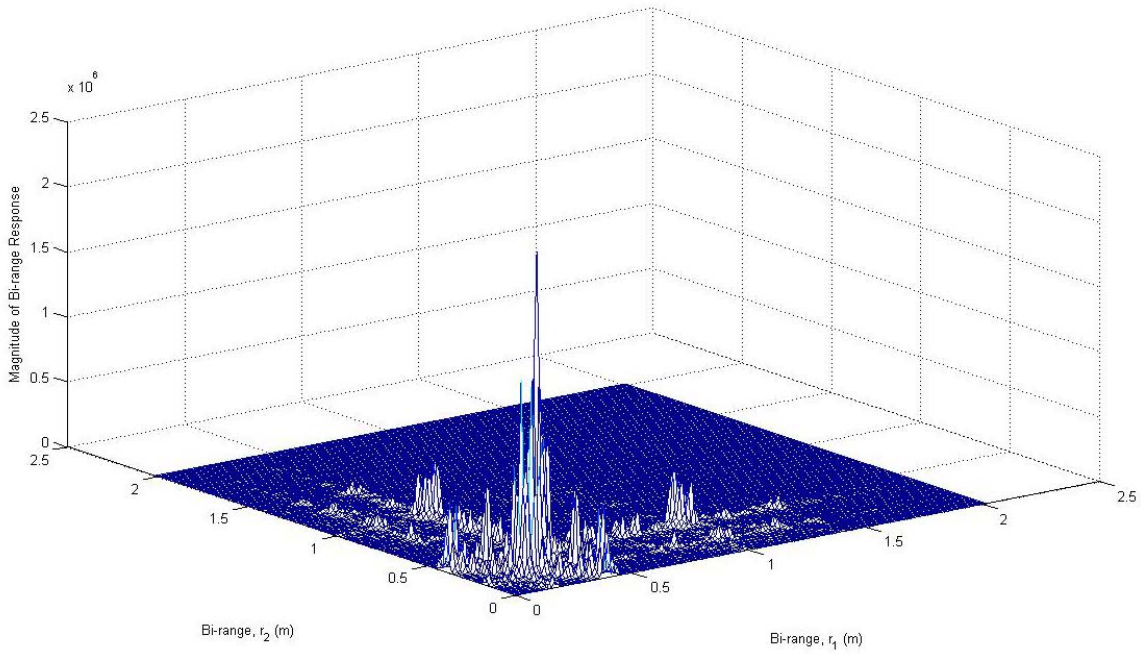

Figure 45 3-D Bi-Range Profile of Backhoe Loader at Aspect Angles of $\theta_{azimuth}$=60° and $\varphi_{elevation}$=30° with HH Polarization

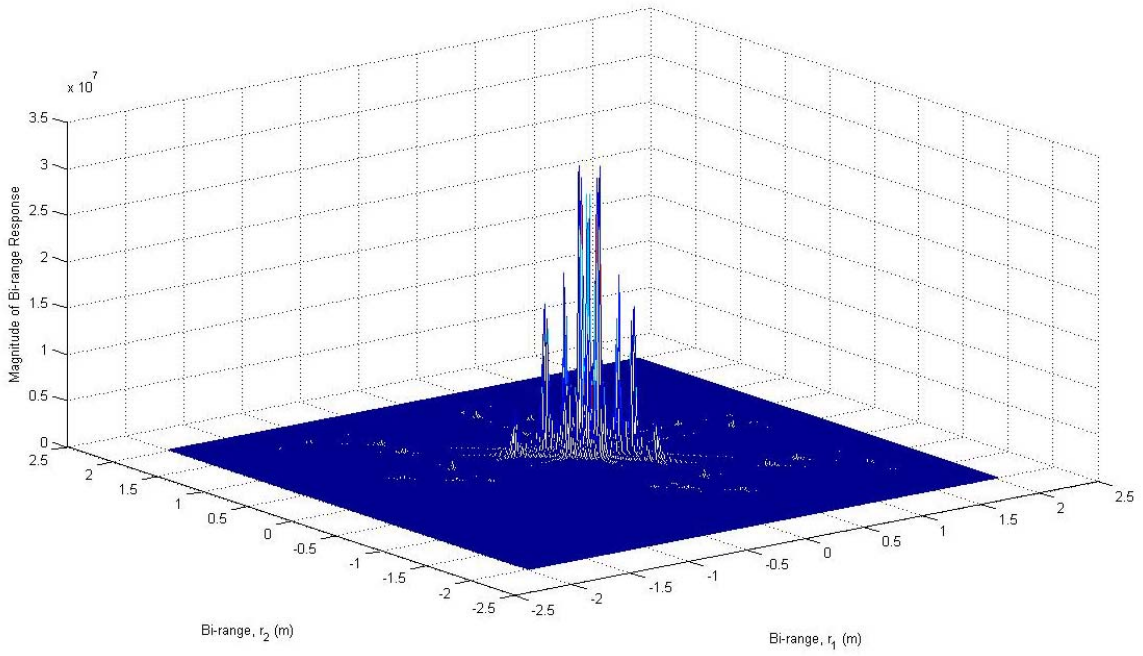

Figure 46 3-D Bi-Range Profile of Backhoe Loader at Aspect Angles of $\theta_{azimuth}$=60° and $\varphi_{elevation}$=30° with HV Polarization

c. 2-D Characteristic Bi-Range Profile ($\theta_{azimuth}$=90°, $\varphi_{elevation}$=0°)

The resulting 2-D characteristic bi-range profiles of the backhoe loader with VV, HH and HV polarizations are shown in Figure 47, 48 and 49 respectively.

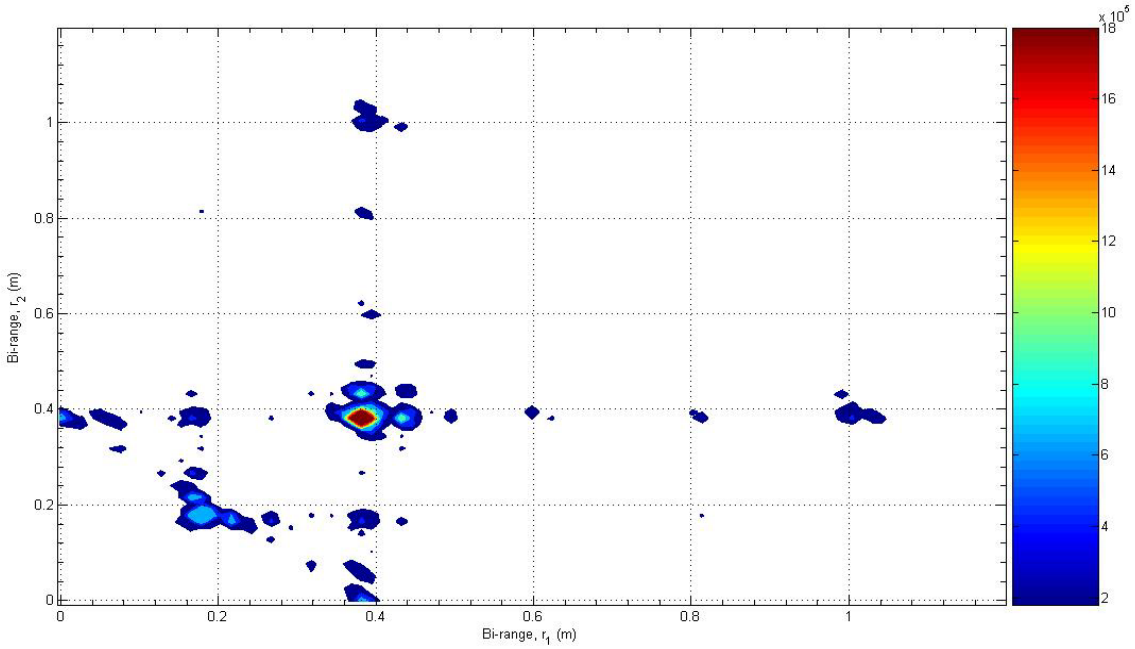

Figure 47 2-D Characteristic Bi-Range Profile of Backhoe Loader at Aspect Angles of $\theta_{azimuth}$=60° and $\varphi_{elevation}$=30° with VV Polarization

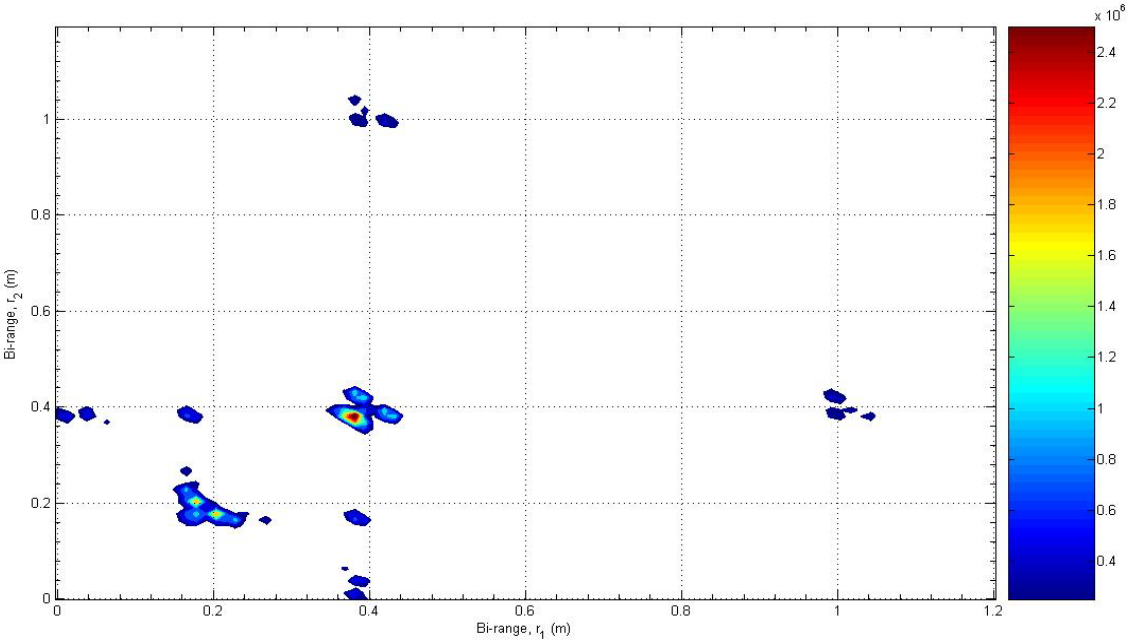

Figure 48 2-D Characteristic Bi-Range Profile of Backhoe Loader at Aspect Angles of $\theta_{azimuth}$=60° and $\varphi_{elevation}$=30° with HH Polarization

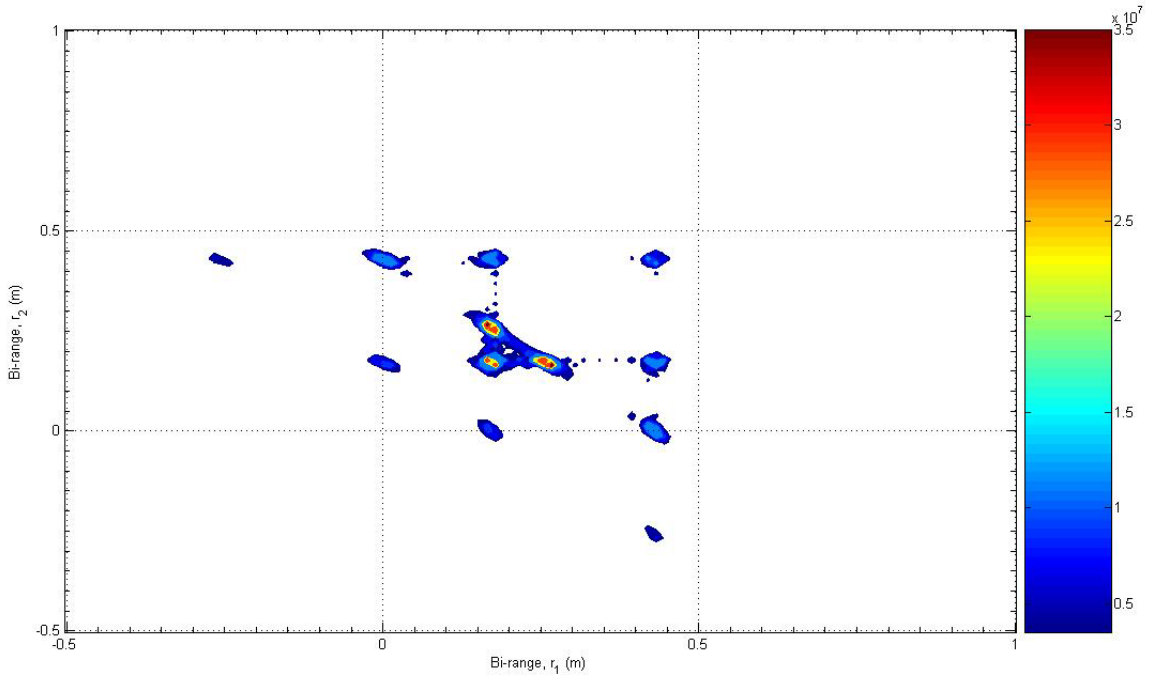

Figure 49 2-D Characteristic Bi-Range Profile of Backhoe Loader at Aspect Angles of $\theta_{azimuth}$=60° and $\varphi_{elevation}$=30° with HV Polarization

B. ANALYSIS OF "BACKHOE DATA DOME" EXPERIMENTATION

In studying and comparing the various radial range and bi-range profiles computed using the "backhoe data dome" experimentation for Test Cases 1, 2 and 3, observations and analysis relating to the uses of radial range profiles, polarization effects and bi-range profiles for target recognition can be rationalized and are discussed in the following sections.

1. Radial Range Profiles

The magnitude of the impulse response versus the range plots of the experimentation results provide a good representation of the one-dimensional radial profile of the backhoe loader from different aspect angles. It can be observed that locations of the peak responses appear to coincide and correspond to the relative positions of dominant individual scattering centers or subcomponents, such as the operator cab, engine compartment, and loader bucket, etc., that present a large RCS and consequently a strong backscattered signal to the radar system as illustrated in Figure 50.

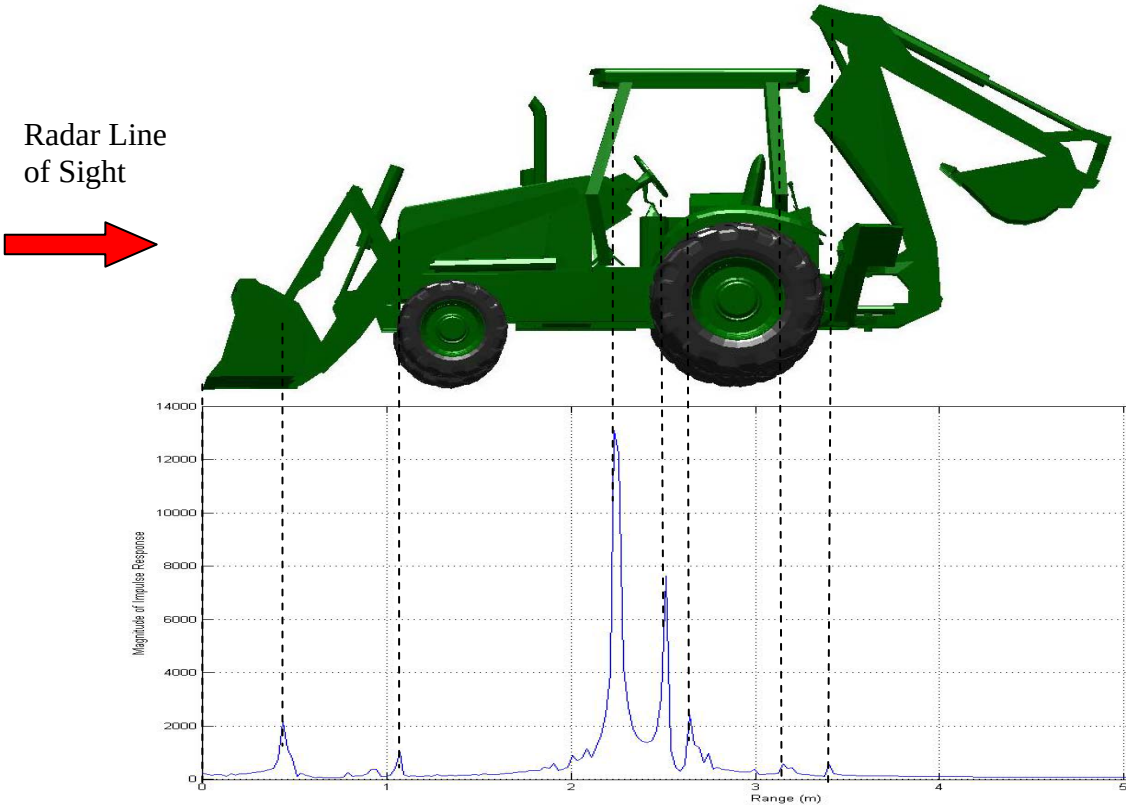

Figure 50 Comparison of Radar Range Profile with Actual Backhoe Loader

While it may seem that the radial range profile can possibly provide a measure of the length dimension of a target of interest along its line-of-sight from the radar system, this inference is usually erroneous and not equivalent to the actual physical target's length due to two effects, as mentioned in Tait (2005). Instead of directly reflecting the radar signal back toward the radar system, multiple scatterers comprising the target and their interactions can result in indirect reflection and delay the round-trip propagation time, which then produces a radial range profile that is longer than the target. Conversely, the other effect results in a shorter radial range profile compared to the actual physical target's length. This disparity is due to the shadowing or masking of one part the target by another part. When a certain part of a target is masked at a particular aspect angle, the obscuration reduces the electromagnetic energy that scattered off of it, and significantly reduces its contribution to the radial range profile.

For example, as also observed in Figure 50, the dipperstick of the backhoe loader is obscured by the engine compartment and operator cab, which then reduces its corresponding response in the radial range profile and results in an apparently shorter backhoe loader.

2. Polarization Effects

The polarization of a radar signal is defined as the direction of the electric E-field as the electromagnetic wave propagates. When a target of interest is illuminated by a linearly polarized signal, two echo signals are reflected back to the radar system; one with the same polarization as the transmitted signal (co-polarized signal) and the other with an orthogonal polarization (cross-polarized signal). The basis of using polarization effects for target recognition is to extract the differences in the radar backscattered signals from a target that is illuminated with different polarization. Although this method seems to be promising for discriminating simple geometrically shaped targets, such as spheres, corner reflectors and straight lengths of wire, etc, it is not as forthcoming for practical complex targets, such as aircraft and vehicles.

For example, it is noted that the 3-D and 2-D bi-range profiles of the backhoe loader for the different test cases are not affected by the polarization of the radar signal as shown by the similarities between the different plots with VV and HH polarizations.

This is probably due to the multiple scatterers or subcomponents interaction within the radar resolution cell that collectively resulted in a composite radar backscattered signal with a different and independent polarization as the transmitted signal. In addition, it is also observed from the 3-D and 2-D bi-range profiles with HV polarization that the peak responses from multiple scatterers' interactions seems to be accentuated by the cross polarization effect.

3. Characteristic Bi-Range Profile

Most importantly, it is obvious from the experimentation results of the different test cases that there exists significant peak responses in the 3-D and 2-D bi-range profiles, implying strong additive multiple interactions between the scatterers or subcomponents

of the backhoe loader, that are characteristic of their bi-range shapes and locations. The positions of the multiple scattering interaction terms, relative to the direct specular scattering terms, correspond directly to the physical separation distances between the major individual scatterers of the backhoe loader.

Therefore, these characteristic bi-range profiles can be drawn on, to highlight and map the unique multiple scattering interaction features and natures of the target which may then be used to compare and match against a reference database that contains bi-range signatures of different target types of potential interest and at all aspect angles of interest for target recognition and identification.

VI. CONCLUSIONS AND RECOMMENDATIONS

> Among the detection systems under development in the DD(X) program is the Multi-Function Radar (MFR). The future MFR will provide Non-Cooperative Target Recognition (NCTR) and Kill Assessment.
>
> — Rear Admiral Philip Balisle, U.S. Navy (2002)

A. SUMMING UP OF THESIS RESEARCH

Radar-based NCTR will be a key capability and cardinal requirement in future radar systems equipped onboard all high-valued military combat platforms and assets, such as fighter aircraft and destroyers, etc. While there are many conventional techniques for the incorporation of NCTR into the next-generation radar systems, this thesis endeavors to expand on the knowledge and utility of the bi-spectral method for effective and robust target recognition and identification.

The first objective of this thesis was to study and mathematically model the direct and indirect multiple interactions of scattering mechanisms of radar backscattered signal. The fundamentals of radar basic operation, electromagnetic wave propagation and scattering mechanisms of electromagnetic waves, when a radar signal intersects any target in its propagation path, were first reviewed. This then provided an insight into the relationships between the target's radar signature and its physical size, geometry, shape, orientation and material composition, which were the basis in formulating the mathematical model of the radar backscattered signal.

A mathematical model which represents the direct specular and indirect multiple scattering interactions of the backscattered radar signal was developed and subsequently verified using an example of a simple three-point scatterers target and the MATLAB program "backscatter_signal.m" to plot the radial range profile.

The second objective of this thesis was to develop a radar NCTR technique of using the bi-spectral signatures of backscattered radar signals for characterization of a target's multiple interactions features. The definitions and mathematical derivations of the bi-spectrum, bi-time and bi-range of the radar backscattered signal were introduced,

together with the concept of using the bi-spectral signatures, also known as the characteristic bi-range profiles of backscattered radar signal as a complementary add-on to augment the radial range profile for target recognition and identification.

The characteristic bi-range profile was then studied and verified through the same example of a simple 3-points scatterer target and the MATLAB program, "bispectral.m" was developed to compute and plot the bi-range profiles of the third-order cumulant or triple correlation of the frequency-domain radar backscattered signal.

To further investigate the potential of using bi-spectra technique for radar target recognition, experimentation based on the AFRL, "Backhoe Data Dome" was conducted. The results and findings for three different test cases were analyzed and found to be promising.

B. RECOMMENDATIONS FOR FUTURE WORK

The novel idea of using the bi-spectral method for radar target recognition, based on the characterization of a target's multiple scatterer interactions term, is a relatively recent development, considering that the concept was initially conceived and proposed as a basis of recognition by Jounty & Walton (1990) during the early nineties. As such, many aspects of this proposed bi-spectal NCTR technique can be further researched, developed and verified. The following sections recommend two areas for which future research and investigation can be considered.

1. Experimentation Based on Actual Radar Signature Measurements of Real Complex Target

For the current thesis, due to the restricted access to classified information, the experimentation to examine the potential of using the characteristic bi-range profile for target recognition and identification is based on the AFRL's public release of the "Backhoe Data Dome, Version 1.0," which consists of simulated wideband (7-13 GHz), full polarization, complex backscatter data from a backhoe loader generated through the use of a CAD model in free space (Lin & Naidu, 2004). While this set of data facilitated the verification of the concept of using a bi-spectral method for target recognition, the

experimentation lacks fidelity in the consideration of the radar bi-spectral signatures and scattering mechanisms from a real complex target in an environment surrounded with clutter and noise.

Given proper security clearance, more comprehensive experimentation, based on classified data sets of actual radar backscattered signal measurements from real complex targets can be examined and analyzed in future research to better understand the robustness of the bi-spectral method and its clutter and noise suppression performance.

2. Bi-spectral Waveform Design

Another area of research interest that can be further investigated and verified for future work is the topic of bi-spectral waveform design. The design of the radar waveform is crucial in the measurement of the radar backscattered signals required to generate the bi-spectral profile. In order to generate bi-range profiles, which are compatible with the reference signature database of different target types of potential interest for target recognition, the radar waveform needs to provide high range resolution measurements and extract discriminating multiple scatterers interaction features of the target.

While the experimentation results from the current thesis seem to suggest that the use of a cross polarized signal can possibly accentuate the peak bi-range profile responses from multiple scatterers' interactions, more in-depth investigation and studies have to be performed in order to understand and validate the polarization characteristics of the multiple scatterers' interactions terms. Apart from the polarization of the radar signal, other radar waveform design parameters like the transmitted frequency, pulse width, pulse repetition frequency, frequency bandwidth and modulation, etc., can also be examined in future research work in order to establish an optimal bi-spectral waveform.

THIS PAGE INTENTIONALLY LEFT BLANK

APPENDIX MATLAB SOURCE CODES

A. SOURCE CODE FOR RADAR BACKSCATTERED SIGNAL

```
%-----------------------------------------------------------------------------------------------------------------------
%       backscatter_signal.m
%
%       This program computes the radar backscattered signal and
%       generates the radial range profile of n points scatterers
%
%       Written by Yeo, Jiunn Wah
%-----------------------------------------------------------------------------------------------------------------------
clear all
n = 3;                  %       Number of point scatter
f = 5:0.01:6;           %       Frequency band in GHz
A = [1 1 1];            %       Amplitude of the scattered signal
R = [0 1.5 3.6];        %       Range between the Radar and point scatter
s = 0;                  %       Initialization of counter
c = 3e8;                %       Speed of light

bandwidth = f(length(f))-f(1);

%       Direct specular scattering term
for count1=1:n
   s=s+A(count1).*exp(i.*2.*pi.*2*R(count1).*1e9.*f./c);%-rand*2*pi);
end

%       Indirect multiple scattering interaction term
for count2=1:n
   for count3=1:n
      if count3~=count2
      s=s+A(count2)*A(count3).*exp(i.*2.*pi.*2*(R(count2)+R(count3)).*1e9.*f./c);
      end
   end
end

%       Plotting of Radial Range Profile
z=fft(s)./length(s);
figure
plot(linspace(-length(z)/2,length(z)/2,length(z))*c/2/bandwidth/1e9, fftshift(abs(z)));
xlabel('Range (m)')
ylabel('Magnitude Impulse Response')
grid on
```

B. SOURCE CODE FOR GENERATING THE THIRD-ORDER CUMULANT AND BI-SPECTRAL PLOTS

```
%-----------------------------------------------------------------------------------------------------------------------
%       bispectral.m
%
%       This program generates the 3-D and 2-D bi-range profile of
%       a radar backscattered signal
%
%       Written by Yeo, Jiunn Wah
%-----------------------------------------------------------------------------------------------------------------------
clear all

%       Call program to compute the radar backscattered signal and
%       generates the radial range profile of n points scatterer
backscatter_signal;

%       Function to generate the third order cumulant of the radar backscattered signal
[cx] = cum3(s,(length(s)-1));

%       Perform Fourier Transform of the third order cumulant to generate the bispectrum
bisp = fftshift(fft2(ifftshift(cx)));

%       Setting the plot limits
x = linspace(-length(bisp)/4,length(bisp)/4,length(bisp))*c/2/bandwidth/1e9;
y = linspace(-length(bisp)/4,length(bisp)/4,length(bisp))*c/2/bandwidth/1e9;
ref = find(x==0);

%       Plotting of the 3-D bi-range profile
figure
mesh(x(ref:length(x)),y(ref:length(y)),abs(bisp(ref:length(bisp),(ref:length(bisp)))));
xlabel('Bi-range, r_1 (m)')
ylabel('Bi-range, r_2 (m)')
zlabel('Magnitude of Bi-range Response')

%       Plotting of the 2-D Characteristic bi-range profile
figure
contourf(x(ref:length(x)),y(ref:length(y)),abs(bisp(ref:length(bisp),(ref:length(bisp)))), [2e4 1.2e5 1.4e5
1.6e5 1.8e5 2e5]);
xlabel('Bi-range, r_1 (m)')
ylabel('Bi-range, r_2 (m)')
grid on
colorbar

%-----------------------------------------------------------------------------------------------------------------------
%       cum3.m
%
%       This function generates the third order cumulant of the radar backscattered signal
%
%       Written by Yeo, Jiunn Wah
%
%       cx      :       the cross cumulant matrix C(m,n) of the radar backscattered signal
%       signal  :       the radar backscattered signal to be processed
%
%       signal_length   :       the maximum argument of the cross cumulant
%-----------------------------------------------------------------------------------------------------------------------
```

```
function [cx] = cum3(signal,signal_length)

%   Assignment and pre-conditioning of signal
signal_1=conj(signal(:));
signal_2=signal(:);
signal_3=signal(:);

N = length(signal_1);

%   Triple correlation of signal
X1 = repmat(signal_1,1,2*signal_length+1);

C2=[zeros(signal_length,1);signal_2(1:signal_length+1)];
R2=[signal_2(signal_length+1:N).' zeros(1,signal_length)];
X2=hankel(C2,R2);

C3=[zeros(signal_length,1);signal_3(1:signal_length+1)];
R3=[signal_3(signal_length+1:N).' zeros(1,signal_length)];
X3=hankel(C3,R3).';

cx=X2*(X1.*X3)/N;
```

C. SOURCE CODE FOR TEST CASE 1

```
%-----------------------------------------------------------------------------------------------------------------------
%       test_case1.m
%
%       This program computes the third order cumulant and bispectrum of the “backhoe
%       data dome” radar backscattered signals for a target orientation of azimuth angle,
%       (θazimuth) = 0° and elevation anlge, (φelevation) = 0°.
%
%       Both radial range and bi-range profiles are processed and plotted over a frequency
%       bandwidth of 5.9058 GHz (from 7.0472 to 12.953 GHz) with VV, HH and HV
%       polarizations.
%
%       Written by Yeo, Jiunn Wah
%-----------------------------------------------------------------------------------------------------------------------
clear all;

%       Load “Backhoe Data Dome” data
load('C:\DOCUME~1\J&C\MYDOCU~1\NPS\Thesis\BACKHO~1\2D_CHA~1\2D_K_S~1\backhoe_el000_az350to100.mat')

c = 3e8;                %       Speed of light
bandwidth = 5.9058;     %       Stimulated frequency bandwidth

sVV_0 = VV(:,141);      %       VV polarized radar signal at θazimuth = 0° and φelevation = 0°
zVV_0 = fft(sVV_0);

sHH_0 = HH(:,141);      %       HH polarized radar signal at θazimuth = 0° and φelevation = 0°
zHH_0 = fft(sHH_0);

sHV_0 = HV(:,141);      %       HV polarized radar signal at θazimuth = 0° and φelevation = 0°
```

```
zHV_0 = fft(sHV_0);

%       Plotting of Radial Range Profile with VV polarization
figure
plot((-length(zVV_0)/2:length(zVV_0)/2-1)*c/2/bandwidth/1e9, (abs(fftshift(zVV_0))))
xlabel('Range (m)')
ylabel('Magnitude of Impulse Response')
title('Radial Range Profile for \theta_a_z = 0 deg and \theta_e_l = 0 deg with VV Polarization')
grid on

%       Plotting of Radial Range Profile with HH polarization
figure
plot((-length(zHH_0)/2:length(zHH_0)/2-1)*c/2/bandwidth/1e9, fftshift(abs((zHH_0))))
xlabel('Range (m)')
ylabel('Magnitude of Impulse Response')
title('Radial Range Profile for \theta_a_z = 0 deg and \theta_e_l = 0 deg with HH Polarization')
grid on

%       Plotting of Radial Range Profile with HV polarization
figure
plot((-length(zHV_0)/2:length(zHV_0)/2-1)*c/2/bandwidth/1e9, (abs(fftshift(zHV_0))))
xlabel('Range (m)')
ylabel('Magnitude of Impulse Response')
title('Radial Range Profile for \theta_a_z = 0 deg and \theta_e_l = 0 deg with HV Polarization')
grid on

%       Computation of third order cumulant and bispectrum
[cxVV_0] = cum3(sVV_0,(length(sVV_0)-1));
bispVV_0 = fftshift(fft2(ifftshift(cxVV_0)));

[cxHH_0] = cum3(sHH_0,(length(sHH_0)-1));
bispHH_0 = fftshift(fft2(ifftshift(cxHH_0)));

[cxHV_0] = cum3(sHV_0,(length(sHV_0)-1));
bispHV_0 = fftshift(fft2(ifftshift(cxHV_0)));

%       Plotting of the 3-D bi-range profile with VV polarization
figure
xVV_0=linspace(-length(bispVV_0)/4,length(bispVV_0)/4,length(bispVV_0))*c/2/bandwidth/1e9;
yVV_0 = linspace(-length(bispVV_0)/4,length(bispVV_0)/4,length(bispVV_0))*c/2/bandwidth/1e9;
refVV_0 = find(xVV_0==0);
refendVV_0 = find(xVV_0>=4.5 & xVV_0<=4.52);
mesh(xVV_0(refVV_0:refendVV_0),yVV_0(refVV_0:refendVV_0),abs(bispVV_0(refVV_0:refendVV_0,
(refVV_0:refendVV_0))));
xlabel('Bi-range, r_1 (m)')
ylabel('Bi-range, r_2 (m)')
zlabel('Magnitude of Bi-range Response')
title('3-D Bi-range Profile for \theta_a_z = 0 deg and \theta_e_l = 0 deg with VV Polarization')

%       Plotting of the 3-D bi-range profile with HH polarization
figure
xHH_0 = linspace(-length(bispHH_0)/4,length(bispHH_0)/4,length(bispHH_0))*c/2/bandwidth/1e9;
yHH_0 = linspace(-length(bispHH_0)/4,length(bispHH_0)/4,length(bispHH_0))*c/2/bandwidth/1e9;
refHH_0 = find(xHH_0==0);
refendHH_0 = find(xHH_0>=4.5 & xHH_0<=4.52);
```

```
mesh(xHH_0(refHH_0:refendHH_0),yHH_0(refHH_0:refendHH_0),abs(bispHH_0(refHH_0:refendHH_0,
(refHH_0:refendHH_0))));
xlabel('Bi-range, r_1 (m)')
ylabel('Bi-range, r_2 (m)')
zlabel('Magnitude of Bi-range Response')
title('3-D Bi-range Profile for \theta_a_z = 0 deg and \theta_e_l = 0 deg with HH Polarization')

%       Plotting of the 3-D bi-range profile with HV polarization
figure
xHV_0 = linspace(-length(bispHV_0)/4,length(bispHV_0)/4,length(bispHV_0))*c/2/bandwidth/1e9;
yHV_0 = linspace(-length(bispHV_0)/4,length(bispHV_0)/4,length(bispHV_0))*c/2/bandwidth/1e9;
refHV_0 = find(xHV_0>=-2.51 & xHV_0<=-2.5);
refendHV_0 = find(xHV_0>=2.5 & xHV_0<=2.51);
mesh(xHV_0(refHV_0:refendHV_0),yHV_0(refHV_0:refendHV_0),abs(bispHV_0(refHV_0:refendHV_0,
(refHV_0:refendHV_0))));
xlabel('Bi-range, r_1 (m)')
ylabel('Bi-range, r_2 (m)')
zlabel('Magnitude of Bi-range Response')
title('3-D Bi-range Profile for \theta_a_z = 0 deg and \theta_e_l = 0 deg with HV Polarization')

%       Plotting of the 2-D characteristic bi-range profile with VV polarization
figure
contour(xVV_0(refVV_0:refendVV_0),yVV_0(refVV_0:refendVV_0),abs(bispVV_0(refVV_0:refendVV
_0,(refVV_0:refendVV_0))), [2e7 4e7 6e7 8e7 1e8 1.2e8 1.4e8 1.6e8 1.8e8 2e8]);
xlabel('Bi-range, r_1 (m)')
ylabel('Bi-range, r_2 (m)')
title('2-D Characteristic Bi-range Profile for \theta_a_z = 0 deg and \theta_e_l = 0 deg with VV
Polarization')
grid on
colorbar

%       Plotting of the 2-D characteristic bi-range profile with HH polarization
figure
contour(xHH_0(refHH_0:refendHH_0),yHH_0(refHH_0:refendHH_0),abs(bispHH_0(refHH_0:refendHH
_0,(refHH_0:refendHH_0))), [2e7 4e7 6e7 8e7 1e8 1.2e8 1.4e8 1.6e8 1.8e8 2e8]);
xlabel('Bi-range, r_1 (m)')
ylabel('Bi-range, r_2 (m)')
title('2-D Characteristic Bi-range Profile for \theta_a_z = 0 deg and \theta_e_l = 0 deg with HH
Polarization')
grid on
colorbar

%       Plotting of the 2-D characteristic bi-range profile with HV polarization
figure
contour(xHV_0(refHV_0:refendHV_0),yHV_0(refHV_0:refendHV_0),abs(bispHV_0(refHV_0:refendHV
_0,(refHV_0:refendHV_0))), [3 5 10 15 20 25 30]);
xlabel('Bi-range, r_1 (m)')
ylabel('Bi-range, r_2 (m)')
title('2-D Characteristic Bi-range Profile for \theta_a_z = 0 deg and \theta_e_l = 0 deg with HV
Polarization')
grid on
colorbar
```

D. SOURCE CODE FOR TEST CASE 2

```
%-----------------------------------------------------------------------------------------------------------------------
%       test_case2.m
%
%       This program computes the third order cumulant and bispectrum of the "backhoe
%       data dome" radar backscattered signals for a target orientation of azimuth angle,
%       (θ_azimuth) = 90° and elevation anlge, (φ_elevation) = 0°.
%
%       Both radial range and bi-range profiles are processed and plotted over a frequency
%       bandwidth of 5.9058 GHz (from 7.0472 to 12.953 GHz) with VV, HH and HV
%       polarizations.
%
%       Written by Yeo, Jiunn Wah
%-----------------------------------------------------------------------------------------------------------------------
clear all;

%       Load "Backhoe Data Dome" data
load('C:\DOCUME~1\J&C\MYDOCU~1\NPS\Thesis\BACKHO~1\2D_CHA~1\2D_K_S~1\backhoe_el000_az350to100.mat')

c = 3e8;                %       Speed of light
bandwidth = 5.9058;     %       Stimulated frequency bandwidth

sVV_90 = VV(:,1401);    %       VV polarized radar signal at θ_azimuth = 90° and φ_elevation = 0°
zVV_90 = fft(sVV_90);

sHH_90 = HH(:,1401);    %       HH polarized radar signal at θ_azimuth = 90° and φ_elevation = 0°
zHH_90 = fft(sHH_90);

sHV_90 = HV(:,1401);    %       HV polarized radar signal at θ_azimuth = 90° and φ_elevation = 0°
zHV_90 = fft(sHV_90);

%       Plotting of Radial Range Profile with VV polarization
figure
plot((-length(zVV_90)/2:length(zVV_90)/2-1)*c/2/bandwidth/1e9, (abs(fftshift(zVV_90))))
xlabel('Range (m)')
ylabel('Magnitude of Impulse Response')
title('Radial Range Profile for \theta_a_z = 90 deg and \theta_e_l = 0 deg with VV Polarization')
grid on

%       Plotting of Radial Range Profile with HH polarization
figure
plot((-length(zHH_90)/2:length(zHH_90)/2-1)*c/2/bandwidth/1e9, fftshift(abs((zHH_90))))
xlabel('Range (m)')
ylabel('Magnitude of Impulse Response')
title('Radial Range Profile for \theta_a_z = 90 deg and \theta_e_l = 0 deg with HH Polarization')
grid on

%       Plotting of Radial Range Profile with HV polarization
figure
plot((-length(zHV_90)/2:length(zHV_90)/2-1)*c/2/bandwidth/1e9, (abs(fftshift(zHV_90))))
xlabel('Range (m)')
ylabel('Magnitude of Impulse Response')
title('Radial Range Profile for \theta_a_z = 90 deg and \theta_e_l = 0 deg with HV Polarization')
grid on
```

```
 %        Computation of third order cumulant and bispectrum
[cxVV_90] = cum3(sVV_90,(length(sVV_90)-1));
bispVV_90 = fftshift(fft2(ifftshift(cxVV_90)));

[cxHH_90] = cum3(sHH_90,(length(sHH_90)-1));
bispHH_90 = fftshift(fft2(ifftshift(cxHH_90)));

[cxHV_90] = cum3(sHV_90,(length(sHV_90)-1));
bispHV_90 = fftshift(fft2(ifftshift(cxHV_90)));

%        Plotting of the 3-D bi-range profile with VV polarization
figure
xVV_90 = linspace(-length(bispVV_90)/4,length(bispVV_90)/4,length(bispVV_90))*c/2/bandwidth/1e9;
yVV_90 = linspace(-length(bispVV_90)/4,length(bispVV_90)/4,length(bispVV_90))*c/2/bandwidth/1e9;
refVV_90 = find(xVV_90==0);
refendVV_90 = find(xVV_90>=2 & xVV_90<=2.0085);
mesh(xVV_90(refVV_90:refendVV_90),yVV_90(refVV_90:refendVV_90),abs(bispVV_90(refVV_90:ref
endVV_90,(refVV_90:refendVV_90))));
xlabel('Bi-range, r_1 (m)')
ylabel('Bi-range, r_2 (m)')
zlabel('Magnitude of Bi-range Response')
title('3-D Bi-range Profile for \theta_a_z = 90 deg and \theta_e_l = 0 deg with VV Polarization')

%        Plotting of the 3-D bi-range profile with HH polarization
figure
xHH_90 = linspace(-length(bispHH_90)/4,length(bispHH_90)/4,length(bispHH_90))*c/2/bandwidth/1e9;
yHH_90 = linspace(-length(bispHH_90)/4,length(bispHH_90)/4,length(bispHH_90))*c/2/bandwidth/1e9;
refHH_90 = find(xHH_90==0);
refendHH_90 = find(xHH_90>=2 & xHH_90<=2.0085);
mesh(xHH_90(refHH_90:refendHH_90),yHH_90(refHH_90:refendHH_90),abs(bispHH_90(refHH_90:ref
endHH_90,(refHH_90:refendHH_90))));
xlabel('Bi-range, r_1 (m)')
ylabel('Bi-range, r_2 (m)')
zlabel('Magnitude of Bi-range Response')
title('3-D Bi-range Profile for \theta_a_z = 90 deg and \theta_e_l = 0 deg with HH Polarization')

%        Plotting of the 3-D bi-range profile with HV polarization
figure
xHV_90 = linspace(-length(bispHV_90)/4,length(bispHV_90)/4,length(bispHV_90))*c/2/bandwidth/1e9;
yHV_90 = linspace(-length(bispHV_90)/4,length(bispHV_90)/4,length(bispHV_90))*c/2/bandwidth/1e9;
refHV_90 = find(xHV_90>=-2.01 & xHV_90<=-2.0);
refendHV_90 = find(xHV_90>=2.0 & xHV_90<=2.01);
mesh(xHV_90(refHV_90:refendHV_90),yHV_90(refHV_90:refendHV_90),abs(bispHV_90(refHV_90:ref
endHV_90,(refHV_90:refendHV_90))));
xlabel('Bi-range, r_1 (m)')
ylabel('Bi-range, r_2 (m)')
zlabel('Magnitude of Bi-range Response')
title('3-D Bi-range Profile for \theta_a_z = 90 deg and \theta_e_l = 0 deg with HV Polarization')

%        Plotting of the 2-D characteristic bi-range profile with VV polarization
figure
contour(xVV_90(refVV_90:refendVV_90),yVV_90(refVV_90:refendVV_90),abs(bispVV_90(refVV_90:r
efendVV_90,(refVV_90:refendVV_90))), [2.5e9 5e9 7.5e9 1e10 1.5e10 2e10 2.5e10]);
xlabel('Bi-range, r_1 (m)')
ylabel('Bi-range, r_2 (m)')
```

```
title('2-D Characteristic Bi-range Profile for \theta_a_z = 90 deg and \theta_e_l = 0 deg with VV Polarization')
grid on
colorbar

%       Plotting of the 2-D characteristic bi-range profile with HH polarization
figure
contour(xHH_90(refHH_90:refendHH_90),yHH_90(refHH_90:refendHH_90),abs(bispHH_90(refHH_90:refendHH_90,(refHH_90:refendHH_90))), [2.5e9 5e9 7.5e9 1e10 1.5e10 2e10 2.5e10]);
xlabel('Bi-range, r_1 (m)')
ylabel('Bi-range, r_2 (m)')
title('2-D Characteristic Bi-range Profile for \theta_a_z = 90 deg and \theta_e_l = 0 deg with HH Polarization')
grid on
colorbar

%       Plotting of the 2-D characteristic bi-range profile with HV polarization
figure
contour(xHV_90(refHV_90:refendHV_90),yHV_90(refHV_90:refendHV_90),abs(bispHV_90(refHV_90:refendHV_90,(refHV_90:refendHV_90))), [18 20 40 60 80 100 120 140 160 180]);
xlabel('Bi-range, r_1 (m)')
ylabel('Bi-range, r_2 (m)')
title('2-D Characteristic Bi-range Profile for \theta_a_z = 90 deg and \theta_e_l = 0 deg with HV Polarization')
grid on
colorbar
```

E. SOURCE CODE FOR TEST CASE 3

```
%-----------------------------------------------------------------------------------------------------------------------
%       test_case3.m
%
%       This program computes the third order cumulant and bispectrum of the “backhoe
%       data dome” radar backscattered signals for a target orientation of azimuth angle,
%       (θ_azimuth) = 60° and elevation anlge, (φ_elevation) = 30°.
%
%       Both radial range and bi-range profiles are processed and plotted over a frequency
%       bandwidth of 5.9058 GHz (from 7.0472 to 12.953 GHz) with VV, HH and HV
%       polarizations.
%
%       Written by Yeo, Jiunn Wah
%-----------------------------------------------------------------------------------------------------------------------
clear all;

%       Load “Backhoe Data Dome” data
load('C:\DOCUME~1\J&C\MYDOCU~1\NPS\Thesis\BACKHO~1\2D_CHA~1\2D_K_S~1\backhoe_el030_az350to100.mat')

c = 3e8;                %       Speed of light
bandwidth = 5.9058;     %       Stimulated frequency bandwidth

sVV_60 = VV(:,981);     %       VV polarized radar signal at θ_azimuth = 60° and φ_elevation = 30°
zVV_60 = fft(sVV_60);

sHH_60 = HH(:,981);     %       HH polarized radar signal at θ_azimuth = 60° and φ_elevation = 30°
zHH_60 = fft(sHH_60);
```

```
sHV_60 = HV(:,981);       %       HV polarized radar signal at θ_azimuth = 60° and φ_elevation = 30°
zHV_60 = fft(sHV_60);

%       Plotting of Radial Range Profile with VV polarization
figure
plot((-length(zVV_60)/2:length(zVV_60)/2-1)*c/2/bandwidth/1e9, (abs(fftshift(zVV_60))))
xlabel('Range (m)')
ylabel('Magnitude of Impulse Response')
title('Radial Range Profile for \theta_a_z = 60 deg and \theta_e_l = 30 deg with VV Polarization')
grid on

%       Plotting of Radial Range Profile with HH polarization
figure
plot((-length(zHH_60)/2:length(zHH_60)/2-1)*c/2/bandwidth/1e9, fftshift(abs((zHH_60))))
xlabel('Range (m)')
ylabel('Magnitude of Impulse Response')
title('Radial Range Profile for \theta_a_z = 60 deg and \theta_e_l = 30 deg with HH Polarization')
grid on

%       Plotting of Radial Range Profile with HV polarization
figure
plot((-length(zHV_60)/2:length(zHV_60)/2-1)*c/2/bandwidth/1e9, (abs(fftshift(zHV_60))))
xlabel('Range (m)')
ylabel('Magnitude of Impulse Response')
title('Radial Range Profile for \theta_a_z = 60 deg and \theta_e_l = 30 deg with HV Polarization')
grid on

%       Computation of third order cumulant and bispectrum
[cxVV_60] = cum3(sVV_60,(length(sVV_60)-1));
bispVV_60 = fftshift(fft2(ifftshift(cxVV_60)));

[cxHH_60] = cum3(sHH_60,(length(sHH_60)-1));
bispHH_60 = fftshift(fft2(ifftshift(cxHH_60)));

[cxHV_60] = cum3(sHV_60,(length(sHV_60)-1));
bispHV_60 = fftshift(fft2(ifftshift(cxHV_60)));

%       Plotting of the 3-D bi-range profile with VV polarization
figure
xVV_60 = linspace(-length(bispVV_60)/4,length(bispVV_60)/4,length(bispVV_60))*c/2/bandwidth/1e9;
yVV_60 = linspace(-length(bispVV_60)/4,length(bispVV_60)/4,length(bispVV_60))*c/2/bandwidth/1e9;
refVV_60 = find(xVV_60==0);
refendVV_60 = find(xVV_60>=2 & xVV_60<=2.01);
mesh(xVV_60(refVV_60:refendVV_60),yVV_60(refVV_60:refendVV_60),abs(bispVV_60(refVV_60:ref
endVV_60,(refVV_60:refendVV_60))));
xlabel('Bi-range, r_1 (m)')
ylabel('Bi-range, r_2 (m)')
zlabel('Magnitude of Bi-range Response')
title('3-D Bi-range Profile for \theta_a_z = 60 deg and \theta_e_l = 30 deg with VV Polarization')

%       Plotting of the 3-D bi-range profile with HH polarization
figure
xHH_60 = linspace(-length(bispHH_60)/4,length(bispHH_60)/4,length(bispHH_60))*c/2/bandwidth/1e9;
yHH_60 = linspace(-length(bispHH_60)/4,length(bispHH_60)/4,length(bispHH_60))*c/2/bandwidth/1e9;
refHH_60 = find(xHH_60==0);
```

```
refendHH_60 = find(xHH_60>=2 & xHH_60<=2.01);
mesh(xHH_60(refHH_60:refendHH_60),yHH_60(refHH_60:refendHH_60),abs(bispHH_60(refHH_60:ref
endHH_60,(refHH_60:refendHH_60))));
xlabel('Bi-range, r_1 (m)')
ylabel('Bi-range, r_2 (m)')
zlabel('Magnitude of Bi-range Response')
title('3-D Bi-range Profile for \theta_a_z = 60 deg and \theta_e_l = 30 deg with HH Polarization')

%       Plotting of the 3-D bi-range profile with HV polarization
figure
xHV_60 = linspace(-length(bispHV_60)/4,length(bispHV_60)/4,length(bispHV_60))*c/2/bandwidth/1e9;
yHV_60 = linspace(-length(bispHV_60)/4,length(bispHV_60)/4,length(bispHV_60))*c/2/bandwidth/1e9;
refHV_60 = find(xHV_60>=-2.01 & xHV_60<=-2.0);
refendHV_60 = find(xHV_60>=2.0 & xHV_60<=2.01);
mesh(xHV_60(refHV_60:refendHV_60),yHV_60(refHV_60:refendHV_60),abs(bispHV_60(refHV_60:ref
endHV_60,(refHV_60:refendHV_60))));
xlabel('Bi-range, r_1 (m)')
ylabel('Bi-range, r_2 (m)')
zlabel('Magnitude of Bi-range Response')
title('3-D Bi-range Profile for \theta_a_z = 60 deg and \theta_e_l = 30 deg with HV Polarization')

%       Plotting of the 2-D characteristic bi-range profile with VV polarization
figure
contour(xVV_60(refVV_60:refendVV_60),yVV_60(refVV_60:refendVV_60),abs(bispVV_60(refVV_60:r
efendVV_60,(refVV_60:refendVV_60))), [1.8e5 4e5 6e5 8e5 1e6 1.2e6 1.4e6 1.6e6 1.8e6]);
xlabel('Bi-range, r_1 (m)')
ylabel('Bi-range, r_2 (m)')
title('2-D Characteristic Bi-range Profile for \theta_a_z = 60 deg and \theta_e_l = 30 deg with VV
Polarization')
grid on
colorbar

%       Plotting of the 2-D characteristic bi-range profile with HH polarization
figure
contour(xHH_60(refHH_60:refendHH_60),yHH_60(refHH_60:refendHH_60),abs(bispHH_60(refHH_60:r
efendHH_60,(refHH_60:refendHH_60))), [2.5e5 4e5 6e5 8e5 1e6 1.2e6 1.4e6 1.6e6 1.8e6 2.0e6 2.5e6]);
xlabel('Bi-range, r_1 (m)')
ylabel('Bi-range, r_2 (m)')
title('2-D Characteristic Bi-range Profile for \theta_a_z = 60 deg and \theta_e_l = 30 deg with HH
Polarization')
grid on
colorbar

%       Plotting of the 2-D characteristic bi-range profile with HV polarization
figure
contour(xHV_60(refHV_60:refendHV_60),yHV_60(refHV_60:refendHV_60),abs(bispHV_60(refHV_60:r
efendHV_60,(refHV_60:refendHV_60))), [3.5e6 4e6 6e6 8e6 1e7 2e7 2.5e7 3e7 3.5e7]);
xlabel('Bi-range, r_1 (m)')
ylabel('Bi-range, r_2 (m)')
title('2-D Characteristic Bi-range Profile for \theta_a_z = 60 deg and \theta_e_l = 30 deg with HV
Polarization')
grid on
colorbar
```

LIST OF REFERENCES

Balisle, P. (2002, April 9). *Statement before the Seapower Subcommittee of the Senate Armed Services Committee on Surface Warfare Systems.* Retrieved on October 5, 2006, from http://www.navy.mil/navydata/testimony/seapower/pmbalisle020309.txt

Bao, Z., Pei, B., Xing, M. (2001). Logarithm Bispectrum-Based Approach to Radar Range Profile for Automatic Target Recognition. *Radar 2001, IEEE Conference Proceedings*

Bao, Z., Shi, Y., Zhang, X. (2001). A new feature vector using selected bispectra for signal classification with application in radar target recognition. *IEEE Transactions on Signal Processing. Vol.49 (No.9).*

Borden, B. (1998). *Radar imaging of airborne target—a primer for mathematicians and physicists.* California: Naval Air Warfare Center Weapons Division China Lake.

Botha, E.C., Spoelstra, J. (1992). *Radar target recognition using multiple bounce scattering terms.* South Africa, Pretoria.: University of Pretoria.

Bullard, B. (1991). Pulse *Doppler Signature of a Rotary-Wing Aircraft*. Atlanta: Georgia Tech Research Institute, Georgia Institute of Technology.

Defence Research and Development Canada. (2005). *Non-Cooperative Target Recognition of Air Targets (NCTR).* Retrieved on June 7, 2006, from http://www.ottawa.drdc-rddc.gc.ca/html/RAST-309-nctr_e.html

Garber, E.D., Jouny, I. and Moses, R.L. (1995). Radar Target Identification Using the Bispectrum: A Comparison Study. *IEEE Transactions on Aerospace and Electronic Systems, Vol. 31, No. 1.*

Jounty, I. and Walton, E.K. (1990). Bispectrum of Radar Signals and Application to Target Classification. *Radio Science, 25(2):101-113.*

Jouny, I. (1994). Description of radar targets using the bispectrum. *IEE Proceeding—Radar, Sonar and Navigation Vol. 141*(3).

Lin, L., Naidu, K. (2004). Data dome: full k-space sampling data for high-frequency radar research. *Proceedings of SPIE, Algorithms for Synthetic Aperture Radar XI, Vol.5427,* 200-207.

Nebabin, V.G. (1995). *Methods and techniques of radar recognition.* Boston: Artech House.

Potter, J. (2005). [Acoustics Sensors] Unpublished lecture notes.

Sadiku, M.N.O. (2001). *Elements of Electromagnetics*. (3rd ed.). New York: Oxford University Press.

Skolnik, M.I. (2001). *Introduction to radar systems*. (3rd ed.). New York: McGraw-Hill.

Tait, P. (2005). *Introduction to radar target recognition*. UK: Institution of Electrical Engineers.

Tzu, S., Hart, B.H., Griffith, S. (1971). *The art of war*. New York: Oxford University Press.

Van Der Heigen, R. (1998). *Aircraft recognition with radar range profiles* (Doctoral dissertation, University of Amsterdam, 1998).

Wolff, C. (1997). *Radar Principles*. Retrieved on August 9, 2006, from http://www.radartutorial.eu/13.ssr/sr04.en.html

INITIAL DISTRIBUTION LIST

1. Defense Technical Information Center
   Ft. Belvoir, Virginia

2. Dudley Knox Library
   Naval Postgraduate School
   Monterey, California

3. Professor Brett Borden
   Physics Department
   Naval Postgraduate School
   Monterey, California

4. Professor Donald L. Walters
   Physics Department
   Naval Postgraduate School
   Monterey, California

5. Professor Phillip E. Pace
   Electrical and Computer Engineering Department
   Naval Postgraduate School
   Monterey, California

6. Professor Andres Larraza
   Physics Department
   Naval Postgraduate School
   Monterey, California

7. Chairman, Physics Department
   Naval Postgraduate School
   Monterey, California

8. Professor Yeo Tat Soon
   Director of Temasek Defence System Institute
   National University of Singapore
   Singapore

9. LT Cole, Zachary
   Naval Postgraduate School
   Monterey, California

10. Yeo Jiunn Wah
    Defence Science and Technology Agency
    Singapore